Energy Absorption in Metal-FRP Hybrid Square Tubes

Roozbeh Kalhor

Dissertation submitted to the faculty of the
Virginia Polytechnic Institute and State University in partial fulfillment of the requirements
for the degree of

Doctor of Philosophy
in
Engineering Mechanics

Scott W. Case, Chair
Marwan Al-Haik
Shane Ross
Garry Seidel

November 30, 2016
Blacksburg, VA

Keywords: Energy absorption, Axial crushing, Metal-composite square hybrid tubes, Neural networks, Multi-objective optimization

Energy Absorption in Metal-FRP Hybrid Square tTubes

Roozbeh Kalhor

ABSTRACT

Lower-cost manufacturing methods have increased the anticipation for economical mass production of vehicles manufactured from composite materials. One of the potential applications of composite materials in vehicles is in energy-absorbing components such as hollow shells and struts (these components may be in the form of circular cylindrical shells, square and rectangular tubes, conical shells, and frusta). However, constructions which result in brittle fracture of the composite tubes in the form of circumferential or longitudinal corner crack propagation may lead to unstable collapse failure mode and concomitant very low energy absorption. As a result, metal-composite hollow tubes have been developed that combine the benefits of stable ductile collapse of the metal (which can absorb crushing energy in a controlled manner) and the high strength-to-weight ratio of the composites. The relative and absolute thicknesses of metal or FRP section has a substantial effect on energy absorption of the hybrid tubes. In particular, likelihood of delamination occurrence raises with increase in FRP thickness. This can reduce the energy absorption capability of the metal-FRP hybrid tubes. Additionally, adding a very thick FRP section may result in a global buckling failure mode (rather than local folding). Until now, there are no studies specifically addressing the effect of FRP thickness on energy absorption of hybrid tubes. In this study, the effects of fiber orientation and FRP thickness (the number of layers) on the energy absorption of S2-glass/epoxy-304 stainless steel square tubes were experimentally investigated. In addition, a new geometrical trigger was demonstrated which has positive effects on the collapse modes, delamination in the FRP, and the crush load efficiency of the hybrid tube.

To complete this study, a new methodology including the combination of experimental results, numerical modeling, and a multi-objective optimization process was introduced to obtain the best combination of design variables for hybrid metal-composite tubes for crashworthiness applications. The experimental results for the S2 glass/epoxy-304 stainless steel square tubes with different configurations tested under quasi-static compression loading were used to validate numerical models implemented in LS-DYNA software. The models were able to capture progressive failure mechanisms of the hybrid tubes. In addition, the effects of the design variables on the energy absorption and failure modes of the hybrid tubes were explained. Subsequently, the results from the numerical models were used to obtain optimum crashworthiness functions. The load efficiency factor (the ratio of mean crushing load to maximum load) and ratio between the difference of mean crushing load of hybrid and metal tube and thickness of the FRP section were introduced as objective functions. To connect the variables and the functions, back-propagation artificial neural networks (ANN) were used. The Non-dominated Sorting Genetic Algorithm–II (NSGAII) was applied to the constructed ANNs to obtain optimal results. The results were presented in the form of Pareto frontiers to help designers choose optimized configurations based on their manufacturing limitations. Such restrictions may include, but are not limited to, cost (related to the number of layers), laminate architecture (fiber orientation and stacking sequence) which can be constrained by the manufacturing techniques (i.e. filament winding) and thickness (as an example of physical constraints).

Energy Absorption in Metal-FRP Hybrid Square Tubes

Roozbeh Kalhor

GENERAL AUDIENCE ABSTRACT

In a car accident, the incident energy must be absorbed by elements of the vehicles to prevent it from being transferred to the occupants. (Indeed, a vehicle that is not damaged in a crash may lead to significant injury to occupants.) Typical energy absorbing elements in a vehicle include hollow shells and struts in the crumple zone, bumpers, and airbags. The focus of this study is on hollow thin-walled tubes in the form of hybrid metal-composite square tubes which have the potential to provide cost-effective structures for energy absorption applications. The behavior of these elements is complicated, requiring computationally intensive and time-consuming computer simulations to analyze their failure and to improve their design. The time required for these simulations may lead to long times before new elements are introduced into the marketplace. Consequently, the objective of this study is to provide an efficient and fast methodology to obtain the best hybrid structures for crashworthiness applications. To support the computational modeling, experimental results obtained from the samples with different configurations tested under quasi-static compression loading were used to validate the models. The effect of fiber orientation, stacking sequence, and thickness of the composite on energy absorption and failure modes were predicted using the models. To reduce the time associated with computational modeling, artificial neural networks (ANNs) were employed to fit the response at selected training points and to generate a pool of responses at other points. These responses may then be used by a designer to choose the best solution for a set of competing design constraints.

To my parents: Shohreh and Asghar

Thank you for your endless support in this journey

For keeping faith on me

For being there when I needed you

Thank you for everything

Acknowledgements

I would like to express my sincere gratitude to my advisor, Dr. Scott W. Case, for the continuous support during my Ph.D., for his patience, motivation, and immense knowledge. He gave me the room and opportunity to try different areas, to fail, and to find the way for which I was truly passionate. I could not have imagined having a better advisor and mentor.

I would like to express my appreciation to my committee members; Dr. Gary Seidel, Dr. Marwan Al-Haik, and Dr. Shane Ross for their advice, encouragement, and insightful comments.

My sincere thanks also goes to BEAM staff including

- Mac McCord and Danny Reed: for being patient and supportive on experimental analysis and helping me to teach ESM 3064 course.
- Darrel Link and Dave Simmons: For their assistance and knowledge on precise fixture/ manufacturing design processes.
- Beverly Williams: for checking and keeping track of us. For giving us advice when we needed.

Last but not least, I want to especially thank my family: my parents, my brother, Reza, and my sister, Ramineh, for their continuous encouragement and support. This accomplishment would not have been possible without them.

Table of Contents

List of Figures

List of Tables

Chapter 1

1. Introduction

1.1. Background

Advances in the transportation industry have continuously increased the number of vehicles in addition to their speed. As a result, injuries and costs resulting from car accidents [1] have also increased. In fact, 95% of all transportation deaths were motorway related. The statistics provided by NHTSA (National Highway Traffic Safety Administration) in 2015 show that automotive fatalities increased by 8% to one death every 89 million miles. In fact, more young Americans die from vehicular crashes than diseases [1]. In another report, the Australian Transport Safety Bureau calculated $15 billion (in AUD) annual economic loss in 1996 because of structural and environmental damage or injuries to people caused by road crashes. The injuries include those resulting from high deceleration and crushing of occupant compartment. Hence, passive energy dissipating structures have been developed over time to reduce the likelihood of injuries.

Consequently, crashworthiness and energy absorption are among the most important parameters in vehicle design. Crashworthiness is the quality of response of a vehicle involved in an accident [1]. Controlled failure modes ensure a stable energy absorption mechanism which leads into better crashworthiness [2]. In general, energy absorption structures should have (1) irreversible energy conversion, (2) restricted and constant reactive load (ideally a rectangular load-displacement response to avoid a high rate of retardation), (3) enough length (to have the ability to absorb more energy), (4) stable and repeatable deformation modes, (5) high specific energy absorption (for better fuel consumption and less pollution), and (6) low cost and easy installation/removal (when replacement is necessary) [1]. In a car accident, the deformation of the elements should

hinder transferring the accident energy to passengers and work to provide a sufficient and safe space for them. Typical energy absorbing systems in a vehicle include: hollow shells and struts (cylindrical, square and rectangular tubes, conical shells, and frusta), bumpers, crumple zones, and the passenger compartment [3]. In this study, the focus is on hollow thin-walled tubes in a car frame such as longitudinal body rails with circular, square, or tapered cross sections (Fig. 1-1a) and front chassis legs (Fig. 1-1b). They resemble the same elements mounted in the area between motor and passenger space and loaded by vehicle bumper or guards [4]. The design of these energy absorbing devices should be combined with the complex knowledge of the accident loads, i.e. the deceleration rates endurable by the human body and the distribution of loads in the vehicle structure [5].

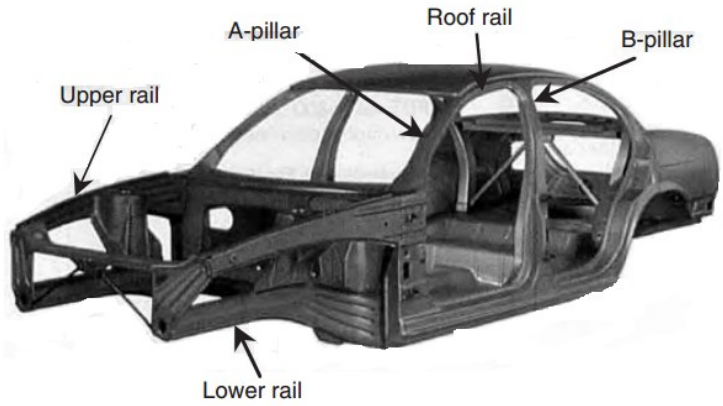

(a)

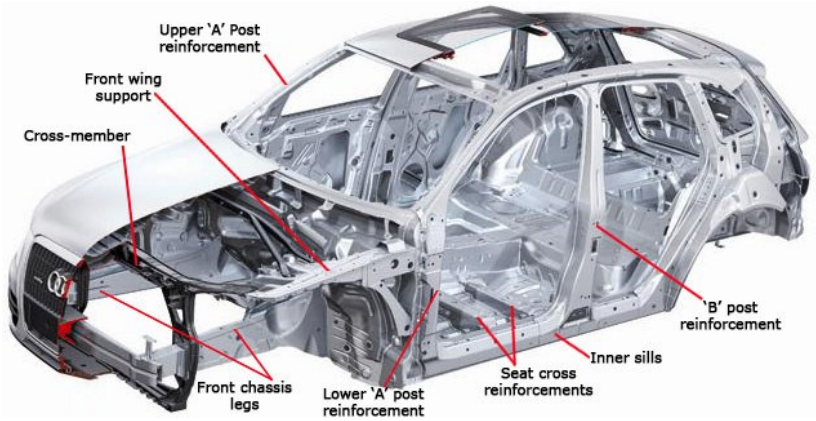

(b)

Fig. 1-1. The structure of a vehicle [1]

The axial crush performance of metal, composite, and hybrid thin-walled structures has been studied under quasi-static and dynamic loading since the 1970s. This axial crushing process begins with elastic compression and bending of the element. As a result, load increases up to a peak value, P_{max}, drops sharply because of local buckling, and continues with oscillations around a mean value, P_{mean} (Fig. 1-3). The details of the deformation process depend on the tube geometry, material characteristics (composite material constituents and laminate design), collapse modes, and loading conditions [3]. The load–displacement curve is used to represent the Specific Energy Absorption (SEA) and load efficiency factor (representative of energy absorption capabilities of crashworthiness performance of energy absorption elements) in the crushing process as follows:

$$\text{SEA} = \frac{\text{Absorbed Energy}}{\text{Mass of the tube}}$$

$$\text{P}_{\text{mean}} = \frac{\text{Area under load} - \text{displacement curve}}{\text{crushing distance}}$$

$$\eta = \frac{\text{P}_{\text{mean}}}{\text{P}_{\text{max}}}$$

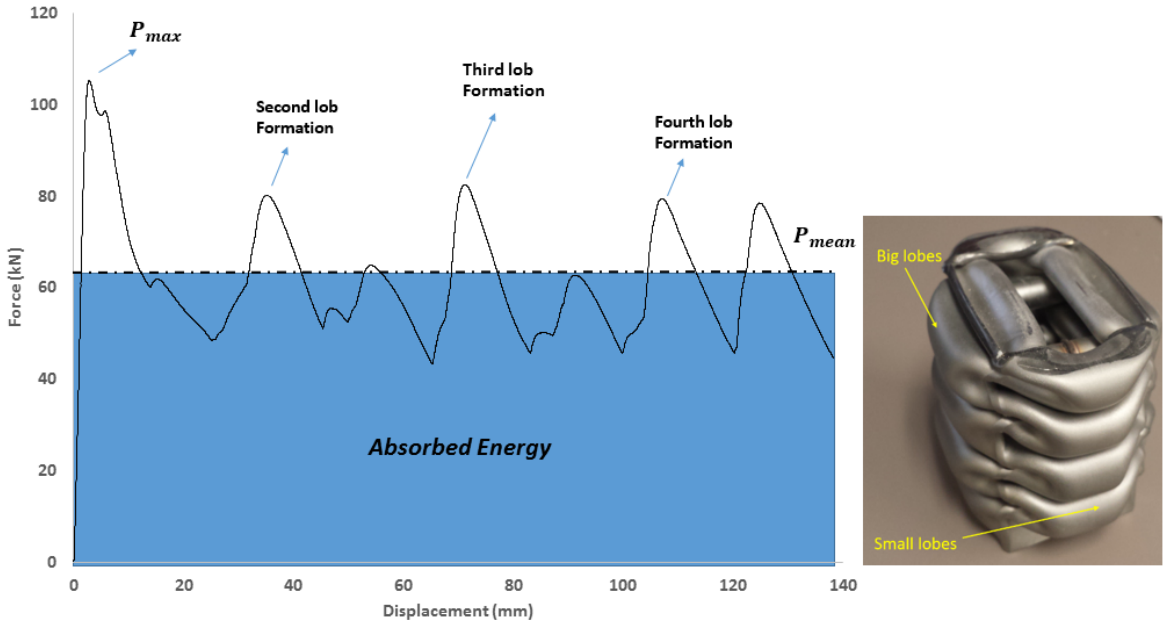

Fig. 1-2. Typical load-displacement curve for hollow square tubes including the ideal load profile (blue area)

The load efficiency factor should be close to unity in order to minimize the presence of rapid changes in the load profile as a result of undesirable collapse modes (i.e. catastrophic failure which causes injuries such as brain trauma to passengers [6, 7]).

To eliminate the effects of inertia and strain rate, energy absorption of hollow thin-walled tubes is usually first studied under quasi-static loading. Previous work has shown that this loading condition produces the same crushing modes as dynamic loading [3].

The application of fiber-reinforced plastics (FRPs) in high performance sports cars [8, 9] and railway vehicles [10] has increased over time because the FRPs can offer weight and cost savings over traditional materials. For instance, the Lamborghini Murcielago presents an entire carbon-fiber/epoxy body including bumpers, fenders, hood, etc. (Fig. 1-3) [11]. FRPs are able to also contribute favorably to crashworthiness. One of the potential applications of composite materials in vehicles is in energy-absorbing components such as hollow shells and struts [3]. In fact, composite materials offer potential design flexibility over traditional materials as there are a large number of design variables that can affect energy absorption

of hybrid and composite tubes, including the stacking sequence or weave pattern of the layers of the composites [12-14], geometry of the tube [12, 15-18], the manufacturing parameters [19], the bonding between the metal and composite sections [20], and environmental conditions including temperature and humidity [19]. However, (1) the cost of carbon fibers ($7.88/kg) compared with steel ($0.37/kg) and aluminum ($1.68/kg) and (2) labor costs for different production methods [21] have historically hindered the use of composite materials in many industrial sectors. However, low-cost manufacturing methods have increased the anticipation for economical mass production of vehicles from composite materials [22]. For instance, the vacuum assisted resin transfer molding (VARTM) method offers 60% reduction in the manufacturing costs compared to other curing processes using an autoclave [23].

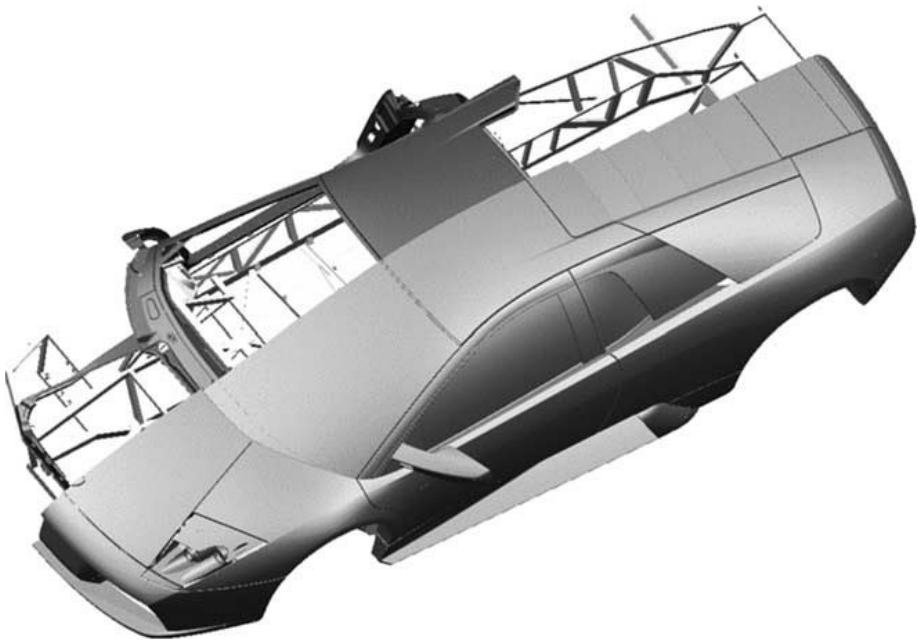

Fig. 1-3. The entire carbon epoxy body of Lamborghini Murcielago made of composite materials over its steel frame [11]

Modern experimental methods coupled with numerical simulations and analytical tools are able to improve the design of thin-walled composite and hybrid structures. In the section that follows, the failure modes of composite hollow and hybrid structures as result of compressive and impact loading are reviewed. Subsequently, different methods for

predicting the resulted failure modes and most relevant material properties in crashworthiness functions such as energy absorption and load efficiency factor are discussed. Finally, different suggested analytical models to predict the crashworthiness functions are presented.

1.2. Experimental studies

1.2.1. Composite structures

As understanding of the failure modes and energy absorption mechanisms of composite materials under different loading conditions (tensile, compressive and bending) in the crushing process can aid designers and manufacturers in producing better hybrid (metal-composite) structures. As a result, the response of composite structures under different loading conditions are categorized in the section.

Fiber breakage, matrix cracking (less energy absorption of thermosetting matrices compared with metal matrices because of their brittle nature), inter-ply delamination (as a result of high shear stresses at the tip of propagating crack which runs between the layers and result in excessive energy absorption), fiber-matrix separation in the form of debonding or pull out (significant contribution of weak interface strength on energy absorption) [3], fiber micro-buckling and kinking, and friction are the most important energy absorption mechanisms in composite materials [24]. The failure modes of a unidirectional laminate under tensile loading include (1) brittle failure with and without fiber pull-out (2) interface shear failure, and (3) delamination. Fibers transverse to loading direction perform as stress concentration points and result in matrix tensile loading, debonding and fiber splitting. Micro-buckling of the unidirectional fibers under compression loading is due to ductile matrices with low stiffness or even weak bonding of fiber and matrix (which cause transverse splitting). When the matrix remains stiff enough to prevent the fibers from buckling, the fibers fail in a shearing mode. Transverse compressive loading of unidirectional composite leads to shear failure of matrix and inter-ply debonding. Finally a laminate under bending loading conditions becomes subjected to the compressive (delamination, matrix

failure, and fiber/matrix interface failure) and tensile failure modes (pullout fiber, unidirectional fiber breakage, matrix cracking, delamination, and interface failure) [3].

- **Failure modes of hollow composite tubes**

In a series of papers, Mamalis et al. [8, 25-27] and Hull et al. [28, 29] studied and categorized the main failure modes of composite hollow structures as follows:

I. Progressive failure mode (Mode I) because of splaying or fragmentation modes which is formed by internal and external fronds. As a result, a debris wedge penetrates in the middle of the fronds including crushed fibers and resin that facilities opening of the main crack. The main energy absorption mechanism for this mode include the main crack propagation (mode I delamination), multiple propagation of axial cracks in the fronds to accommodate flattening, transverse cracking at the roots of fronds, formation of fronds (Mode II delamination between layers), and finally a large frictional energy absorption between (1) the debris wedge and internal/external fronds, (2) moving platen and internal/external fronds, and (3) sliding adjacent delaminated layers (Fig. 1-4) [26].

II. Brittle fracture failure mode of the energy absorption element in the form of circumferential or longitudinal corner (in the case of square cross section because of local stress concentrations) crack propagation (Mode II or sliding mode). The failure mode in the shell in addition to mid-length unstable collapse mode result in catastrophic separation of the shell into irregular shapes.

III. Progressive folding and hinging of composite tubes which is the same as plastic folding formation in thin-walled metal and plastic tubes.

In general, Mode I has the highest energy absorption because of the different identified absorption mechanisms. Frictional energy dissipation has the most significant contribution to the energy absorption. The unstable collapse, Mode III, results in the least energy absorption. Energy absorption associated with crack propagation is estimated to be only 5-20% of total absorbed energy [30-32]. Usually, crushing of different elements leads to one or combination of the crushing failure modes based on different parameters affecting the

response (such as geometry, fiber orientation, and material properties of the matrix and fibers).

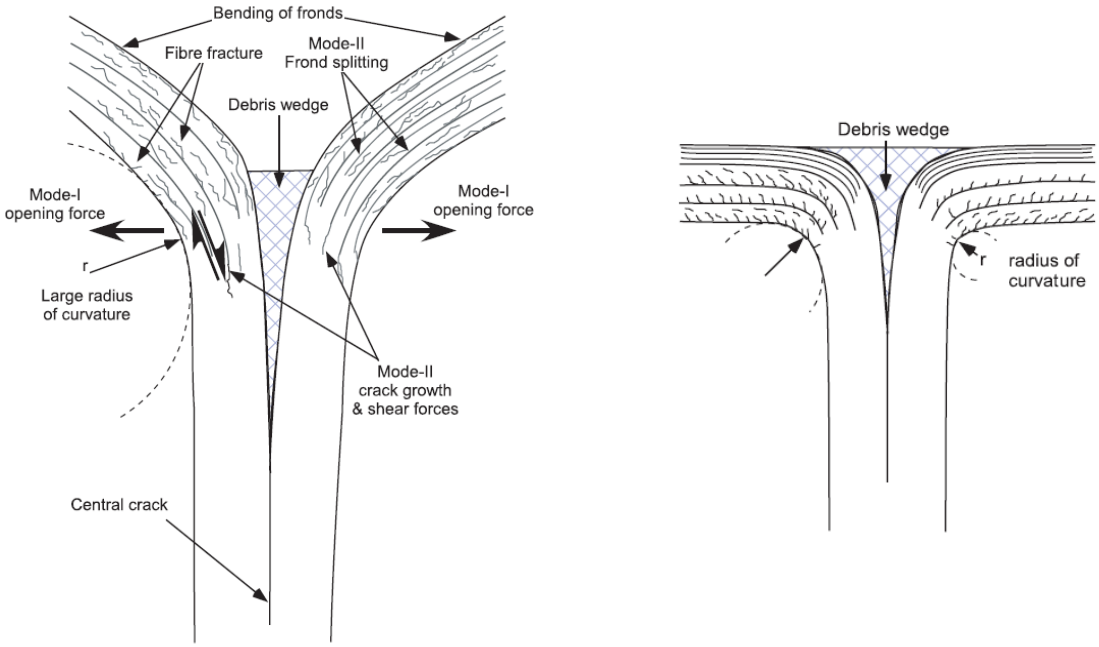

Fig. 1-4. Splaying (Mode I) and sliding (Mode II) in axial crushing [33]

- **Effect of different parameters on energy absorption**

There is a large number of parameters that can affect the energy absorption of hybrid and composite tubes, including the constituents (the fiber and matrix materials), stacking sequence or weave pattern of the layers of the composite [12-14], the geometry of the tube [12, 15-18], the manufacturing parameters [19], and the environmental conditions including temperature and humidity [19].

- **FRP constituents**

The effect of fiber and matrix strain-to-failure on the energy absorption ability of graphite fibers reinforced composite tubes was investigated by Farley [34]. T300/934, T300/5245, AS-4/934 and AS-4/5245 in the form of prepreg sheets were used to make different samples. Composites made from AS-4 carbon fibers exhibited a 20% greater strain-to-failure compared than those made from T300 carbon fibers. Farley found that a matrix with higher

strain-to-failure resulted in greater energy absorption by reducing the interlaminar cracking between plies. He also observed the crushing pattern of the tubes depends on the strain-to-failure of both matrix and fiber. In addition, he suggested less brittle fibers such as Kevlar can also change the folding pattern of composite tubes from the splitting mode to a progressive failure mode [35]. Moreover, he found that fiber orientation can also have a significant influence. Fibers with higher strain-to-failure are more effective in absorbing energy when oriented circumferentially (90° with respect to the tube axis). In another study, carbon fiber/epoxy and carbon fiber/polyether ether ketone (PEEK) unidirectional composite tubes were tested under axial compressive loading [36]. The PEEK composites were better able to resist crack growth parallel to the fibers than the epoxy composites. Furthermore, the interlaminar Mode I fracture toughness parallel to fibers for PEEK matrix is over 10 times greater than epoxy matrix. Hence, for a 0° orientation, the carbon/PEEK tubes were able to absorb greater energy than the carbon/epoxy tubes.

Overall, epoxy matrix materials absorb greater energy compared to vinyl ester and polyester matrices. However, epoxy is five times more expensive than polyesters. Vinyl ester resins have better energy absorption, adhesion, and fatigue properties than polyester while costing less than half as much [37].

In general, combinations of carbon/glass fiber and epoxy are the most studied form of composite materials under axial compressive loading (quasi-static and dynamic) [10, 23, 27]. Ochelski et al. [23] showed 20% lower Specific Energy Absorption (SEA) for glass/epoxy compared with carbon/epoxy. Kevlar/epoxy showed a lower energy absorption compared than carbon and carbon/Kevlar epoxy for circular composite tubes [10] because of the ductility of Kevlar fibers compared with carbon fibers. This ductility leads to buckling or ductile progressive failure similar to metal tubes [5]. Silk/epoxy [38], PVC [39], and aramid/epoxy [27] square tubes also showed a ductile progressive crushing mode without debris formation which is specific to brittle materials.

- **Stacking sequence and fiber orientation**

Changes in stacking sequence of a composite laminate are able to affect the flexural stiffness, delamination occurrence, and the behavior of a material (transitioning from being brittle to ductile) [27]. Hull [40] showed a nonlinear trend between energy absorption and fiber orientation of the layers of glass/polyester tubes. Varying the fiber orientation from $[\pm 35°]$ to $[\pm 65°]$ changed the failure mode from the splaying to the fragmentation crushing mode. In another study [41], unidirectional carbon/PEEK composite tubes with $0° \leq \theta \leq \pm 25°$ were crushed and showed the progressive splaying mode. However, the $\theta = \pm 30°$ combination catastrophically failed by compressive shear fracture. Ramakrishna [41] showed increasing θ more than $\theta = 15°$ in the $[\pm\theta]$ stacking sequence reduced the mode II fracture toughness and specific energy absorption.

Woven fabrics (Fig. 1-5) were regularly used on hand lay-up manufacturing methods because of easy handling process. They are also able to interrupt crack propagation and improve impact strength because of their waviness [24]. The progressive modes in woven fabrics are different from UD fabrics based on warp to weft ratios (axial to hoop tube directions). Berry and Hull [42] investigated the fragmentation or splaying failure modes of woven fabrics which depended on the warp/weft ratio.

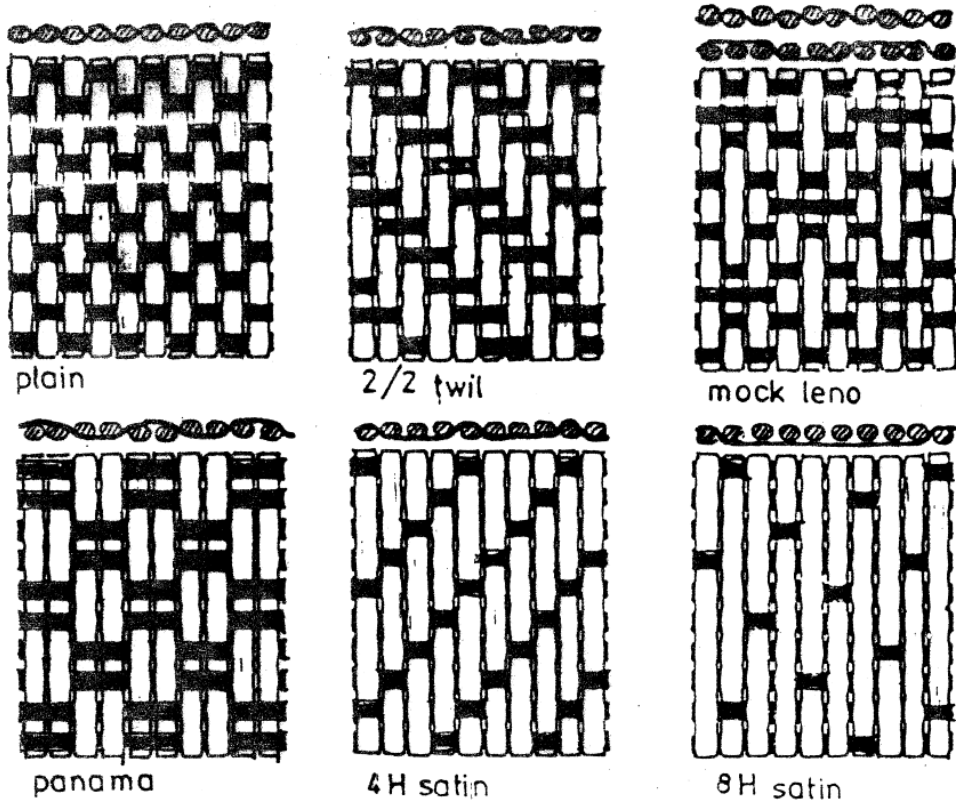

Fig. 1-5. some of weave pattern styles of woven fabrics [43]

- **Geometry**

It was also found that increasing the wall thickness of composite may increase energy absorption [12]. On the other hand, FRPs were found to be particularly effective for dynamic specific energy absorption for slender tubes [17]. The effect of the ratio of FRP thickness to outer tube diameter on the energy absorption and the deformation modes of carbon fiber/PEEK composite tubes was investigated in [34, 44, 45] and the non-linear variation of energy absorption with respect to the FRP-thickness/tube diameter ratio was demonstrated by Farley [46]. A reduction in the ratio can lead to an increase in energy absorption, at least for thermoset-based composite tubes. Palanivelu et al. [18] investigated progressive axial crush performance of different geometrical shapes (Fig. 1-6) of composite tubes manufactured by hand lay-up method from unidirectional E-glass fabrics and polyester resin under quasi-static loading. Square and hexagonal cross sections showed a change from

catastrophic failure to progressive failure as the ratio varied from 0.045 to 0.083. In addition, special geometrical shapes (e.g. the conical circular shape) provided more specific energy than the others. Mamalis et al. [47] studied the effect of tube wall slenderness on energy absorption which showed an increase with increasing the ratio of t/D. In addition, composite tubes having circular cross-sections were found to be more effective than the square and rectangular cross sections in energy absorption [36, 48].

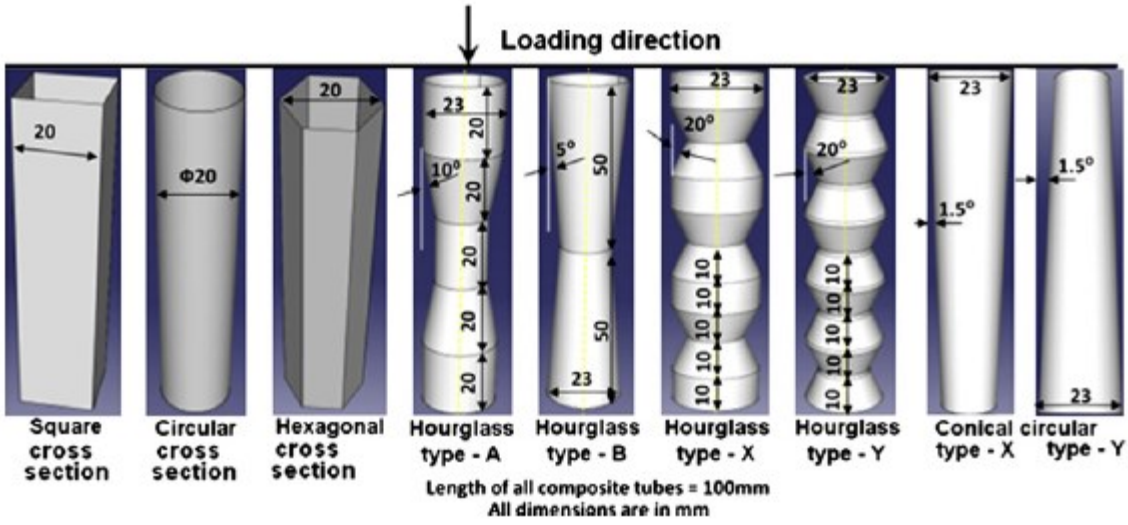

Fig. 1-6. The effect of different geometries for composite tubes on crashworthiness parameters [18]

Specific energy absorption capability depends on the absolute value of t, rather than the t/D ratio, and it increases with increasing t up to a certain value [49]. In addition, increasing the number of layers in FRP improves energy absorption because of its direct effect on [*D*] matrix [21]. However, this will increase the material and manufacturing costs. The effect of thickness on crashworthiness parameters and the collapse mode of conical CFRP tubes was investigated by Mamalis et al. [26]. Thin tubes were buckled as a result of Mode II failures and thick tubes failed by progressive Mode I or catastrophic Mode III [26]. In addition, increasing the semi-apical angle of frusta and half angle of cone vertex decreased the SEA [23, 50].

Geometrical reinforcement of circular tubes with radial GFRP webs [2] using radial-corrugated composite tubes [51] was able to increase the SEA and stabilize the loading profile.

- **Strain rate**

The rate-dependent response of matrix materials has been shown to affect the energy absorption differently for different materials. For example, increasing the strain rate increased the energy absorption for polyester matrices; for vinylester the change could be either positive or negative [52]. Vinylester resin absorbed significantly more energy than polyester resin in quasi-static tests but not in dynamic tests. A comparison between carbon woven fabric/epoxy composite tubes under quasi-static and dynamic loadings showed higher peak load, multiple local peaks, and more absorbed energy for dynamic loading [53].

Farley et al. [54] investigated the effect of crushing speed ranging from 0.01 to 12 m/s on circular composite tubes with $[0/\pm\theta]_2$ and $[\pm\theta]_2$ stacking sequences in which θ was chosen to be 15, 45, 75 degrees. The crushing modes and interlaminar crushing behavior were affected by changing crushing speed for Gr-E (Thornel 300-Fiberite 934) and K-E (Kevlar 49-Fiberite 934). When the fiber orientation changed from 45 to 75, the effect of crushing speed was increased, the mechanical response was matrix dominated, and as result effect of interlaminar crack growth on energy absorption was increased.

- **Triggering Mechanisms**

A triggering mechanism is employed to begin the crushing process. In the absence of an effective triggering mechanism, high maximum loads during accidents resulting in lumbar spine injuries of passengers was reported by Laananen et al. [55]. Therefore, in an ideal energy absorber, the ratio of mean crushing load to maximum load upon sudden crash should approach unity because of safety concerns. As a result, triggers are introduced to achieve progressive failure and acceptable deceleration, control the collapse modes, and avoid catastrophic failure, particularly in composite tubes [56]. The effect of triggers on energy absorption was the focus of several previous studies. Examples include the use of

edge chamfering (Fig. 1-7a) [41], steeple or tulip (Fig 1-7b) patterns [57] (resulting in circumferential and axial cracks, respectively) for square [57, 58] and circular [18] tubes, and external triggering mechanisms such as crush cups and plug initiators (outward and inward) (Fig. 8) [59, 60]. Triggers used for metal tubes include edge chamfering, hole discontinuities [61, 62], sinusoidal relief patterns [63] to control the wavelength of progressive buckle development , and triggering dents [64].

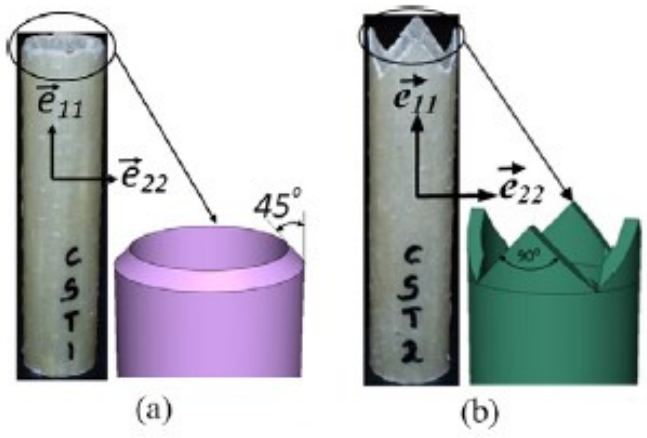

Fig. 1-7. Two different triggering mechanisms (a) chamfered (b) tulip [18]

Hou et al. [65] showed a strong nonlinear negative relation between radius of plug initiator and load uniformity factor. A combination of chamfered and inward plug crush cup was introduced [60] to obtain the highest SEA and lowest initial peak load.

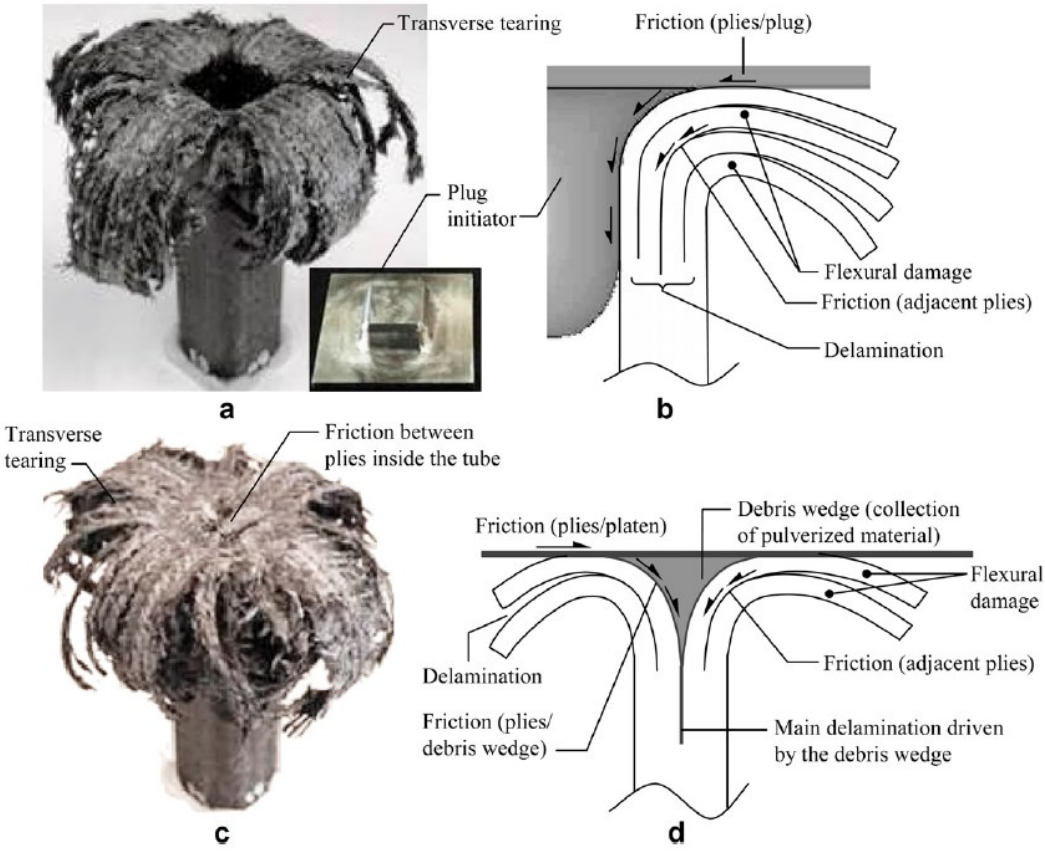

Fig. 1-8. Major failure mechanisms involved in axial crushing of braided composite tubes tested (a,b) with and (c,d) without an external plug initiator [22].

- **Processing parameters**

The effects of resin properties and resin processing factors like mold temperature, post-cure time, and resin composition on crush behavior of thermoset composite produced by resin transfer molding were also investigated [66]. The effect of higher concentrations of voids produced by VARTM (with the advantage of cost reduction) compared with autoclave cure (2.52% versus 0.17%) was studied on SEA [21]. It was reported the relatively high void formation did not affect SEA.

- **Effect of material properties on energy absorption**

In the process of crushing, different parameters have significant effects on different regions of the load-displacement profile. The initial crushing phase is dominated by the

flexural rigidity of the FRP which is related to constituent materials, stacking sequence, and number of layers [27]. The slope of the initial phase was higher for carbon/epoxy fiber reinforced composites (CRFP) compared with glass/acrylic resin and aramid epoxy composites (with the same thickness and stacking sequence) because of higher bending stiffness [23]. In addition, a higher fiber volume fraction cause greater stiffness and flexural rigidity [27]. Increasing the number of layers (higher thickness) created higher slope. After the initial maximum load, the load dropped significantly because of the first delamination formation but increased with lower slope as a result of lower flexural stiffness of delaminated FRP. During the crushing process, the loading oscillated around a mean crushing load as a result of flexural and frictional resistance. The effect of different stacking sequences such as $[\pm 45]_{ns}$, $[\pm 90]_{ns}$, and $[\pm 0]_{ns}$ were also studied on the crushing of CFRP rectangular sections. Tensile and compressive strain to failure for $[\pm 45]_{ns}$ was reported to be much higher than $[\pm 90]_{ns}$ and $[\pm 0]_{ns}$ laminates with lower modulus of elasticity. Hence, $[\pm 45]_{ns}$ composites showed a ductile behavior (considering the brittle nature of CFRP laminates) under crushing process and fracture of the fiber was not observed. (The same behavior for was seen for aramid FRPs because of the ductile nature of aramid fibers) [27].

Daniel et al. showed that SEA is associated with interlaminar shear strength [67]. The relation between Mode I and II fracture toughness and SEA was also proved by Ghaseminejad [32] and Hadavinia [68] for CFRPs and GFRPs. There are linear correlations between energy absorption parameters (maximum and mean crushing loadings and SEA) and compressive strength and shear modulus [10]. Farley et al. [34, 69] found an inverse relationship between energy absorption of carbon/epoxy composite tubes with carbon fiber stiffness. Warrior et al. [37, 70] observed SEA increases with increasing the Mode I fracture toughness of the matrix. The positive effect of stitching on G_{Ic} and SEA was also shown [70, 71].

1.2.2. Metal-composite hybrid structures

Combinations of different materials such as composite tubes with different fibers [69, 72], metal-composite hybrid tubes, foam-filled composite tubes, carbon nanotube or zinc oxide/carbon fiber epoxy composites hybrid tubes, etc. having the same geometry are able to produce different failure modes and energy absorption mechanisms. Over the past decade,

there has been considerable interest in reinforcing steel structures used in aeronautical and civil structures with FRPs. FRPs are often used in the form of hybrid metal-composite tubes in vehicle structures.

When used as energy absorbing elements in vehicle construction, steel-composite hybrid tubes have the benefits of the stable, ductile collapse of the steel (which can absorb crush energy in a controlled manner and solves the unstable interlaminar and interlayer crack propagation of composite tubes) and the high strength-to-weight ratio of the composites. As a result, they have the potential to enable better fuel consumption and reduced emission in vehicles [13]. They are also used as web girders in ships [56], sacrificial cladding for protecting civil structures against blast attacks [18] and for retrofitting [19] or rehabilitation [20] of metallic structures to increase their strength and their ability to face industrial or marine environmental conditions that can deteriorate the base material.

There are competing effects in regard to the composite and metal thickness and their effects on energy absorption in metal-composite hybrid tubes. When more layers are used, delamination is more likely to occur [17], reducing energy absorption. Bambach [73] concluded that strength-weight and energy-weight ratios decreased with the slenderness of the metal. Additionally, adding a very thick composite section may result in a global buckling mode of failure (rather than local folding) but there are no studies we are aware of specifically addressing the effect of composite thickness on energy absorption of hybrid tubes. Hence, there is a need to investigate the effects of fiber orientation and FRP thickness (the number of layers) on the energy absorption of hybrid steel-FRP tubes.

Testing of metal-composite hybrid tubes under quasi-static and dynamic loadings showed that the collapse modes were progressive and identical for steel SHS and steel-CFRP SHS with only one composite layer. However, steel-CFRP SHS with two composite layers exhibited delamination failures only under dynamic loading; however, these delaminations did not significantly affect the mean crushing load [17]. To relate the quasi-static loading to dynamic crushing load in the modeling process, the strain rate effect was added to yield stress of steel section using Cowper-Symonds expression.

The adhesion between the metal and the composite is also of importance in terms of the mode of failure exhibited [74]. The adhesive, in addition to being strong and stiff, should be compatible with steel and composite and durable in harsh environmental conditions. Heat and humidity are able to affect the adhesion behavior. In fact, the most important factor in the long term behavior of unprotected adhesively bonded metal joints is the presence of high humidity and liquid water [74]. Surface preparation (such as removal of surface contamination or chemically surface activation and modification) is able to produce an interface resistant to hydration. Abrasion or grit blasting are among the methods which have regularly been used to prepare metal surface. Adhesives such as methacrylate show the best combination of strength, stiffness, vibration damping, and sealing behavior compared with epoxy polyurethane and epoxies [11]. Boucht et al. [75] used different surface treatment methods before bonding the composite to aluminum tubes including degreasing (which removes the contaminants inhibiting chemical bond formation [74]), chromic-sulfuric etching, anodizing, and sulfuric etching. However, they were not able to find a clear relation between better adhesion and specific energy absorption.

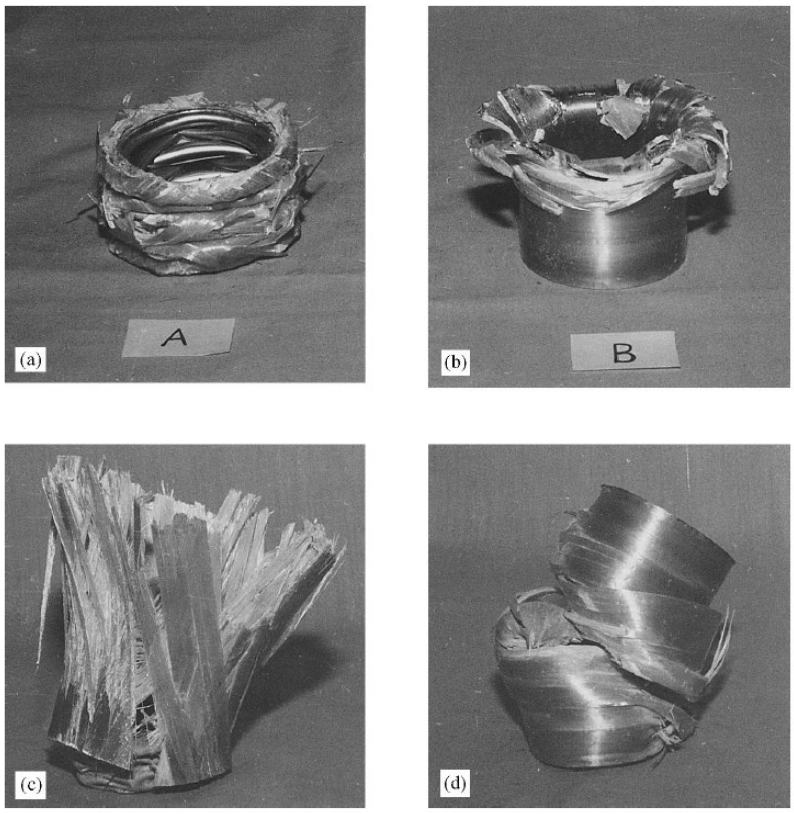

Fig. 1-9. Failure modes observed for cylindrical metal-composite hybrid tubes in the experiments are (a) compound diamond, (b) compound fragmentation, (c) delamination, and (d) catastrophic failure [12]

The effect of stacking sequence and fiber orientation on energy absorption of metal-composite hybrid tubes were studied by Kim et al [76] in which $[0/90]_n$ (n=1, 2, …) showed better crashworthiness parameters in comparison to a $[90]_{2n}$ stacking sequence. The $[90]_{2n}$ sequence hindered the plastic deformation of metal tubes as a result of carbon fiber stiffness in the in hoop direction. However, the reinforcement was not sufficient, leading to failure at the corners when the first crushing lobe was formed, resulting in low energy absorption. In the case of $[0/90]_n$ specimens, high stiffness and bending resistance of the FRP in the axial direction and the reinforcement of the axial fibers by the transverse fibers decreased the debonding and delamination failure modes (which happened for $[0]_{2n}$ stacking sequence). Using a $[45/-45]_n$ stacking sequence led to ductile behavior and scissoring effects in which2

peak loads were observed. This changed the crushing mode and increased the initial peak load compared with two other stacking sequences.

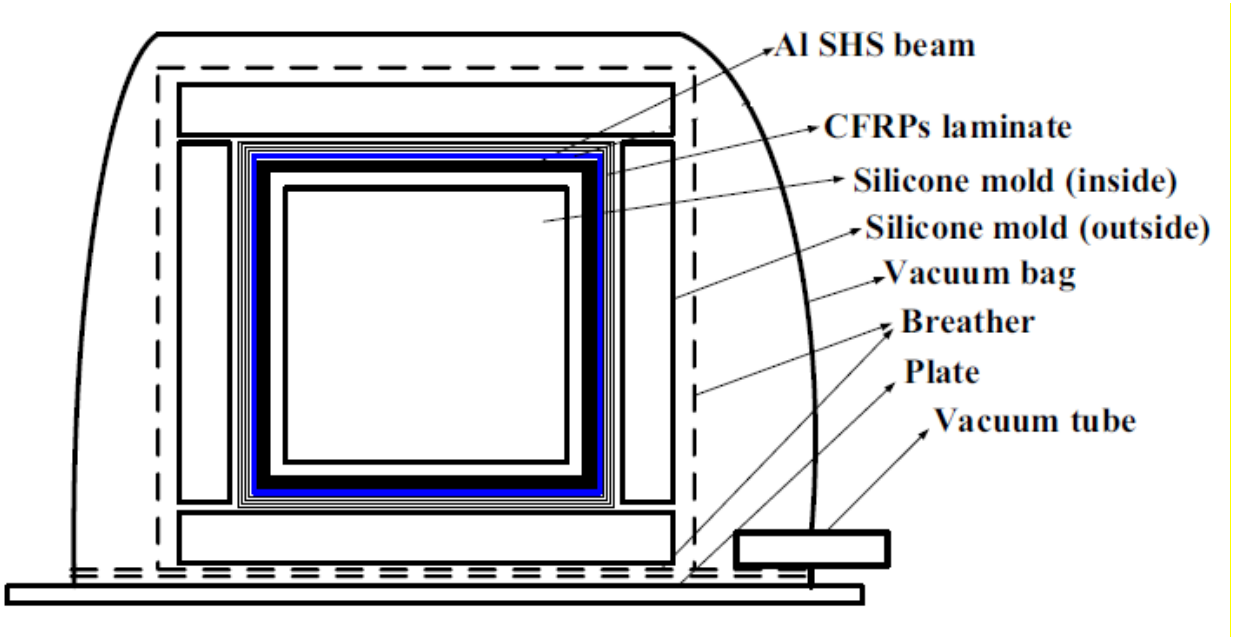

Fig. 1-10. Vacuum bag for making the Al/CFRP hybrid SHS beam [76]

1.3. Numerical studies

There are obviously a large number of design variables which have the potential to affect energy absorption. Because a full experimental study of these design variables is impractical, numerical studies must play a major role in identifying the best combination of design variables. However, in contrast to composite-only tubes, there are only a limited number of previous studies in numerical modeling of metal-composite hybrid tubes.

In general, to model failure, after the failure surface is reached, the elastic properties are degraded based on one of two different degradation methods: progressive and continuum damage mechanics (CDM). Progressive failure models use a ply discount method (ply-by-ply failure) which depends on the loading conditions. CDM models utilize a continuing deterioration of the elastic properties. These CDM models employ a number of damage variables (estimated through sensitivity studies) which change continuously from 0 (no damage) to 1 (complete failure) but often cannot be experimentally obtained. Because of the

anisotropic and heterogeneous nature of composite materials, the relationship between the microstructure and macroscopic strain-stress responses is very complicated. Therefore, CDM models are presently the only ones that have the ability to find the relationship between microstructure details such as voids and microcracks and mechanical properties using internal state variables [77]. Composite tubular structures such as braided (plug-initiated and un-initiated) [22, 78] and woven fabric [24, 79] have been modeled with continuum damage mechanics (CDM) based models, introduced by Matzenmiller, Lubliner, and Taylor (MLT), using LS-DYNA. The MLT approach was used [80] and modified to consider a linear elastic loading and unloading which has helped to model energy absorption in composite tubes. Another continuum damage mechanics based model (user defined) named CODAM (COMposite DAMage) was developed for composite materials in university of British Colombia [22, 78, 81] with promising results in damage evolution/propagation and simulations of splaying failure mode (plugged and unplugged initiated [78]). The model considers a pre-defined debris wedge and simulate the delamination between all plies by tie-breaks elements. Compared to damage mechanics based models, the MAT54 ‘‘Enhanced Composite Damage’’ element in LS-DYNA needs fewer experimental input parameters [82] but it is sensitive to some non-physical parameters determined by try-and-error method and final experimental failure modes.

Palanivelu et al. [83, 84] studied the effect of delamination, axial cracks, and initial geometric imperfections using shell elements and Chang-Chang failure criterion for glass polyester circular and square tubes. (Shell elements were chosen because capturing the damage mechanism with solid elements is difficult and time-consuming [85]) They used two approaches: a single layer and two layered shell elements. Because of the absence of delamination in their model, the predicted crashworthiness parameters differed from the experimental results.

The composite damage model MAT58 in LS-DYNA was also used to simulate axial crushing of braided composite tubes by multiple shell elements through the thickness to count for multi-layer laminate. The layers interacted by an interface strength based tiebreak elements to simulate the delamination failure modes. The interface strength was not directly

measured by experiments and but was tuned by linking it to interlaminar fracture toughness (Mode I and II) which was measured experimentally using a double cantilever beam (DCB) test [70]. In addition, in the study, the unloading compressive path was corrected [81]. It was found that interlaminar fracture toughness can have a significant role on SEA because it affects the main central inter-wall crack propagation and subsequent frond bending. Jacob et al. [86] examined the effect of fiber orientation and stacking sequence on the interlaminar fracture toughness of composite crash boxes using Belytschko-Lin–Tsay quadrilateral shell elements. Another method to model the delamination failure mode is to use cohesive zone elements which can be implemented as user defined models (UMAT) in LS-DYNA [87]. However, beside the potential need to consider delamination in order to capture the correct failure mode in simulation of composite tubes, the energy absorption directly related to delamination was reported to be around 1-3% of the total SEA. The value small compared to material damage growth (65% for plug initiated and 80% un-initiated tubes) and frictional dissipation energy because of debris wedge, between the tube and the plug, and between the plies.

El-Hage et al. [88] investigated aluminum-composite square hybrid tubes under quasi-static loading using LS-DYNA software. They used a filament-wound E-glass fiber-reinforced composite. Because of filament winding limitations, they limited their study to fiber orientations between $\pm 30°$ and $90°$ with respect to tube axis. To model the FRP and aluminum sections, Belytschko-Tsay quadrilateral shell elements were used. The aluminum section was modeled using piecewise linear isotropic plasticity (MAT24) (von Mises flow rule). To model FRP section, a composite damage model (MAT54) was used. MAT54 uses Chang-Chang failure criterion—a modified Hashin equation considering the non-linear shear stress-strain behavior. In the model, composite behaves linearly until failure and continues to non-linearity when damage happens based on ply-discount theory. Laminated shell theory was also activated to correct the assumption of uniform constant shear strain through the thickness. As a result of using single shell element, the out of plane fracture modes were not modeled. The comparison of their model with experiments was also limited: the results were compared with experiments for two composite architectures with symmetric crushing

modes only. The transverse fiber orientation was identified as the best stacking sequence for the FRP section with a non-linear behavior reported between the mean crushing load and fiber orientation. They also presented an empirical equation based on different parameters such as thickness and stacking sequence to predict the mean crushing load. Kalhor et al. [14] used the same numerical modeling approach together with experimental results from [88] to optimize stacking sequences of composite layers under dynamic loading.

In order to reduce the computational cost of the numerical modeling, several groups constructed different functions (e.g. structural weight [89], load vs. displacement [90], energy absorption, mean and peak crushing load [91-94]) which were subsequently employed to optimize only the shape and geometry of the energy absorbers within the design limitations. Weighted surrogate-based approaches [95, 96], meta-modeling techniques [97], Kriging models [92], Artificial Neural Networks (ANN) [90, 91], and Response Surface (RS) [98-100] methods are among the important methods used in previous studies for optimization problems.

Chapter 2

2. Metal-FRP square tubes under axial compressive loading

In hybrid (metal-FRP) tubes, the relative and absolute thicknesses of each material has a substantial effect on energy absorption. In particular, delamination can reduce the energy absorption capability of the tube. Additionally, adding a very thick composite (FRP) section may result in a global buckling mode of failure (rather than local folding) but there are no studies we are aware of specifically addressing the effect of FRP thickness on energy absorption of hybrid tubes. In this study, we investigate the effects of fiber orientation, stacking sequence, and FRP thickness (the number of layers) on the energy absorption of hybrid steel-FRP tubes. In addition, we demonstrate a geometrical trigger which has positive effects on the collapse modes, delamination in the FRP, and the crush load efficiency of the hybrid tube.

2.1. Sample construction and test procedure

Square cross-section multipurpose 304 stainless steel tubes with 1.65 and 2.11 mm thicknesses, nominal length of 200 mm, and nominal width of 25.4 mm were wrapped with 36 wt% S2-glass/HexPly® 8552 (S2GL/8552) prepreg sheets from Hexcel Corporation (Salt Lake City, UT) to make the hybrid samples. HexPly® 8552 is an amine cured mid-toughened

and high-strength epoxy resin. Its glass transition is approximately 200°C and it is curable by vacuum bag and by autoclave. The curing cycle for the prepreg (Fig. 2-1) includes applying full vacuum pressure (1 bar), heating at 3°C/*minute* up to 110°C, holding for 60 minutes, heating again up to 180°C, holding for 2 hours and finally cooling at 3°C/*minute*.

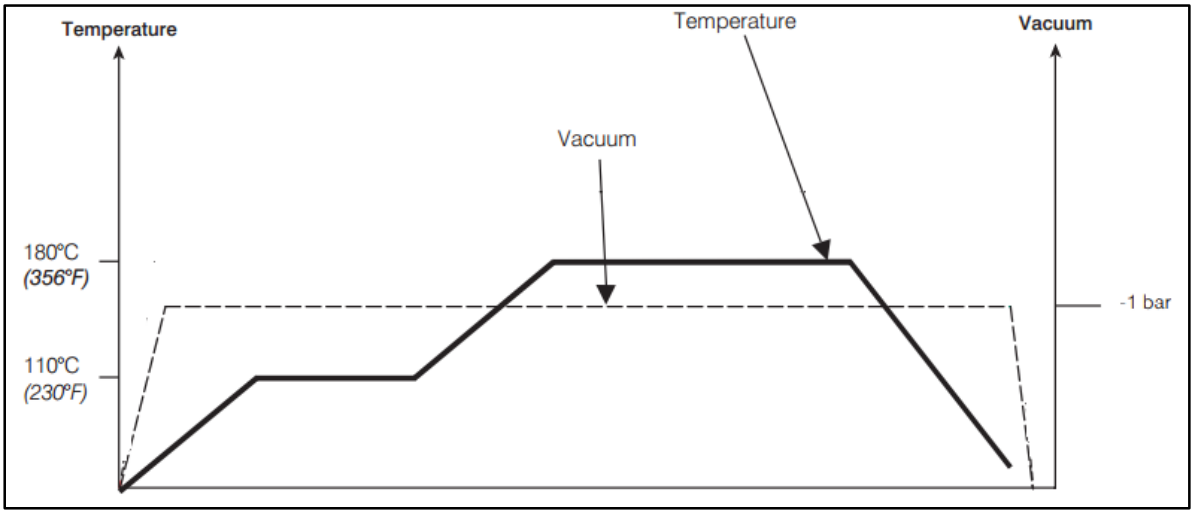

Fig. 2-1. Curing cycle for S2GL/8552 prepreg

To construct the hybrid tubes for the study, the surface of the steel tubes was roughened using 80 grit sandpaper and then degreased with acetone. In addition, one side of each steel tube was chamfered at an angle of ~45° to produce a trigger that lowers the maximum load during the initial crushing process. Four stainless steel samples (identified as ThinMCNTrig) were also cut at the start of third lobe formation after two successive symmetric (2 opposite lobes out and two opposite lobes in) folding formation to present a different triggering mechanism. Prepreg sheets consisting of 8, 16, 24, or 32 layers were cut for different samples and then overwrapped around the steel tube using the hand lay-up method with an overlap of half of a tube side width to reduce the likelihood of early fracture [17]. Each sample was then cured according to the schedule shown in Fig. 2-1.

Table 2-1 shows different designed configurations to address the effects of thickness and stacking sequence of the FRP section. Each sample is titled based on thickness of the metal section (ThinM and ThickM), number of layers of the FRP section, and stacking sequence family of the layers. In each configuration, 90° layer was used to avoid the splitting mode for

the metal section, to help the energy absorption by axial crack of the layer around corners, and to have better bonding to stainless steel [13, 76]. In addition, $\mp 15°$, $\mp 30°$, and $\mp 45°$ layer coordination are used to vary the axial to transverse stiffness ratios (varying the resistance to the applied load and the confinement of the plastic deformation). A 0° layer was also combined with the other layers in the direction of loading to make the tube stiffer in lobe formation. ThinMC845, ThinMC2445, ThinMC3245 were designed with the same stacking sequence as ThinMC1645 to study effect of the FRP section thickness on energy absorption. ThinMCNTrig has the same stacking sequence and number of layers of ThinMC1645 samples but with the mentioned triggering mechanism.

The hybrid samples were crushed between two hardened steel plates at displacement rates of 6 mm/min using an MTS 810 testing frame with 250 kN load cell (Fig. 2-2). To obtain the average crushing performance parameters, 4 samples for each configuration were tested. In each test, load-displacement data was collected at rate of 100 Hz.

Table 2-1. Dimensions and stacking sequences of hybrid tubes

Sample Name	Metal thickness (mm)	Composite Thickness (mm)	Number of composite layers	Stacking Sequence
ThinM	1.65	-	0	-
ThickM	2.11	-	0	-
ThinMC1690	1.65	1.6	16	$[90/0/0/90]_{2s}$
ThinMCNTrig	1.65	1.6	16	$[90/\mp 45/0]_{2s}$
ThickMC1690	2.11	1.6	16	$[90/0/0/90]_{2s}$
ThinMC3245	1.65	3.6	32	$[90/\mp 45/0]_{4s}$
ThinMC2445	1.65	2.4	24	$[90/\mp 45/0]_{3s}$
ThinMC1645	1.65	1.6	16	$[90/\mp 45/0]_{2s}$
ThinMC845	1.65	0.8	8	$[90/\mp 45/0]_{s}$
ThinMC830	1.65	0.8	8	$[90/\mp 30/0]_{s}$
ThinMC815	1.65	0.8	8	$[90/\mp 15/0]_{s}$

Fig. 2-2. Hybrid samples crushed up to 150 mm under quasi-static loading by hydraulic MTS 810 testing frame with 250 kN load cell

2.2. Results and Discussion

The crushing modes observed in the bare metal tubes (ThinM and ThickM) are shown in Fig. 2-2. These consist of (1) splitting mode (2) symmetric mode (2 collapse lobes in and 2 out), and (3) mixed mode (a combination of 4 collapse lobes out with the symmetric mode). The maximum load for tubes which fail via the splitting mode is followed by very low energy absorption since the only mechanism to absorb energy is progressive axial crack on the corners.

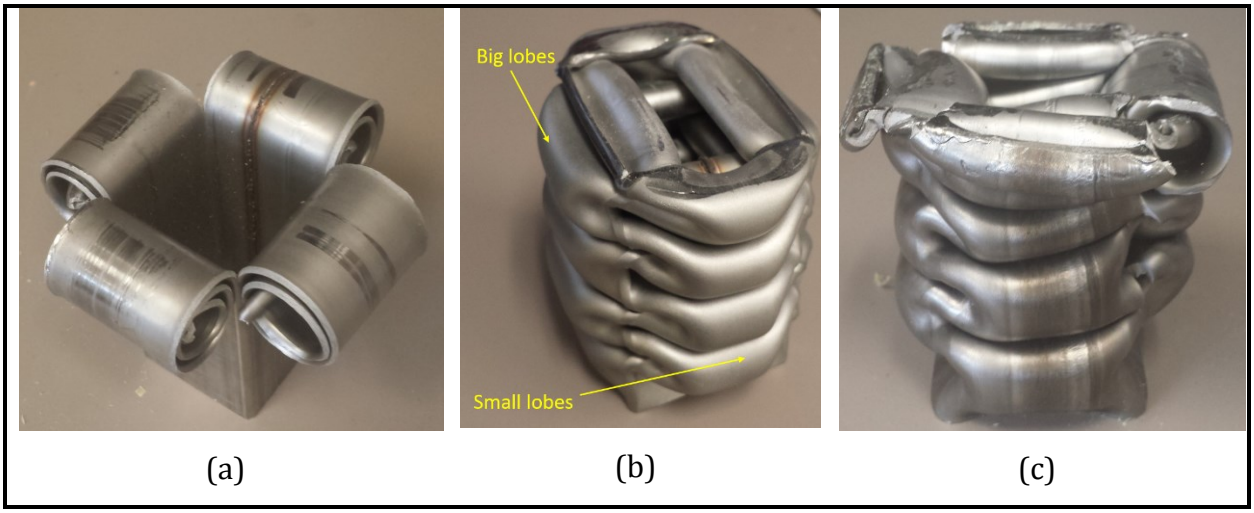

Fig. 2-3. 3 different modes for metal tubes (a) splitting mode (2) axisymmetric mode (3) mixed mode

The crushing modes for thin metal tubes (ThinM) is mostly symmetric in which the load fluctuates based on the lobe formation after the first peak load. Since the four sides are straight at first, the load needed to buckle them is the highest. Subsequently, after each complete lobe formation, the two adjacent sides are bent, making the load lower. The smaller peaks in thin metal load-displacement data (Fig. 2-3) are related to the smaller lobes. Cases in which the lobes are of approximately equal size correspond to approximately the same size peak in the load-displacement plot. For thick tubes (ThickM), the mode transitions from four lobes outward at first is followed by the symmetric mode. The second sharp peak load is related to the four out lobe formation.

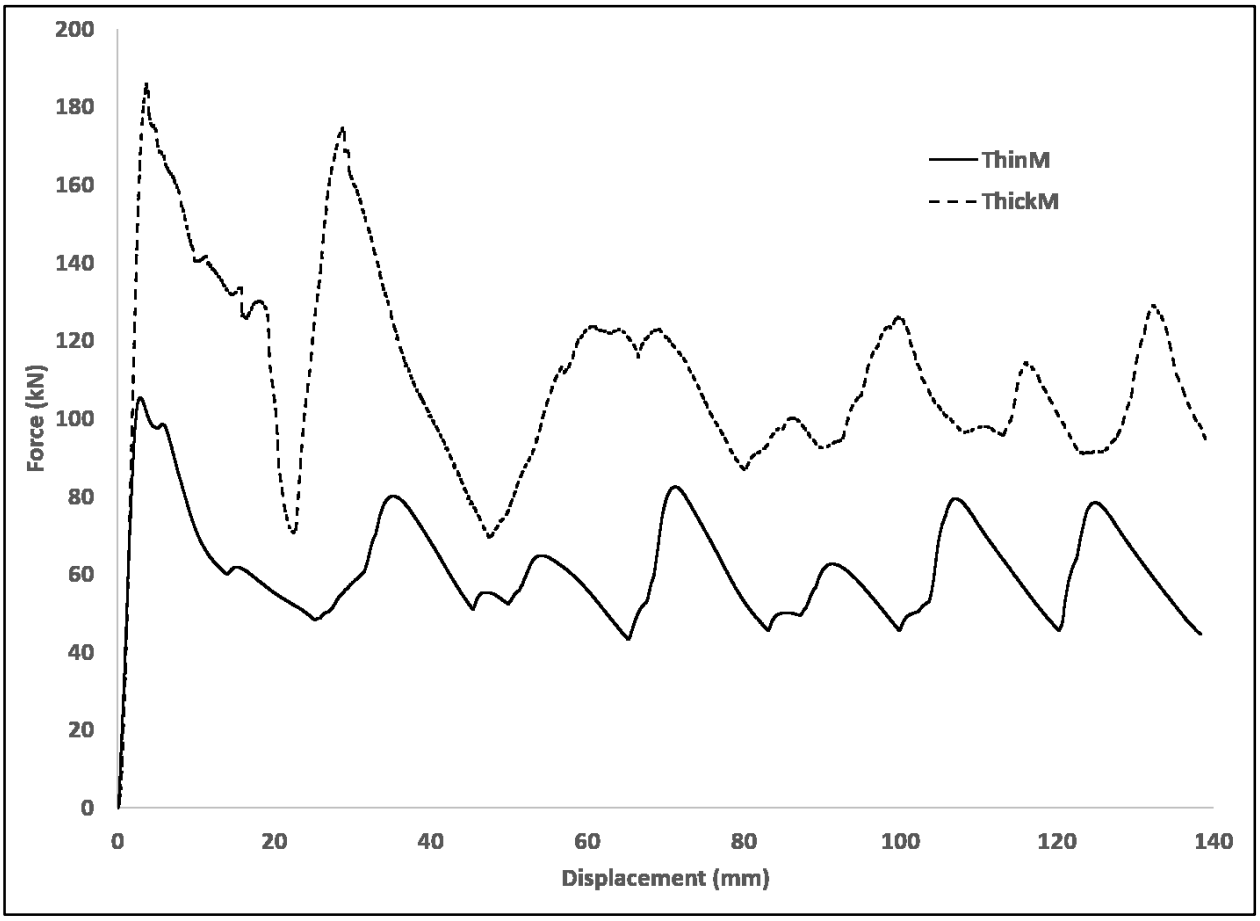

Fig. 2-4. Load-displacement changes for thin and thick metal tubes based on collapsing modes

In general, the role of using FRP layers around metal tubes is inhibiting the metal tubes from global buckling [13]. However, based on experiments, the FRP layers provide other advantages as well: (1) preventing the splitting mode in metal tube that happened in approximately one fourth of bare thin metal (ThinM) specimens leading to very low energy absorption and (2) lowering the magnitude of the load oscillation around the maximum value. The overall energy absorption is a combination of metal plastic deformation as well as fracture of fiber and matrix associated with axial splitting around the corners, interlaminar crack propagation, inter-ply delamination, and friction between the layers for FRP section.

Maximum load, mean crushing load at 125 mm, and the ratio between the specific absorbed energy (SAE) of hybrid and metal tubes for each configuration are summarized in Table 2-2 with standard deviation values in parentheses. Generally, Table 2-2 shows how adding a FRP section can increase the energy absorption of metal tube significantly but the

results also indicate that by changing the stacking sequence of the FRP section with respect to tube axis the mean crushing load and maximum load changes (based on ThinMC845, ThinMC830, ThinMC1690, and ThinMC1645 samples) and the mean crushing load and maximum load increase with increasing number of layers (based on ThinMC845, ThinMC1645, ThinMC2445). In addition, for the ThinMC8 family, it appears pretty clear that SAE decreases with the decrease in fiber angle. A significant observation is the decrease in energy absorption for samples consisting of thin tubes reinforced with eight FRP (composite) layers (ThinMC815, ThinMC830, and ThinMC845) that exhibit the symmetric crushing mode in comparison to bare thin metal samples that exhibit the same crushing mode (ThinM) (Fig. 2-5). Besides the fact that adding the FRP section improved the energy absorption (with a linear fashion), the effect of using the FRP section on thinner tubes is more significant than on thicker tubes. The effect is because the thinner tubes have greater buckling deformations [17] resulting in an increase in crush load efficiency for ThinMC1690 in comparison with the same parameter for thin metal (ThinM sample); contrary to thick metal values (ThickMC1690). In addition, the new triggering mechanism that leads the initial collapsing mode to be symmetric increased the load efficiency factor 12.85% with a small change in the $\frac{\mathrm{SAE_{hybrid}}}{\mathrm{SAE_{metal}}}$ ratio of 2.8% (because of the decreasing the initial peak). These results show the potential to optimize tube design parameters to obtain better energy absorption. This potential may be realized by developing numerical modeling limited to change of stacking sequence of the FRP section to predict the behavior, validating then through the experiments presented in this work (Indeed, this is the goal of an ongoing study.)

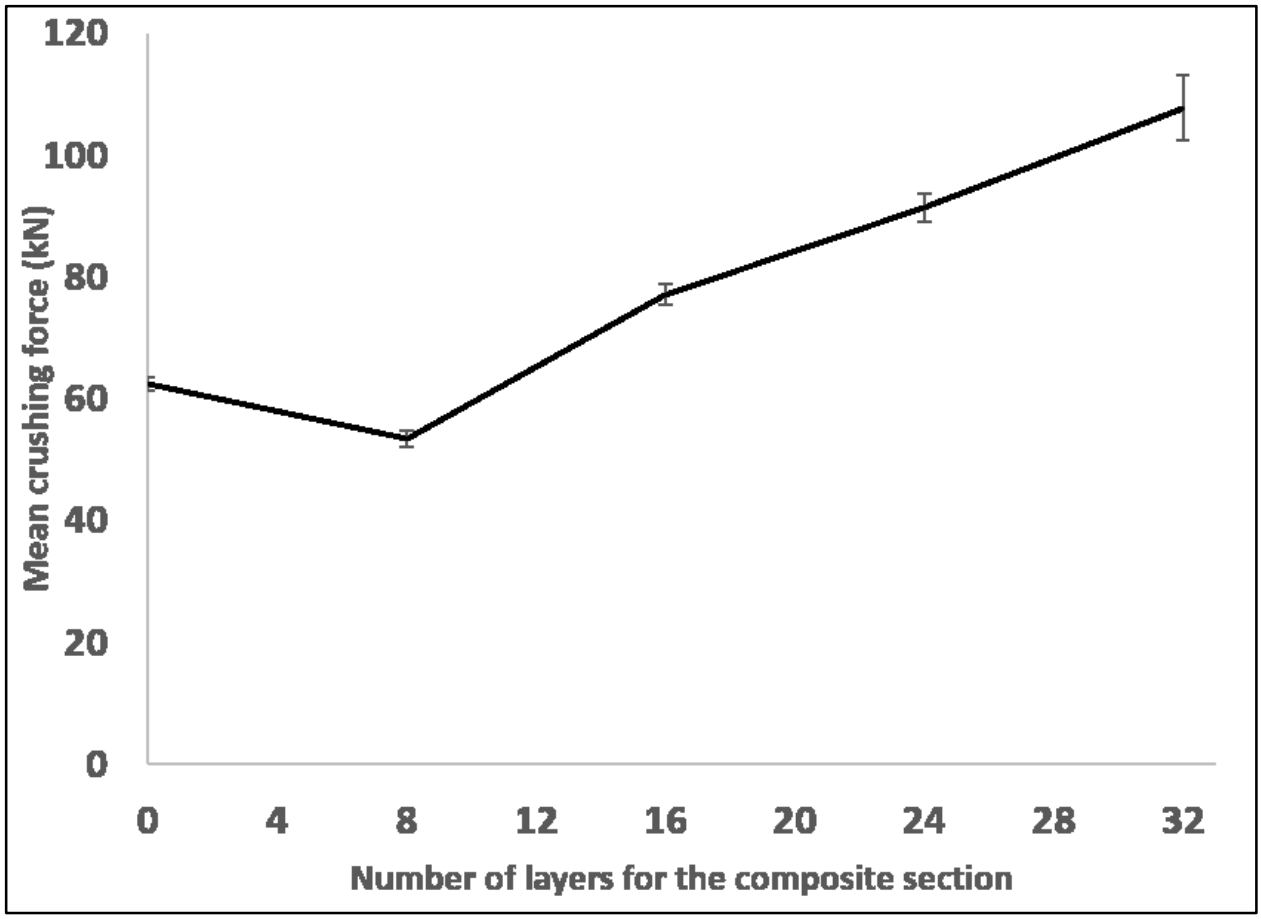

Fig. 2-5. Nonlinear changes of mean crushing load based on number of layers for FRP section of hybrid tubes

Table 2-2. Crush performance parameters of the metal and hybrid tubes

Sample Name	$P_{max} - kN$ (SD)	$P_{mean}@125mm$ kN (SD)	$\frac{P_{mean}}{P_{max}} * 100$	$\frac{P_{mean}}{mass}$ $(\frac{kN}{kg})$	$\frac{\text{SEA}_{hybrid}}{\text{SEA}_{metal}}$ [1]	Crushing mode
ThinM[2]	106.4 (2.8)	53.4 (15.7)	50.2	128.4	1	Symmetric and Splitting
ThinM	107 (3.9)	62.4 (1.1)	58.4	170	1.32	Symmetric
ThickM[3]	161 (1.8)	81.4 (24.6)	50.6	172.4	1	Mixed and Splitting
ThickM	161 (1.6)	98.7 (1.6)	61.3	209	1.2	Mixed
ThinMC1690	136 (3.3)	82.7 (1.1)	60.8	182	1 .42	Symmetric and Mixed
ThinMCNTrig	114 (10.8)	75 (2.6)	65.6	165	1.3	Symmetric
ThickMC1690	190 (8.3)	114 (5.1)	60.2	210	1.22	Symmetric and Mixed
ThinMC3245	190 (6.4)	107.8 (5.3)	56.8	185.9	1.45	Symmetric
ThinMC2445	156 (6.0)	91.4 (2.1)	58.6	178	1.4	Mixed
ThinMC1645	133 (5)	77.1 (1.8)	58.1	169	1.32	Symmetric and Mixed
ThinMC845	108 (5.3)	53.4 (1.3)	50.8	140	1.09	Symmetric
ThinMC830	105 (2.9)	52.7 (1.3)	51.8	138	1.07	Symmetric
ThinMC815[4]	107	52.35	49	134	1.04	Symmetric

Our experimental results indicate that early delamination decreases the energy absorption capability of the composite. One of the factors controlling the likelihood of delamination failure is fiber orientation. For example, Fig. 2-6 highlights the delamination that occurred between the 30° layers in two of four ThinMC830 samples. A general observation was that the amount of delamination became more visible when fiber orientation was closer to 0°.

[1] The specific energy absorption of each configuration is divided by the specific energy absorption of general metal tube condition (including symmetric and splitting crushing modes)
[2] The results include the splitting mode of the metal tube.
[3] The results include the splitting mode of the metal tube
[4] The result of a single test is shown.

Fig. 2-6. One of samples with $[90/\mp 30/0]_s$ *stacking sequence which has delamination in one side*

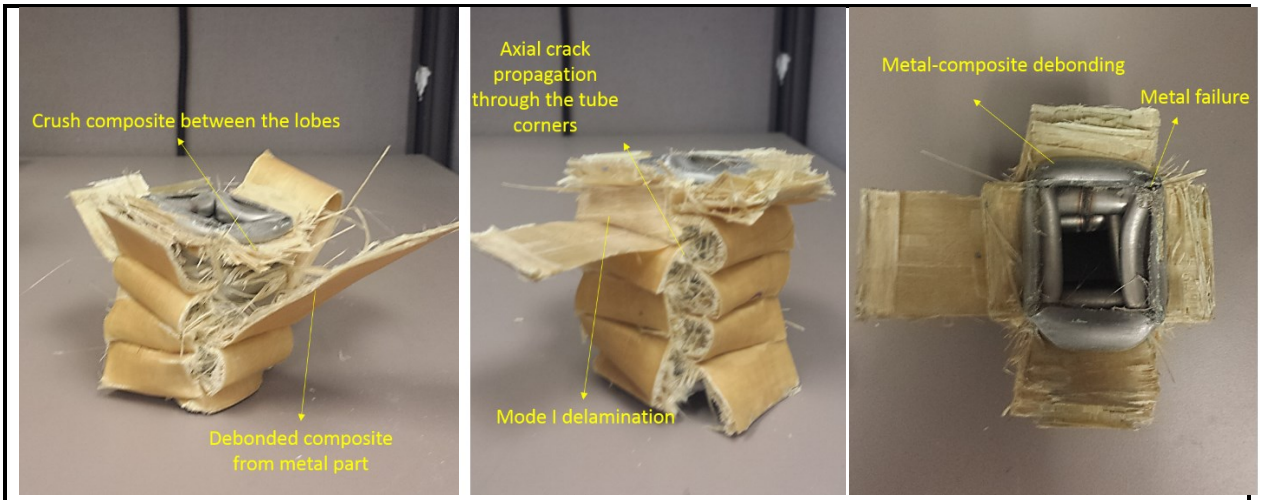

(a) (b) (c)

Fig. 2-7. ThinMC1690 sample 1 shows crushed composite between the metal lobes and debonded composite form metal part (b and c) ThinMC1690 sample 2 shows axial crack propagation thorough tube corner and some metal failure

The most important observation in axial crush performance of hybrid tubes is the development of two different crushing modes: (1) the symmetric mode through the tube (Fig. 2-7 (a) and Fig. 2-9) (2) mixed mode formation in metal tube along with crushed composite between the lobes of metal tube (Fig. 2-8 and Fig. 2-9). The symmetric mode results in just one peak load followed by small load oscillations around mean crushing load as the crushing progresses. The mixed mode results in two large initial picks associated with two continuous formation of outside lobes followed by the symmetric mode.

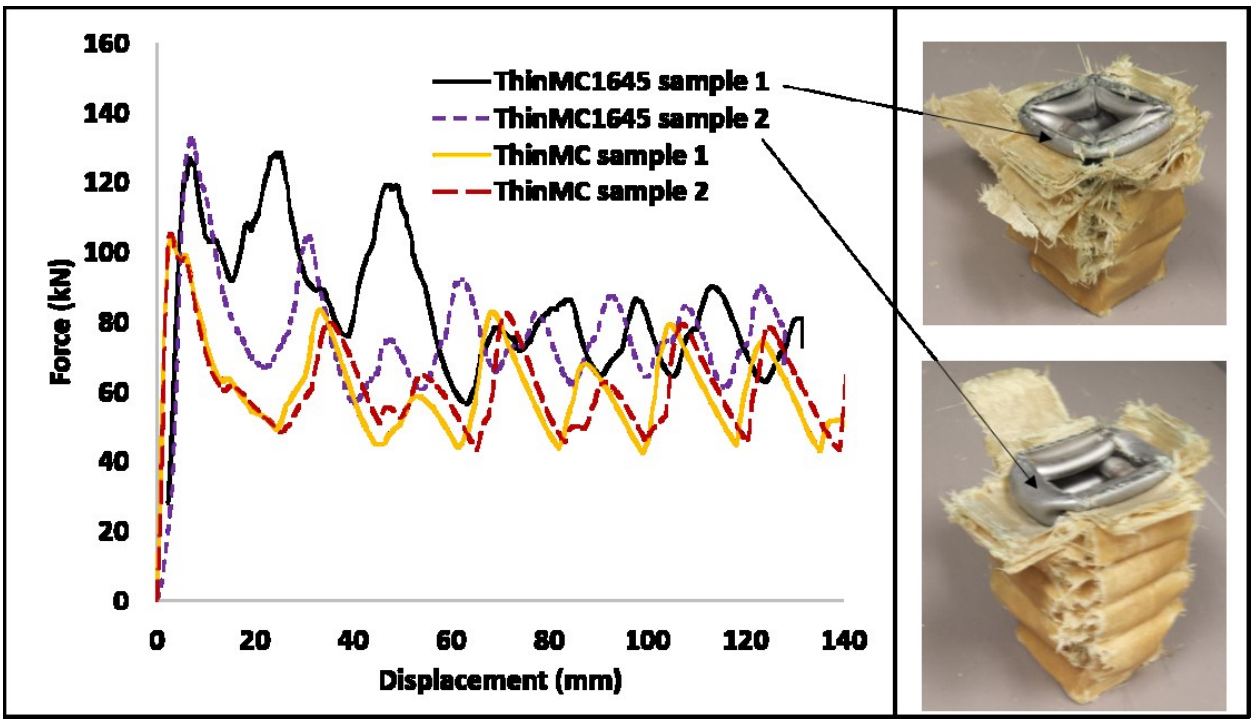

Fig. 2-8. Laod-displacement behavior for 2 different ThinMC1645 hybrid and thin metal samples

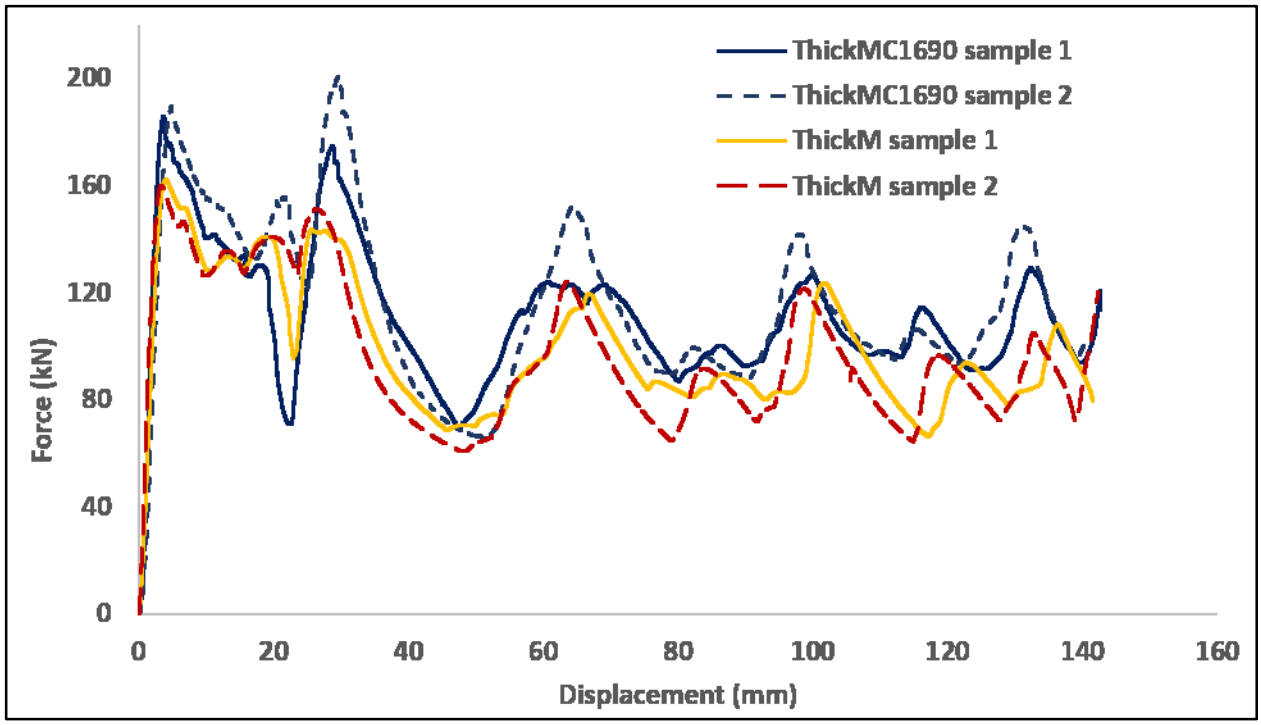

Fig. 2-9. Load-displacement behavior of 2 different ThickMC1690 hybrid and thin metal samples

A number of previous studies discussed the ability of the FRP to increase the energy absorption of hybrid tubes [12, 16, 62, 101, 102]. However, this work demonstrates that this capability is a function of a number of factors including the number of FRP layers. In fact, for the hybrid tubes with 8 layers (Fig. 2-10), the lobes occur at smaller crushing displacement and the middle small peaks are lower than those for the bare metal tubes (ThinM samples) because the composite brittleness allows the lobes to form faster and does not allow as much plastic deformation of the metal. Furthermore, it does not allow the lobes to be equal at the end (in contrast to the metal tube).

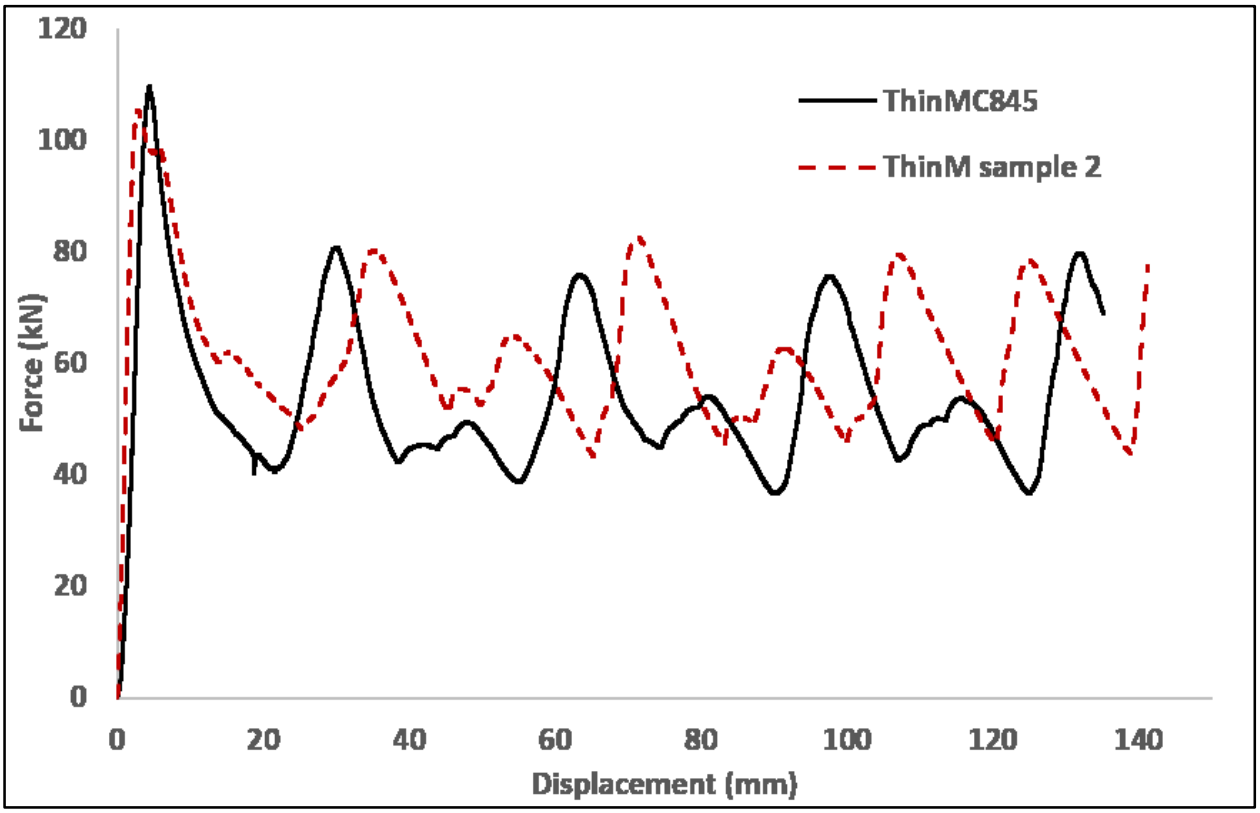

Fig. 2-10. Load-displacement behavior of ThinM and ThinMC845 samples

Because a crush load efficiency close to unity is very important to safety of passengers in an accident and avoiding the mixed collapse mode in the metal that is correlated to large peak loads following the initial peak load is desirable, a new triggering mechanism is presented here that is based on an initial plastic deformation (Fig. 2-11) in metal tube. Hybrid tubes constructed using these initially plastically deformed tubes exhibit increases in crush load efficiency up to 12.85% comparing to original tubes (ThinMC162 that have 45° angle trigger) with small sacrifice in SAE. Fig. 2-12 shows the load displacement results for both triggers and how the new trigger can control the collapse mode and initial load. In fact, the new trigger (1) decreased the peak load and increased the crush load efficiency by an initial weakening and (2) changed the collapse mode to symmetric with advantages of smaller oscillation of load around mean crushing force comparing the mixed mode.

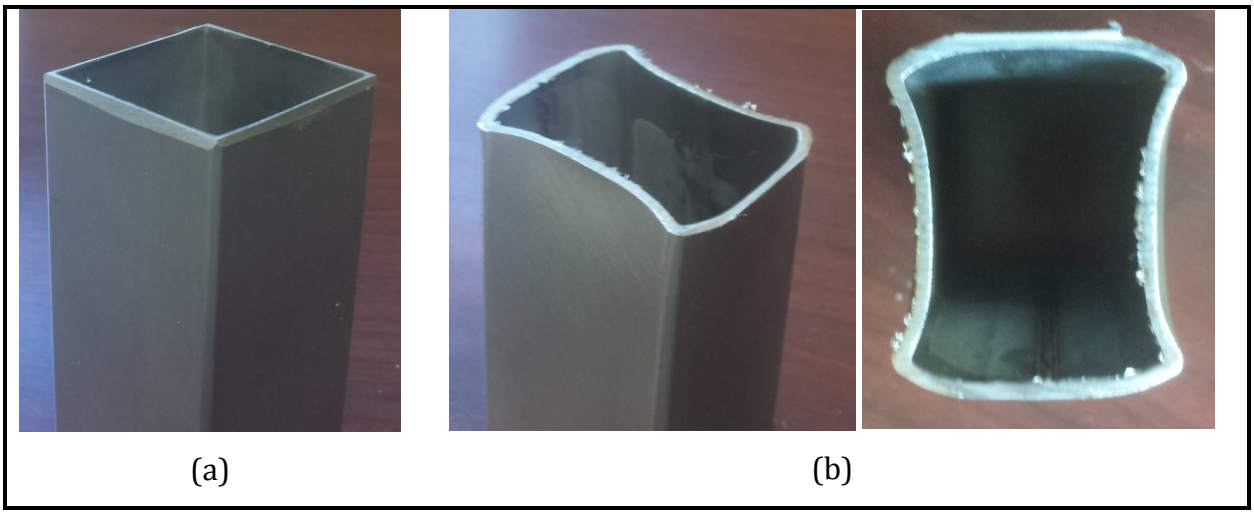

Fig. 2-11. Triggering mechanisms (a) initial 45° tappered (b) initial applied deformed tube

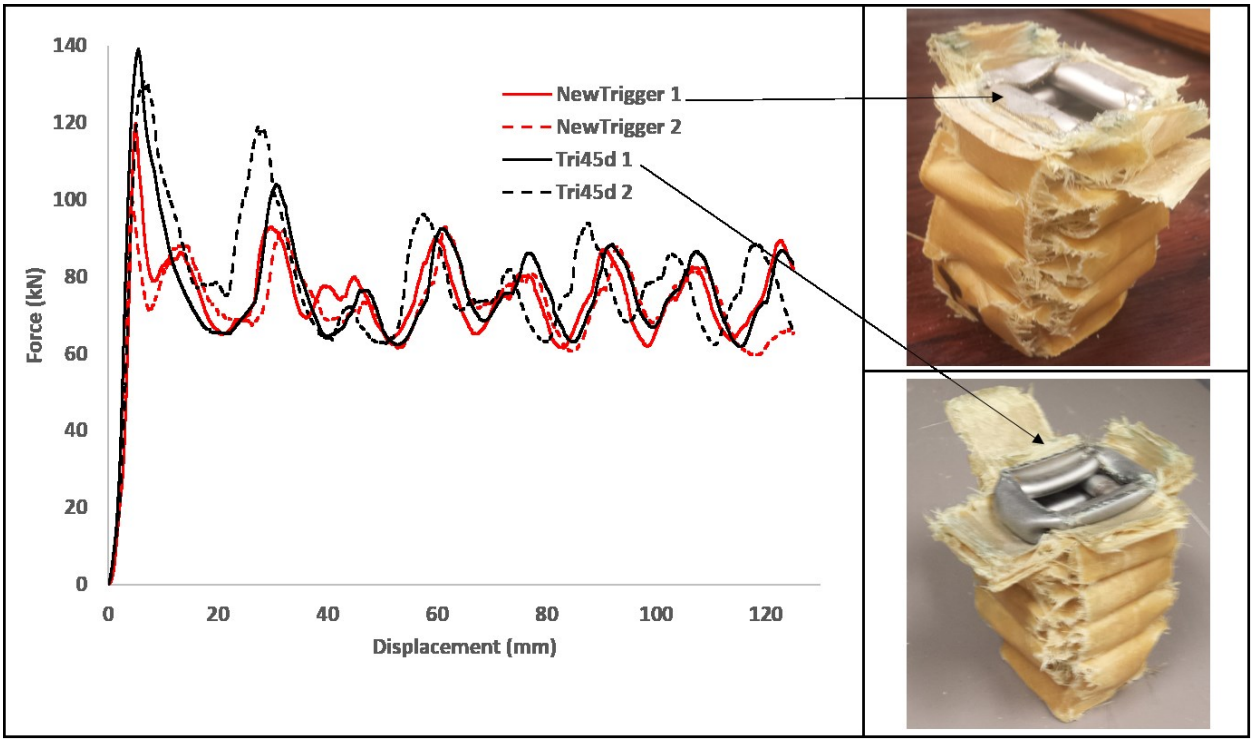

Fig. 2-12. Load displacement results for both triggers (ThinMC1645 and ThinMCNTrig samples) including initial 45° tappered and initial applied deformed tube

2.3. Conclusions

In this study, the effects of different fiber orientation, stacking sequences and thicknesses of FRP section were investigated on collapse mode, crush load efficiency, and the specific absorbed energy of hybrid tubes in comparison with bare metal tubes. It was shown how overwrapping composite around stainless steel metal tube can (1) change its collapsing mode from splitting mode (with very low energy absorption) to symmetric or mixed mode (with much higher energy absorption) and (2) lower the oscillation around mean crushing load. It was also emphasized on the higher effect of strengthening slender metal tubes with FRPs. Based on experiments, it was shown that number of layers of the FRP section in the hybrid tubes has a significant effect the energy absorption. In some cases, the addition of composite to the metal tube may even decrease the energy absorption. A new triggering mechanism was proposed that changes the collapse mode to a symmetric mode and as a result improves the crush load efficiency in hybrid tubes.

In general, the experimental results indicate that the thickness of the metal and FRP sections and the stacking sequence of the FRP layers in the hybrid tubes is so important that there is a need to model the response hybrid tubes. Such a model can help explain counterintuitive behavior (such as the reduced energy absorption exhibited by tubes with 8 layers of FRP).

Chapter 3

3. Numerical Modeling of the effects of FRP thickness and stacking sequence on energy absorption of metal-FRP square tubes

Hybrid metal-composite tubes have the potential to provide cost-effective, energy-absorbing structures for automotive applications. To provide guidance to enable the optimum design of these structures, square hybrid tubes consisting of S2 glass/epoxy composites and 304 stainless steel were modeled numerically. The models were validated with experimental results obtained from quasi-static crushing tests conducted on different combinations of two design variables: stacking sequence and thickness of the FRP section. The effects of the design variables on the energy absorption and failure modes of the hybrid tubes were explained using the models. Subsequently, the results from the numerical models were used to obtain optimum crashworthiness functions. The load efficiency factor (the ratio of mean crushing load to maximum load) and ratio between the difference of mean crushing load of hybrid and metal tube and thickness of the FRP section were introduced as the functions. To connect the variables and the objective functions, back-propagation artificial neural networks (ANN) were used. The Non-dominated Sorting Genetic Algorithm–II (NSGAII) was applied to the constructed ANNs to obtain optimal results in the form of Pareto Frontier solutions. The result is an efficient methodology to obtain the best combination of design variables for hybrid metal-composite tubes for crashworthiness applications.

3.1. Experimental

3.1.1. Materials and sample construction

Prepreg consisting of 36 wt% S2-glass/HexPly® 8552 (S2GL/8552) from Hexcel Corporation (Salt Lake City, UT) was used to fabricate samples for obtaining material properties. HexPly® 8552 is an amine cured mid-toughened and high-strength epoxy resin with a glass transition of approximately 200°C. Samples were cured using the vacuum bagging technique. Stainless steel tubes and sheets (type 304) were obtained from the Phoenix Company (Bethlehem, PA). The curing cycle for the laminates included applying full vacuum pressure (1 bar), heating at 3°C/minute up to 110°C, holding for 60 minutes, heating again to 180°C, holding for 2 hours, and finally cooling at 3°C/minute. Hybrid square tubes were also constructed from S2 glass/epoxy composites and 304 stainless steel with different stacking sequences and thicknesses. The same curing cycle was employed as was used for the laminates. For the metal and hybrid samples, the ends of the metal tube were chamfered at an angle of ~45° to trigger progressive collapse.

3.1.2. Mechanical testing

Tensile properties of the stainless steel parts were determined in accordance with ASTM E8. Dog-bone shaped samples were cut from the sides of the 304 stainless steel tube as well as rolled sheets. Subsequent to the cutting process, the edges were ground to remove any stress concentrations. Tensile, compression, and shear properties of the composite parts were also obtained in accordance with ASTM D3039, D3410, and D3518. General purpose EA-06-125TM-120 strain gages from Vishay Precision Group (Micro-measurements, Raleigh, NC) were used to measure strains during the course of the tests (Fig. 3-1). For the compression tests, front and back gages were used to monitor the amount of bending which took place.

Hybrid square tubes were also constructed from S2 glass/epoxy composites and 304 stainless steel with different stacking sequences and thicknesses. The ends of the metal tube were chamfered at an angle of ~45° to trigger progressive collapse. The tubes were crushed at the rate of 6 mm/min using an MTS 810 testing frame with 250 kN load cell [103]. During

the test, the load and actuator displacement from the load frame were recorded using a custom LabView program.

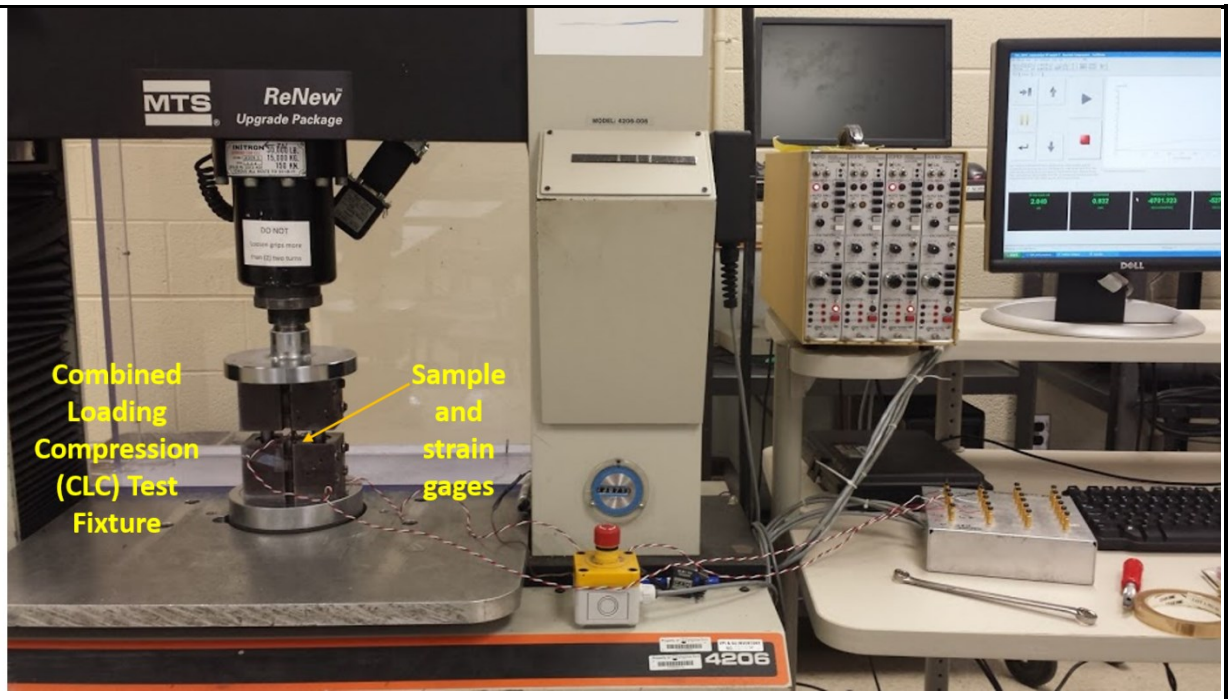

(a)

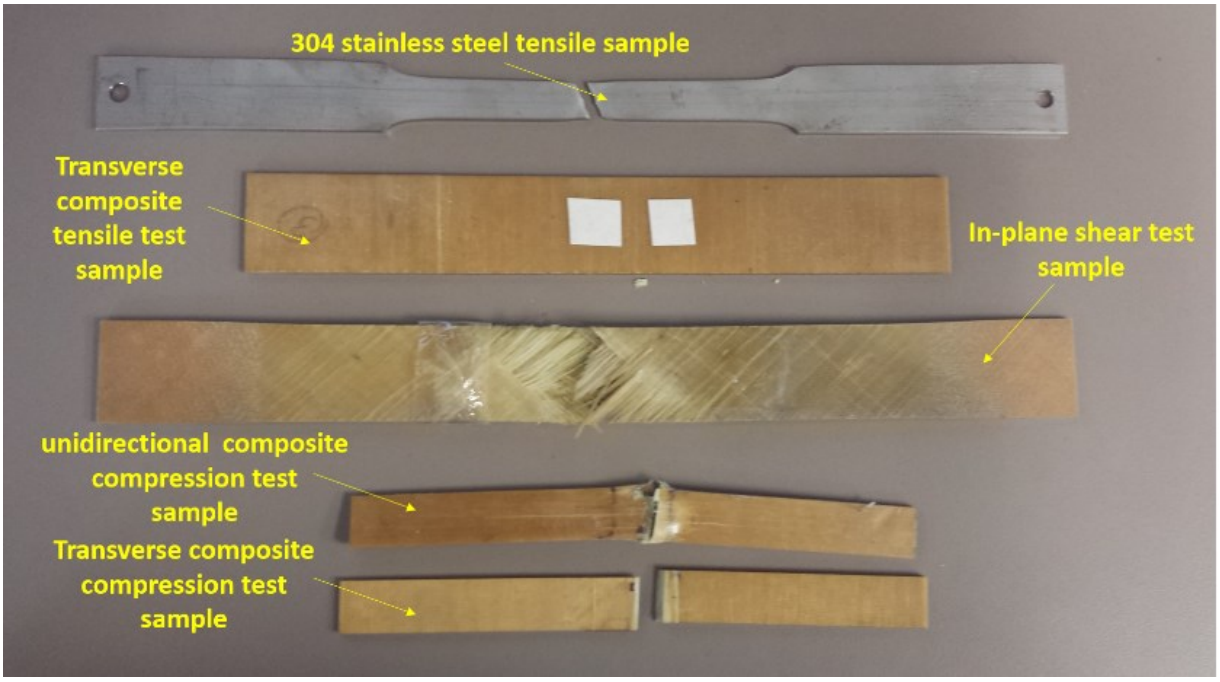

(b)

Fig. 3-1. (a) Combined loading compression test (ASTM 3410) (b) In-Plane shear test (ASTM 3518) (c) typical fracture modes for different mentioned samples

Hybrid square tubes were also constructed from S2 glass/epoxy composites and 304 stainless steel with different stacking sequences and thicknesses. The ends of the metal tube were chamfered at an angle of ~45° to trigger progressive collapse. The tubes were crushed at the rate of 6 mm/min using an MTS 810 testing frame with 250 kN load cell [104].

3.2. Experimental Results and Discussion

Fig. 3-1 shows typical tensile stress-strain curves for the stainless steel specimens produced from the rolled plate as well as the tube sides. It shows piecewise linear plasticity response for the material with elasto-plastic behavior [105]. The steel tubes (austenitic steel) were initially in sheet form which were then bent into a tube shape and welded. Naturally, this fabrication process can introduce strain hardening into the material in the tubes (This strain hardening is reflected in the results of Fig. 3-2). Hence, some residual stresses or strain hardening could have been produced during rolling, bending, and welding (steep thermal gradient) such as general localized tensile residual stresses that can be equal or even greater than the yield strength of a material [106]. One of main objectives of this study is modeling the metal numerically and such residual properties complicate the modeling. It was observed in experiments that the elastic absorbed energy (related to the elastic region) was recovered in the crushing process after unloading the hybrid tube. Consequently, the elastic region does not have an effect on the energy absorption results reported in this study. Therefore, stress-strain data for the as-fabricated tubes after yielding extracted from the tensile test results are summarized on Table 3-1.

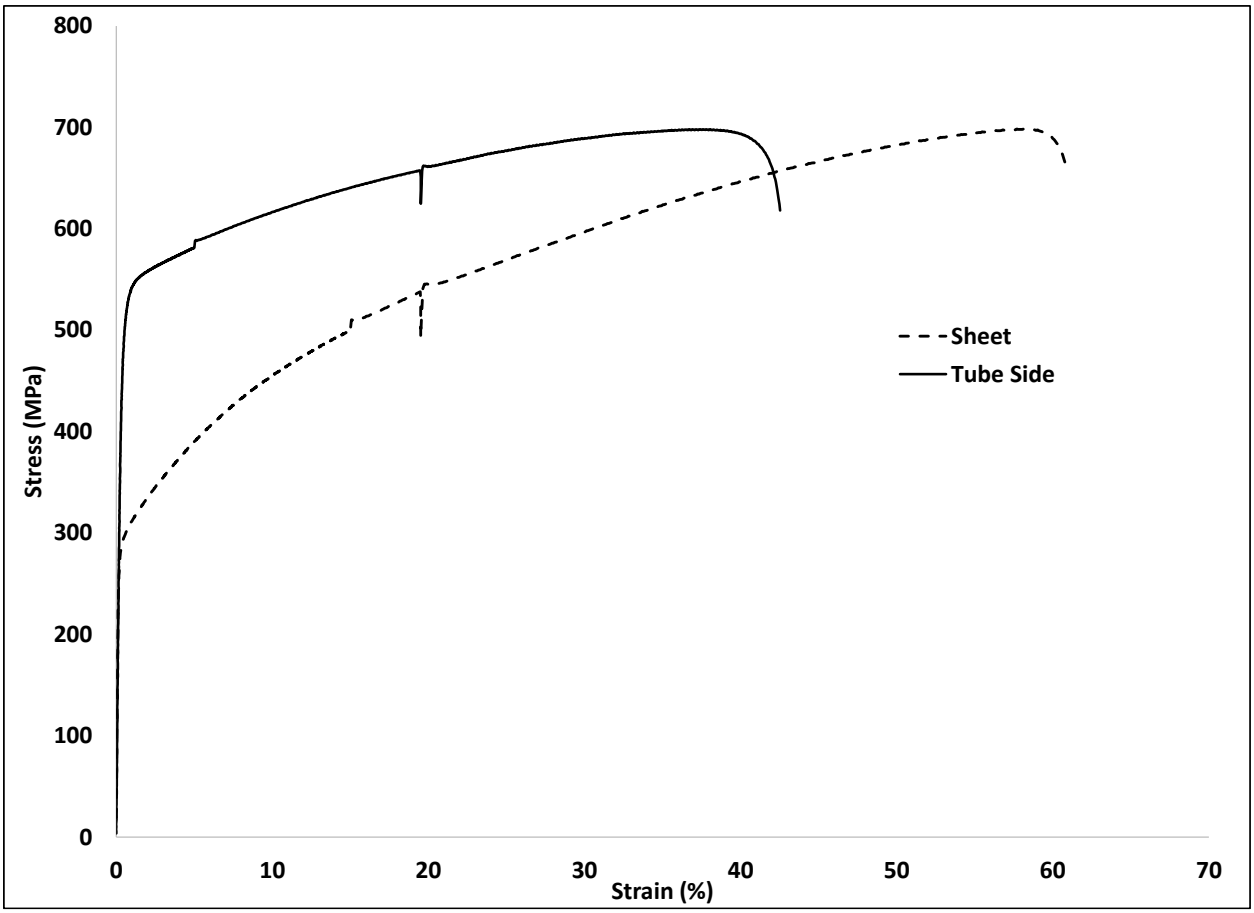

Fig. 3-2. Tensile stress-strain curves for the stainless steel specimens from the raw material in sheet form and a sample extracted from the tube side

Table 3-1. Tensile properties of as-fabricated 304 stainless steel tubes after yielding (the plastic region) as well as Elastic Modulus

Elastic Modulus (GPa)	Plastic Strain (%)	~0	5	10	15	20	25	30	35
190	Stress (Standard Deviation)	502.6 (21.4)	580.2 (15.8)	611 (12.7)	633.8 (10)	652.8 (11.2)	665.8 (10.6)	675.7 (11.6)	680.6 (13.6)

To show the effect of welding on the experimental results, the strain in the x-direction was measured for a metal tube that exhibited the 4-lobes out folding formation (Fig. 3-3) in the middle of welded and unwelded sides using Digital Image Correlation (DIC). There is negligible difference between the measured strains for the sides. As a result, authors concluded the effect of welding and the associated heat affected zone on the load-displacement data is insignificant.

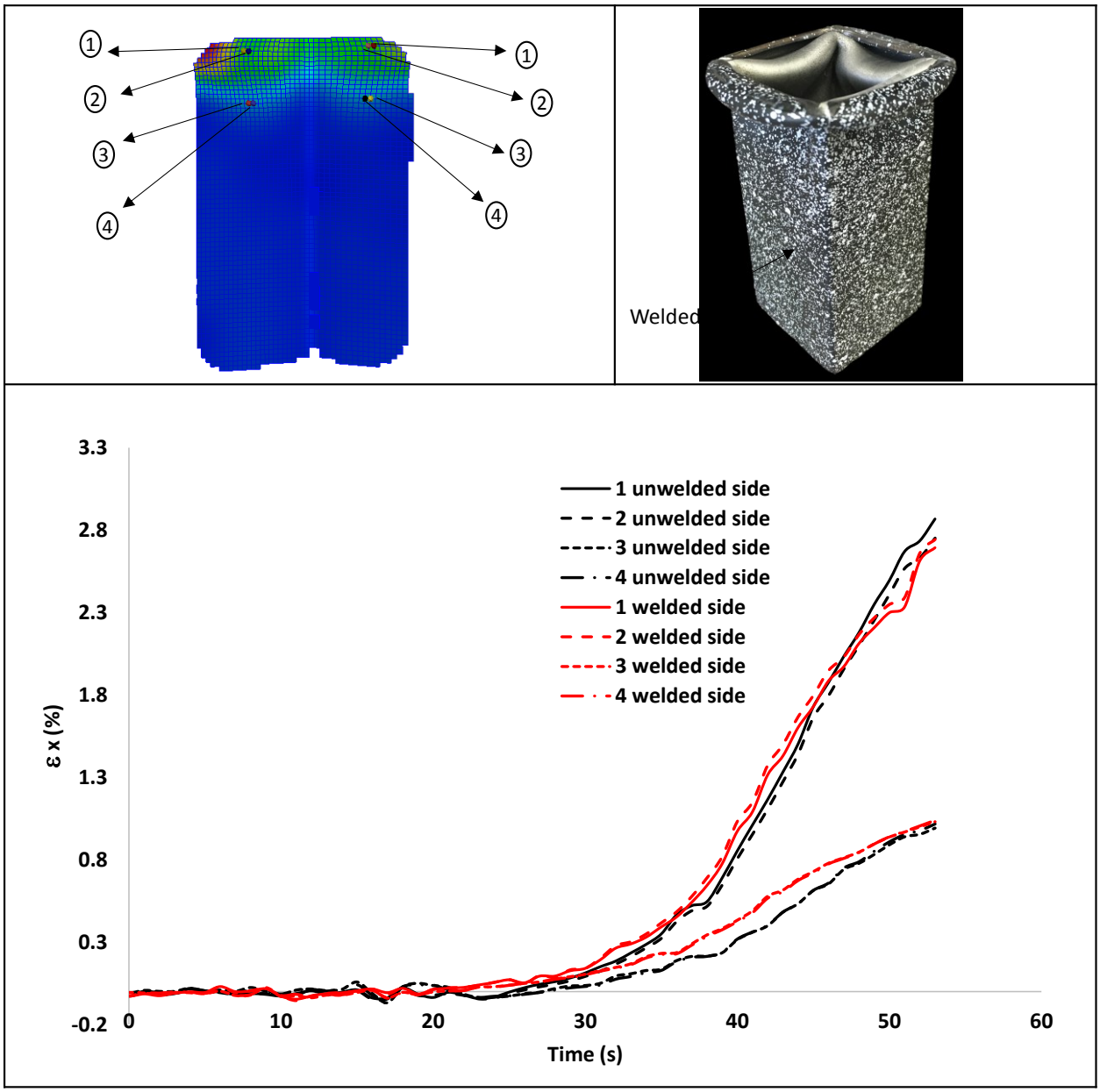

Fig. 3-3. Strain in x-direction measured by Digital Image Correlation (DIC) in unwelded and welded sides

The mechanical properties of S2-glass/HexPly® 8552 (S2GL/8552) composites obtained from the tests are summarized in Table 3-2. For each property, the average and the standard deviation values are presented based on results from at least 5 samples. For the numerical models, the average value of the compression and tensile moduli was used. The strain-at-

failure values in the fiber and transverse directions are important parameters in the numerical studies. They were directly measured in this work unlike in previous studies [18, 88] in which they were obtained numerically. The value of the out-of-plane shear modulus was obtained using the composite cylinder model because of the difficulty of obtaining such a value experimentally [107].

Table 3-2. Mechanical properties of S2-glass/HexPly® 8552 (S2GL/8552) composite

Property	Description	Average Value (Standard Deviation)
ρ_c	Density (kg/m^3)	1760
E_{ft}	Young's modulus in fiber direction under tensile loading (GPa)	46.5 (4.94)
E_{mt}	Young's modulus in transverse direction under tensile loading (GPa)	12.1 (0.73)
E_{fc}	Young's modulus in fiber direction under compression loading (GPa)	42.6 (0.33)
E_{mc}	Young's modulus in transverse direction under compression loading (GPa)	12.9 (0.67)
G_{12}	In-plane shear modulus (GPa)	4.47 (0. 58)
υ_{21}	Minor Poisson's ratio	0.09354
X_t	Tensile strength in fiber direction (MPa)	1480 (47.3)
X_c	Compressive strength in fiber direction (MPa)	820 (59.6)
Y_t	Tensile strength in transverse direction (MPa)	40.2 (8.91)
Y_c	Compressive strength in transverse direction (MPa)	145 (5.73)

ε_{ft}	Strain at failure in fiber direction under tensile loading (%)	3.28 (0.68)
ε_{fc}	Strain at failure in fiber direction under compressive loading (%)	1.84 (0.15)
S	In-plane shear strength (MPa)	149 (5.67)

Table 3-3 shows the dimensions, stacking sequences, and crushing modes of the hybrid tubes from reference [103] which are mentioned in this study.

Table 3-3. Dimensions and stacking sequences of hybrid tubes

Sample Name	Metal thickness (mm)	composite Thickness (mm)	Stacking Sequence	Crushing mode(s)
ThinM	1.65	-	-	Symmetric
ThickM	2.11	-	-	Mixed
ThinMC3245	1.65	3.6	$[90/\mp 45/0]_{4s}$	Symmetric and Mixed
ThinMC2445	1.65	2.4	$[90/\mp 45/0]_{3s}$	Mixed
ThinMC1645	1.65	1.6	$[90/\mp 45/0]_{2s}$	Symmetric and Mixed

3.3. Numerical modeling

The numerical model includes the metal tube, the composite overwrap, and the loading plate (modeled as a rigid wall) (Fig. 3-4). One end of the tube is fully clamped. The other end is in contact with the rigid wall which moves at a constant speed of 100 mm/s and has 100 kg mass. To reduce the time steps in quasi static loading, the mass of the models is scaled

1000 times as suggested in reference [88]. For each of the cases examined, the ratio of the total kinetic energy to the total internal energy is very low (less than 5%) over the crushing distance. Therefore, mass scaling does not introduce artificial loads due to inertia effects and the crushing load-displacement response is independent of the scaling. Two models were built and meshed by LS-DYNA PrePost and solved by LS-DYNA solver (one for the metal tube and one for the hybrid tube). The steel tube (with nominal length of 200 mm, nominal width of 25.4 mm, and nominal thickness of 1.65 mm for thin metal and hybrid tubes and 2.11 for thick tubes) was meshed using 1 mm $\times$ 1 mm 8-noded hexahedral solid elements (based on a mesh convergence study) using ELFORM=1 (in solid element formulation) with hourglass control to prevent zero-energy shapes. The composite in the hybrid tubes was meshed with 1 mm $\times$ 1 mm reduced integration Belytschko-Tsay shell elements that can capture the response of each layer by an integration point. Lamination shell theory is also activated in the elements to simulate the shear stress through the thickness.

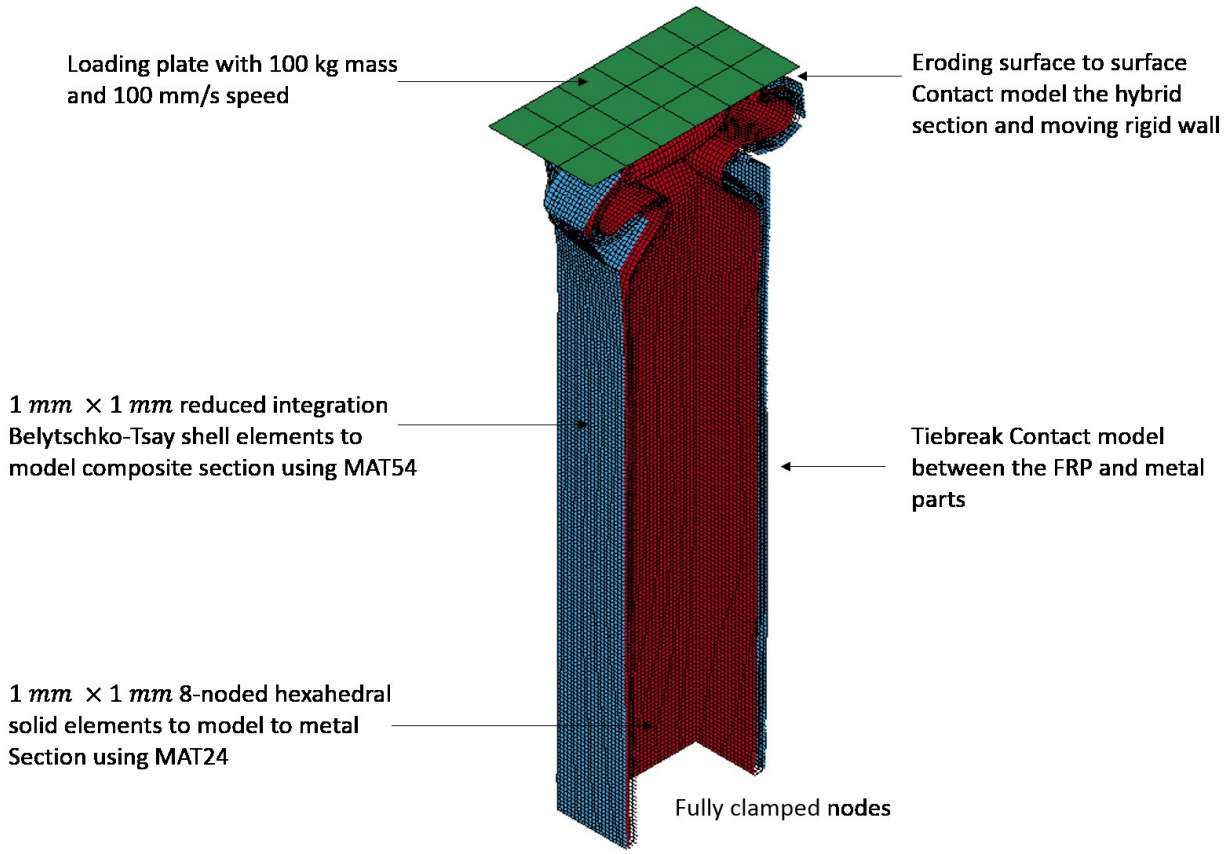

Fig. 3-4. Half sectioned meshed model including the metal tube, the composite overwrap, and the loading plate

The material model used for the steel section is MAT 24 which is based on piecewise linear isotropic plasticity. In order to model the composite part, MAT_ENHANCED_COMPOSITE_DAMAGE (MAT 54) was employed. This material model is specifically designed for unidirectional laminates and is based on the Chang-Chang failure model which provides linear behavior until fracture followed by a post-failure degradation rule and a non-linear shear stress-strain. This model was chosen because the number of parameters in the material model is considerably fewer than the number of parameters in continuum mechanics based material models such as MAT59 and MAT162 [108]. However, there are still some parameters such as ALPH, BETA, FBRT, TFAIL, and SOFT that are required to model stable progressive failure and which cannot be measured experimentally. Detailed definitions of these parameters can be found in the study by Feraboli et al. [108].

DFAILT (strain-at-failure under uniaxial tensile loading) and DFAILC (strain-at-failure under uniaxial tcompressive loading) are the strain at failure in the fiber direction under tensile and compression loading, respectively.

The Contact_Eroding_Single_Surface card was used in order to prevent the interpenetration of both solid and shell elements in both the metal and the composite parts. To construct the hybrid tubes, the surfaces of the stainless steel tubes were roughened and the prepreg sheets were overwrapped around them [18]. Therefore, there was not a separate adhesive layer between the composite and metal sections. A Contact-Tiebreak-Nodes-Only card was used to model the contact which is able to simulate the frictional energy dissipation between the metal and FRP parts (based on cohesive crack concept [22]). The contact between the tube and the rigid wall was modeled with Contact_Eroding_Surface_To_Surface to avoid the penetration of elements through the wall.

The numerical model was able to model the symmetric progressive and mixed crushing modes for the hybrid tube. Table 4 shows the value of each parameter used in the model based on its definition. The other material properties are given in Table 2 in reference [109]. Some of the values were calibrated based on the crushing deformation of the tubes. The SOFT parameter was the only non-physical parameter in the material models able to change the load-displacement behavior of the tubes. This parameter is associated with the strength of elements just before crushing in which the values greater than 1 lead to parameter activation. Fig. 3-5 shows how different values of the SOFT parameter affected the load-displacement curve and the progressive failure of the tube. The load-displacement curves are similar. However, for values of the SOFT parameter below 0.6, the composite part is too brittle, fracturing without bending with the metal part—a behavior which is inconsistent with the behavior observed in the experiments. For values of SOFT above 0.6, the load-displacement results are not sensitive to the chosen parameter for the cases investigated. As a result, a value of SOFT $= 0.75$ *was chosen.*

Table 3-4. Definition and values chosen for untested parameters

Variable	Related to Card	Short definition	Value used
TFAIL	-	element deletion time step	0.25
ALPH	-	weighing factor of nonlinear shear stress	0
SOFT	-	crush front parameter	0.75
FBRT	-	stress reduction term	1
BETA	-	Weighing factor for shear stress	0
FS	All contact cards	Static coefficient of friction	0.3
FD	All contact cards	Dynamic coefficient of friction	0.3
NFLF (N)	Contact_Tiebreak_Nodes_Only	Normal force related to debonding	50
SFLS (N)	Contact_Tiebreak_Nodes_Only	Shear force related to debonding	50

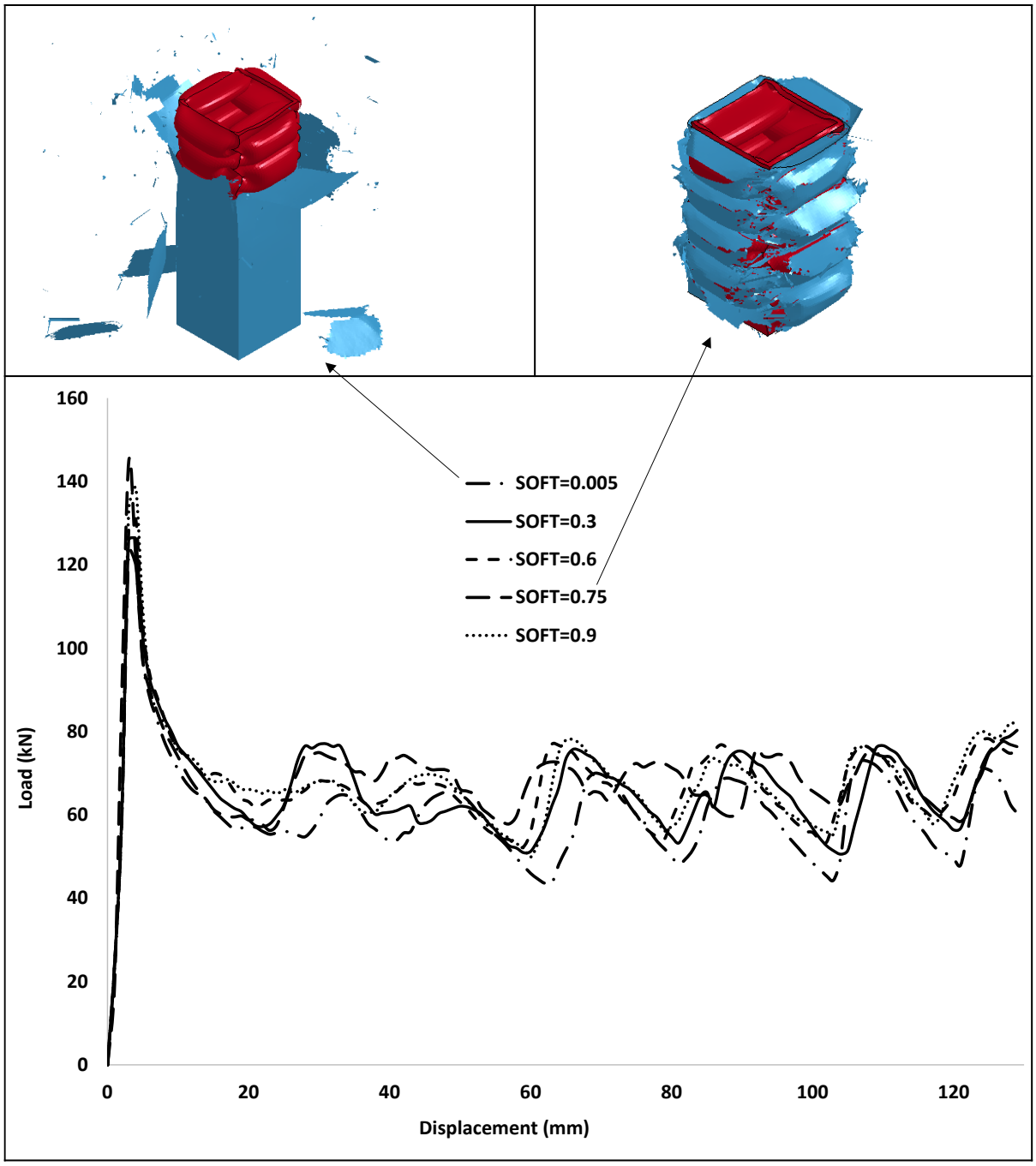

Fig. 3-5. Load-displacement variation with respect to SOFT parameter

3.4. Numerical results

Table 3-5 shows the experimental results compared with simulated response in which the deformation was calculated based on the displacement of the upper rigid wall and the load

data was obtained from the contact card between the hybrid tube and the rigid wall. The quantitative comparison that the maximum load from the numerical results is systematically higher than the experimental results but is within ~13% of those values. For the mean crushing loads, the results are generally within ~10% of the experimental values—in some cases greater than the experiments; in other cases less than the experiments.

Table 3-5. Quantitative comparison of numerical and experimental [103] results for different configurations

Sample Name	P_{max} (kN) (Exper.)	P_{mean}@125mm kN (Exper.)	P_{max} (kN) (Num.)	P_{mean}@125mm kN (Num.)	$Error\ in$ P_{max} (%)	$Error\ in$ P_{mean} (%)
ThinM	107 (3.9)	62.4 (1.1)	121	55.7	13.1	-10.7
ThickM	161 (1.6)	98.7 (1.6)	168	107	4.3	8.4
ThinMC3245	190 (6.4)	107.8 (5.3)	194	99.3	2.1	-8
ThinMC2445	156 (6.0)	91.4 (2.1)	177	82.1	13.5	-10.2
ThinMC1645	133 (5)	77.1 (1.8)	145	69	9	-10.5

In the experiments, thin and thick stainless steel tubes showed a combination of symmetric, mixed, and splitting progressive crushing modes. The developed model agreed well with the load-displacement data of thin and thick tubes (Fig. 3-6). The failure modes of thin tubes obtained from numerical modeling are comparable with the experimental results. Fig. 3-6 shows the failure pattern for thick tube which does not completely match the experiments. However, it is able to capture the starting and finishing lobe formations that are 4 lobes out and 2 lobes out/2 lobes in, respectively. The initial slope (which is related to flexural stiffness of the walls) and the subsequent lobe formation following peak load (which is the result of the bending of two opposite side and changes in the bending rigidity) are also in good agreement with the experimental results (both load-displacement response and crushing modes). One of the characteristics of the mixed failure mode (related to thick tubes)

is significant variation in the nature of load-displacement response which was modeled to a reasonable agreement. In fact, large variations in the crushing response of thick tubes were related to 4 lobes out and shorter peaks are related to 2 lobes out/2 lobes in the symmetric mode [18]. (The first lobe pattern from bottom of thin metal tube's numerical modeling represents the 4 lobes out and the first pattern from its top exhibits the 2 lobes out/2 lobes in crushing mode.)

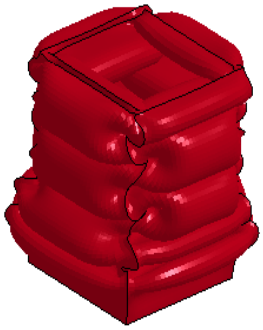 Numerical modeling (Thin metal)	 Experimental pattern (Thin metal)	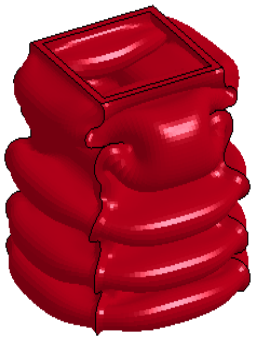 Numerical modeling (Thick metal)	 Experimental pattern (Thick metal)

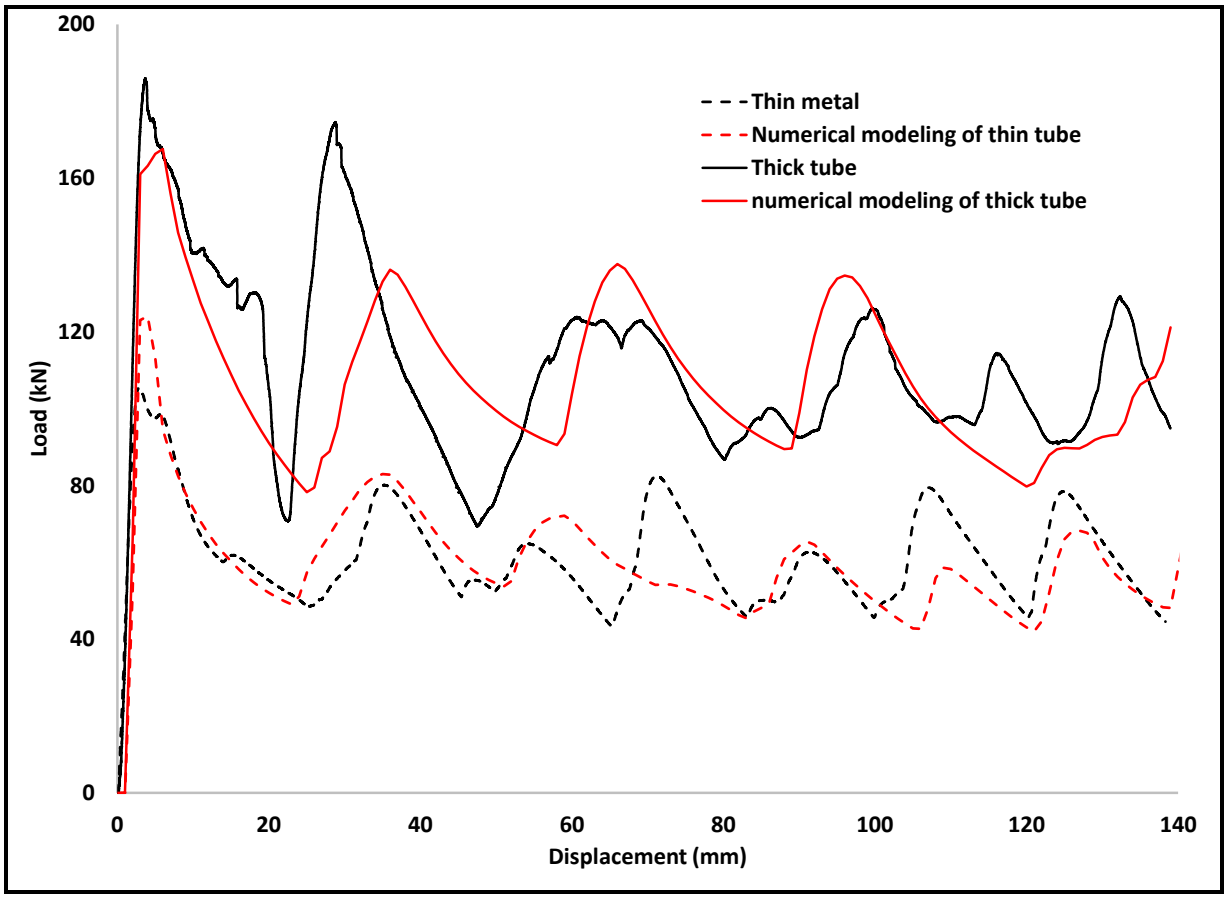

Fig. 3-6. Numerical modeling of thin and thick tubes in comparison with experimental results [103]

Figs. 3-7 and 3-8 show the numerical models for the symmetric crushing mode of hybrid tubes with $[90/\mp45/0]_{2s}$ and $[90/\mp45/0]_{4s}$, respectively, as examples of the predicted crushing behavior of the hybrid tubes in comparison with the experimental results [103]. Once again, there was good correlation between the observed and predicted load-displacement data and the crushing mode of the tubes. For $[90/\mp45/0]_{2s}$ stacking sequence, the numerical model followed the experimental folding pattern (symmetric failure mode); however, the magnitudes of the peaks do not agree. Fig. 3-7 includes the deformed shapes just before each peak. In general, the composite section follows the folding pattern of the metal section in hybrid metal-composite tubes. Local variations in wall thickness (non-uniformity) and material properties of the hybrid wall are able to change the results.

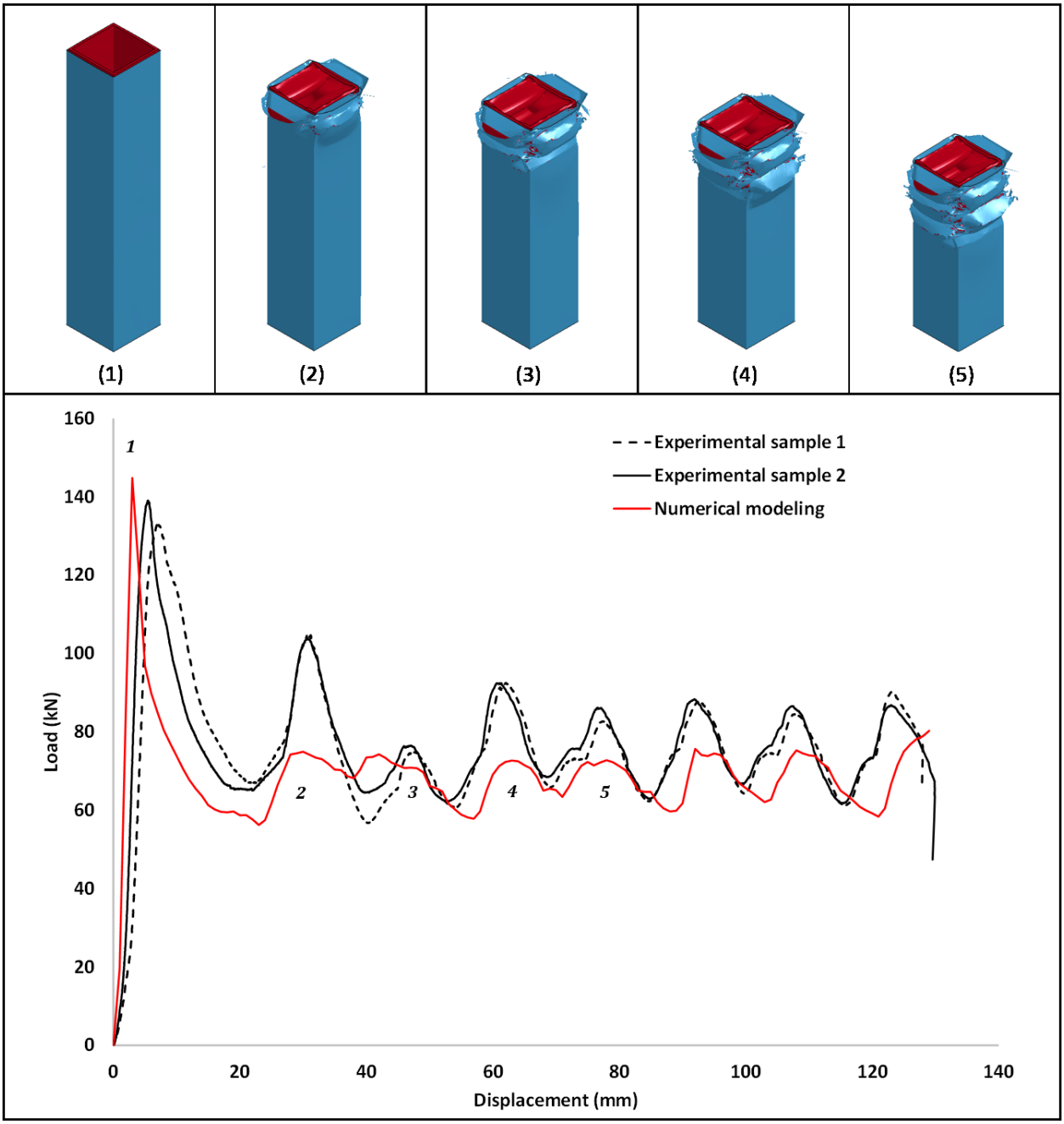

Fig. 3-7. Comparison between numerical modeling and experimental results for hybrid tubes with $[90/\mp 45/0]_{2s}$ *stacking sequence*

Fig. 3-9 shows the resulting Von-Mises stress of $[90/\mp 45/0]_{2s}$ stacking sequence (which was experimentally evaluated) for the first two folding for metal during the course of axial compressive loading. Because the stacking sequence is quasi-isotropic, the resulted stress for the metal part is symmetric (Fig. 7). Fig. 3-10 also shows the damage parameter of Chang-Chang failure criterion for the composite section [45]. However, LS-DYNA is also able to show the fiber and matrix failure in tensile and compressive directions for each layer (integration point) in each stage by activating NEIPS and MAXINT variables in DATABASE_EXTENT_BINARY card.

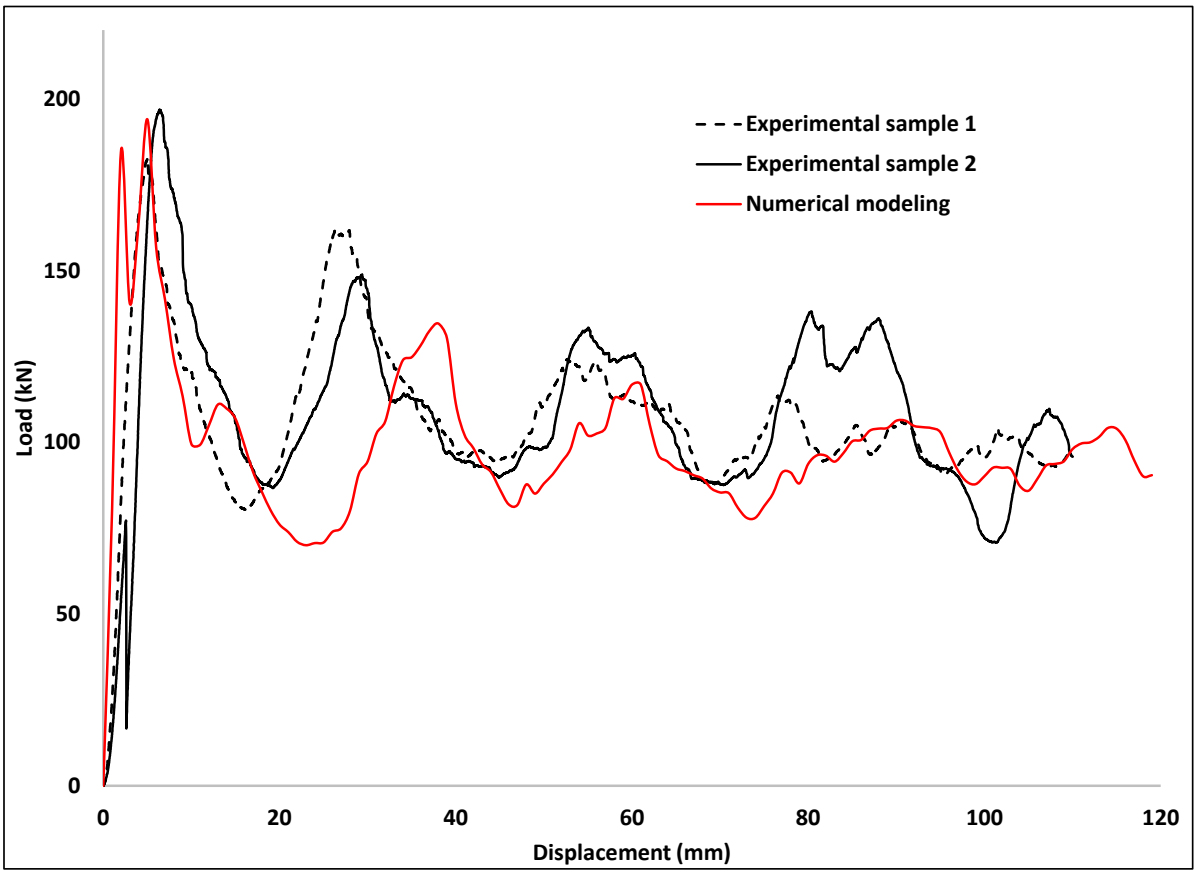

Fig. 3-8. Comparison between numerical modeling and experimental results for hybrid tubes with $[90/\mp 45/0]_{4s}$ *stacking sequence*

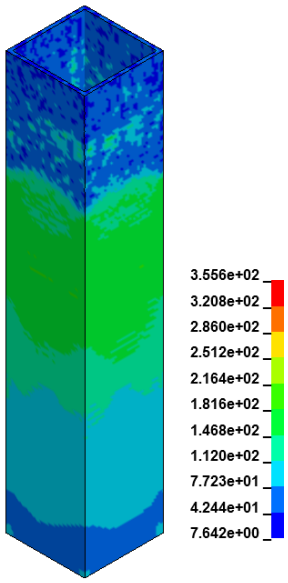

Displacement: 1 cm

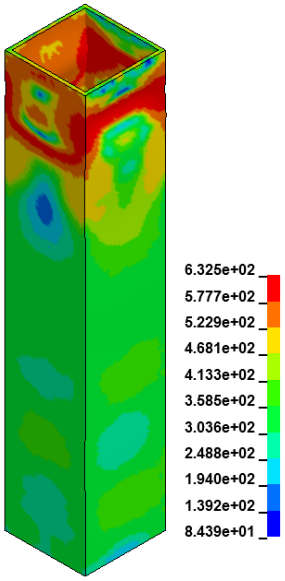

Displacement: 5 cm

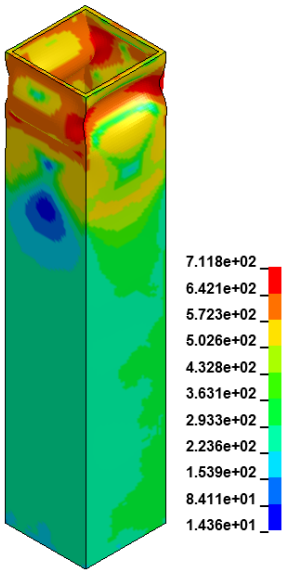

Displacement: 10 cm

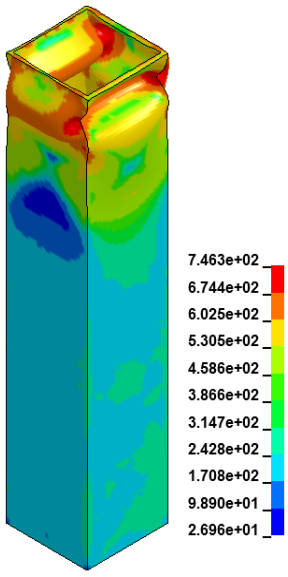

Displacement: 15 cm

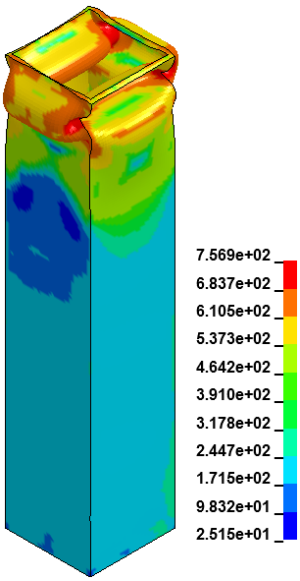

Displacement: 20 cm

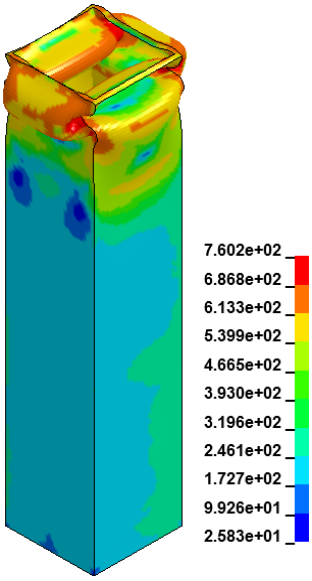

Displacement: 25 cm

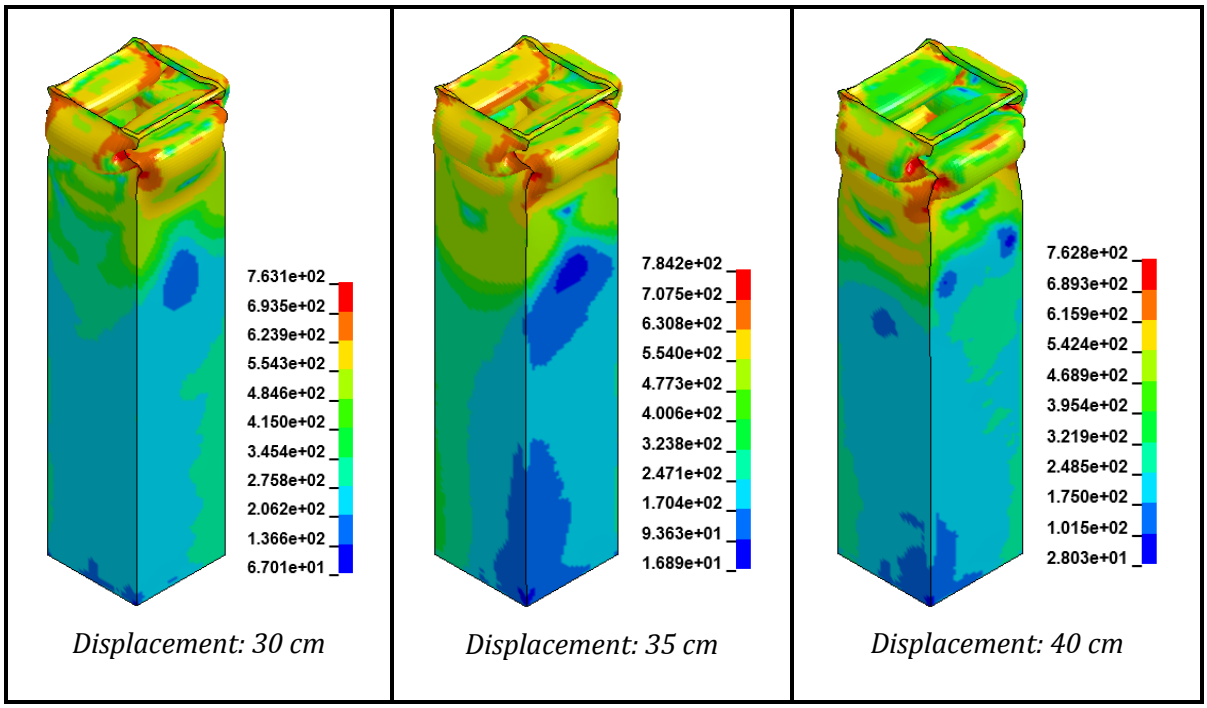

Displacement: 30 cm | *Displacement: 35 cm* | *Displacement: 40 cm*

Fig. 3-9. Von-Mises stress for metal section for the two first folding

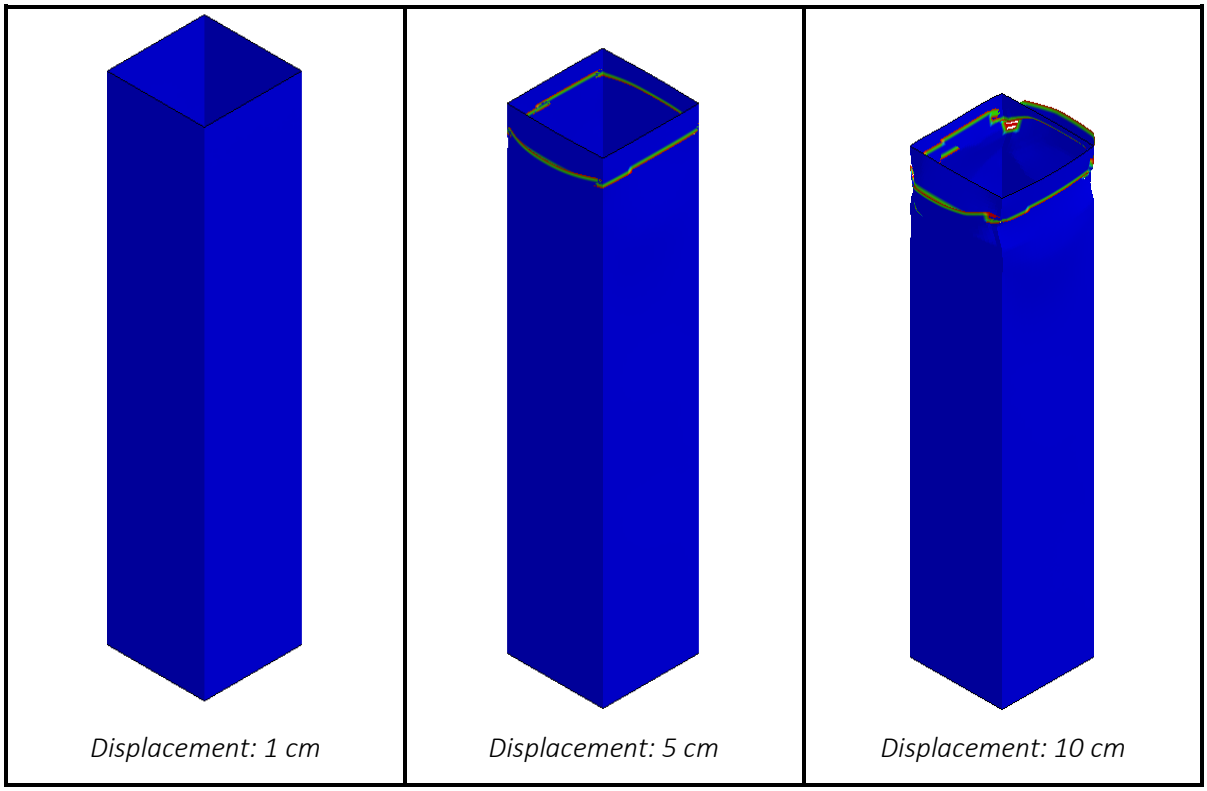

Displacement: 1 cm | *Displacement: 5 cm* | *Displacement: 10 cm*

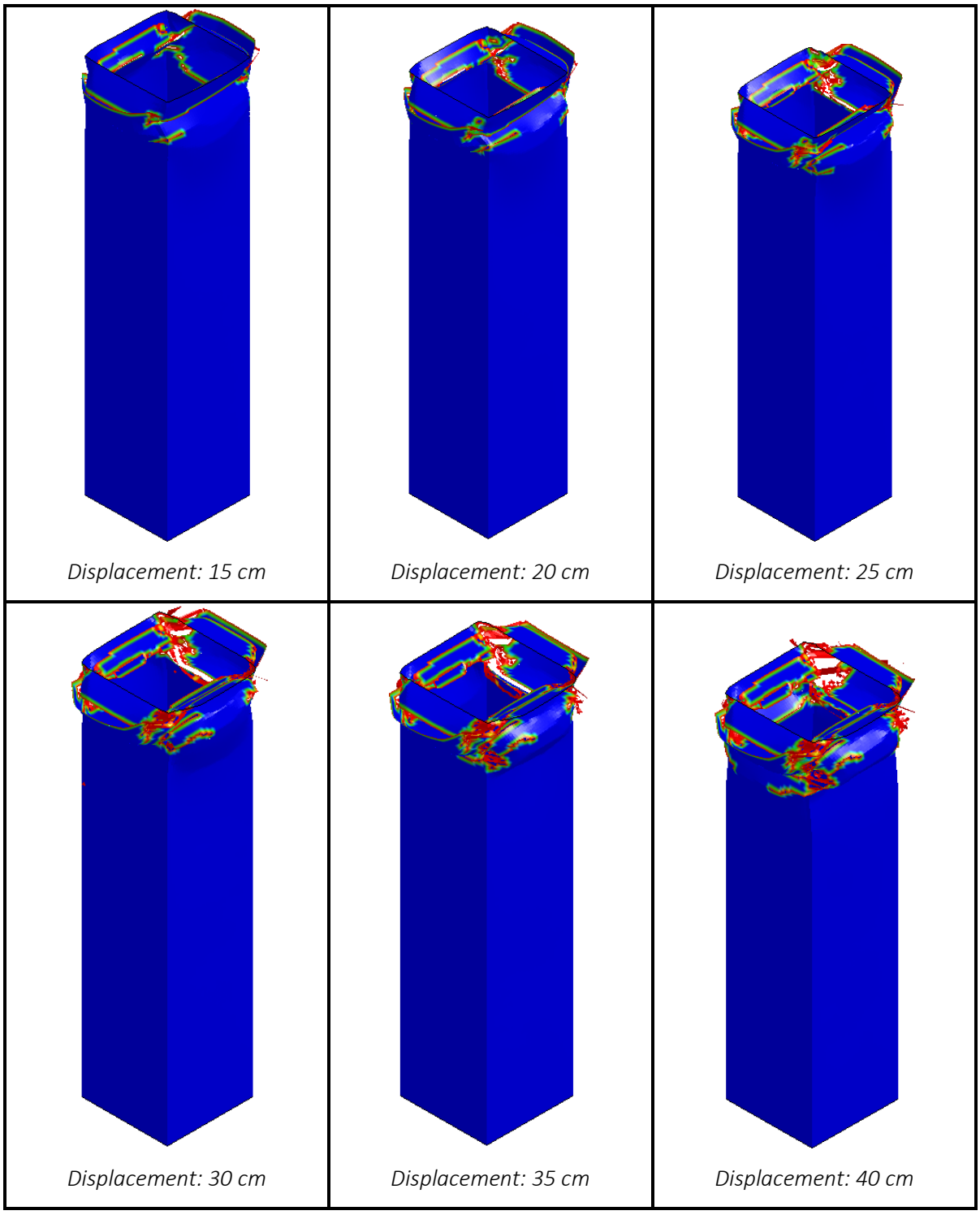

Fig. 3- 10. Damage parameter for the composite section for the two first folding. The blue and red colors show the elements are intact or damaged, respectively.

It is apparent that the energy absorption depends on design variables such as adhesive failure and changes in crushing behavior of the metal tube by thickness and stacking sequence (the latter has a big impact) of the composite section. Hence, additional numerical tests were conducted to examine the changes in the load-displacement results under the influence of different stacking sequences qualitatively (the deformed shapes shown in Fig. 3-11) and quantitatively (Table 3-6). Fig. 3-11 shows that folding behavior (especially in the first and second completed lobes) can be changed with stacking sequences (the images in the right side of the figure shows how the folding behavior of metal section changes as the result of stacking sequences). Based on the results, incorrect combinations of thickness [103] and stacking sequence of the composite section can result in less energy absorption compared to the metal tube.

Table 3-6. Crashworthiness functions as a result of changing stacking sequence and thickness of the composite section of metal-composite square hybrid tubes

Design variables	16 layers			24 layers			32 layers		
Stacking sequence	$P_{mean}(kN)$	$P_{max}\ (kN)$	$PMTC$	$P_{mean}(kN)$	$P_{max}\ (kN)$	$PMTC$	$P_{mean}(kN)$	$P_{max}\ (kN)$	$PMTC$
[90/−15/15/0]	68.9	158.8	4.0625	86	174.5	9.8	91	185	8.9
[90/−30/30/0]	70.7	162.3	5.1875	82.2	169	8.3	93.1	194.7	9.6
[90/−45/45/0]	68.9	144.8	4.0625	82.1	177	8.2	99.3	194	11.5
[90/−60/60/0]	66.4	135.3	2.5	80.1	163.6	7.4	86	205.9	7.4
[90/−75/75/0]	65.5	124.54	1.9375	76	167.6	5.7	82.4	226.2	6.3
[90/0/45/0]	70.8	156	5.25	85	161.5	9.4	95.4	189	10.3
[90/0/90/0]	67.4	138.8	3.125	85.5	162	9.6	92.3	210.6	9.3

[90/45/90/0]	67	133.7	2.875	80.2	147.6	7.4	84.6	212.1	6.9
[90/60/0/0]	69.5	157.4	4.4375	88.3	183	10.8	96	193.8	10.5

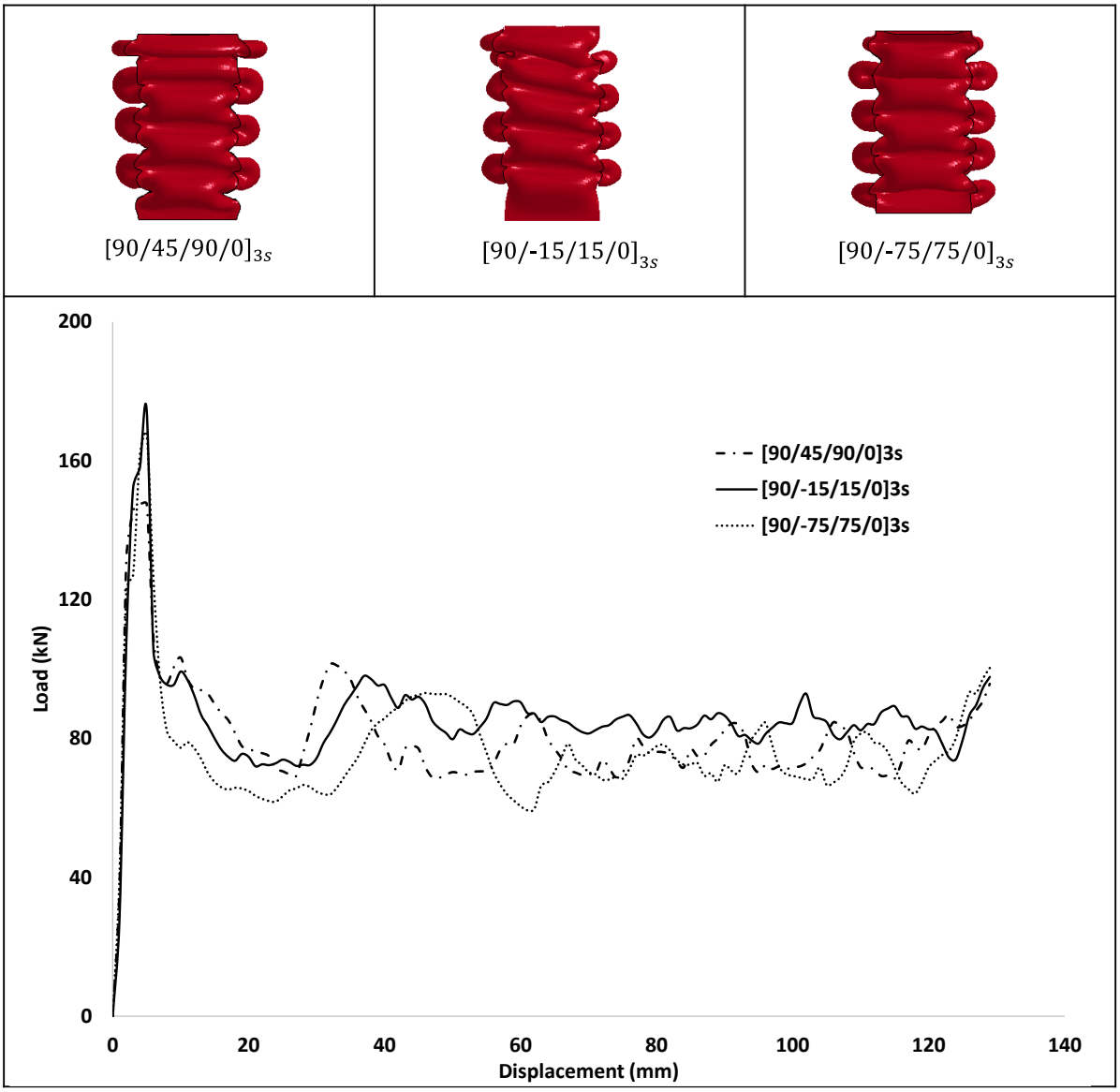

Fig. 3-11. Numerical modeling of hybrid tubes with $[90/45/90/0]_{3s}$, $[90/-15/15/0]_{3s}$, *and* $[90/75/-75/0]_{3s}$ *stacking sequences and their effects on metal folding behavior*

To demonstrate the importance of different thickness and stacking sequence of the composite section of the hybrid tubes on crashworthiness functions, a different set of design variables and their resulting simulated response are presented in Table 6 in which

$$\text{PMTC} = \frac{\text{P}_\text{m} \text{ of hybrid tube } - \text{ P}_\text{m} \text{ of metal tube}}{\text{Thickness of the composite section}}$$

The crashworthiness function PMTC was chosen to study the increase in mean crushing load of the hybrid tube compared with the metal tube with respect to the increase in the thickness of the composite section. The basis for choosing the thickness of the composite section is because of its relationship to both cost and mass of the hybrid tubes (considering relatively negligible cost for material and manufacturing of the metal tubes). The results (Table 3-6 and Fig. 3-11) show that thickness and stacking sequence of the composite section are both effective in changing the crashworthiness functions. In addition, there are highly non-linear relations between the crashworthiness functions and the design variables. For all of the configurations, the $[90/-75/75/0]_{ns}$ stacking sequence has the lowest mean crushing load. In addition, Fig. 3-12 shows the trend of changes in mean crushing load for $[90/\theta_1/\theta_2/0]_{ns}$ which is the same for n=2, 3, and 4 except for two conditions: $[90/-15/15/0]_{ns}$ *and* $[90/-60/60/0]_{ns}$. However, the rate of increasing of mean crushing load is different for the configurations with respect to thickness (Fig. 12). Fig. 3-13 shows that the rate of increase in PMTC decreases with increasing number of layers from 16 to 32 layers. It approaches a flat region and shows that increasing the number of layers of the composite section more than 32 layers may not improve the PMTC values. Finally, the non-linear relations between crashworthiness functions and design variables show the requirement for multi-objective optimization to find the best combination of design variables.

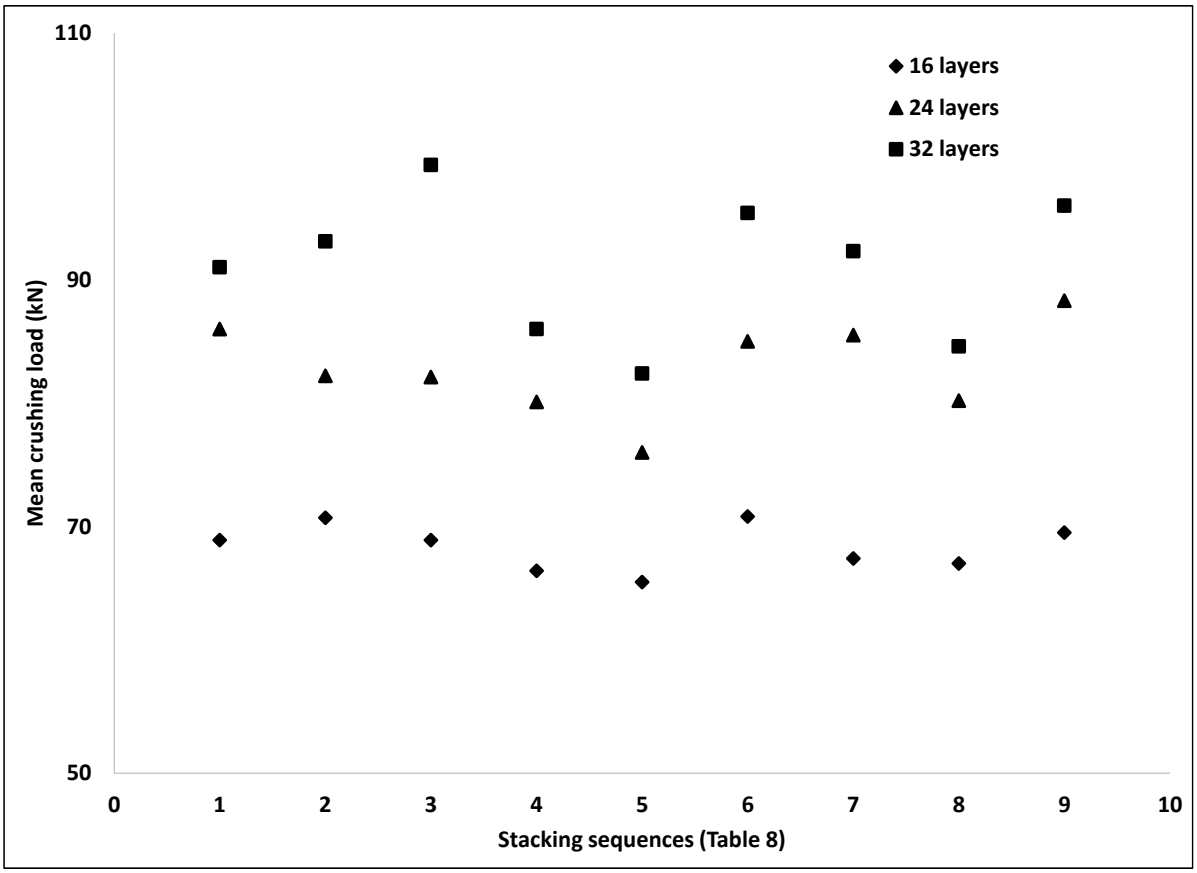

Fig. 3-12. Mean crushing load for every stacking sequences from Table 8

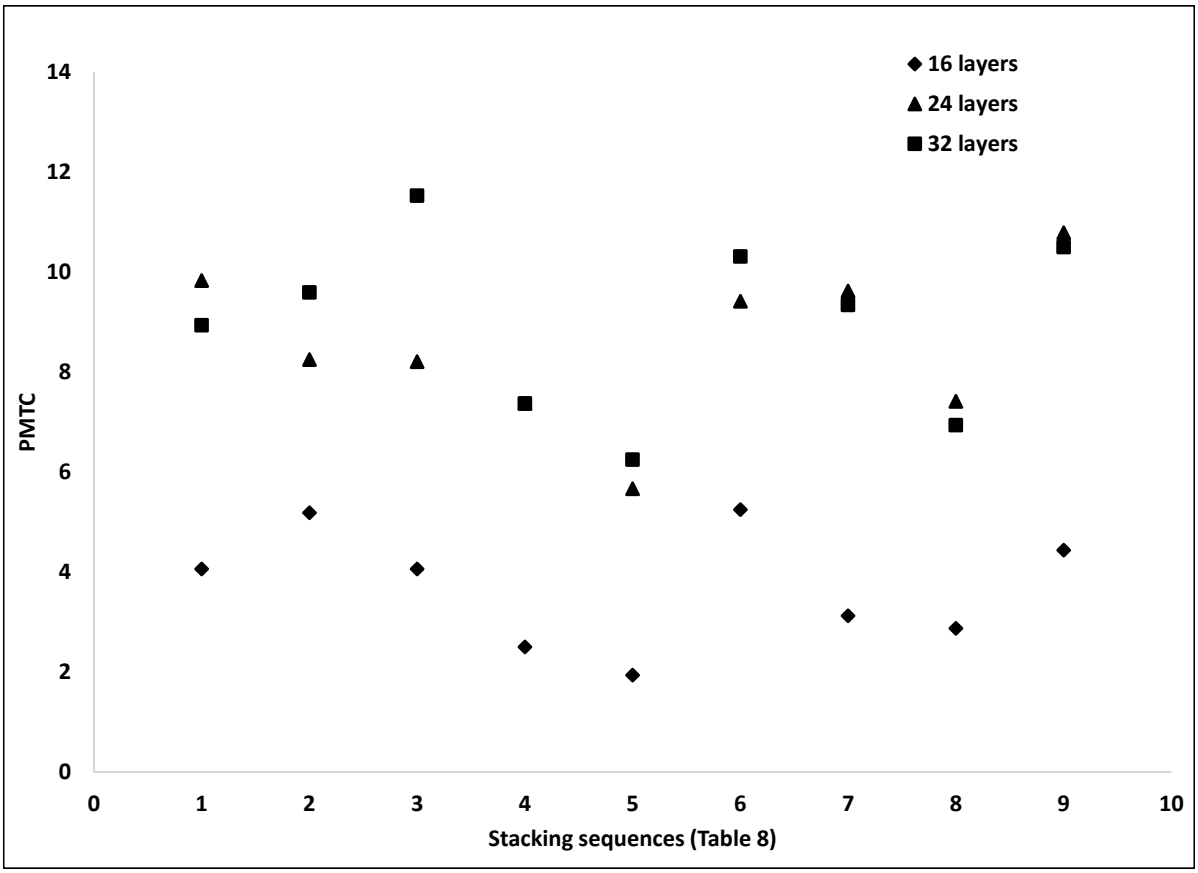

Fig. 3-13. PMTC based on changes in stacking sequences in Table 8 for different number of layers

3.5. Optimization Process

To overcome the computational cost of numerical modeling, surrogate based models are usually employed to fit the resultant objective functions at some known training points and generate a pool of responses on the other points. In addition, in design problems, specifically for structures under impact loading, there are often multiple conflicting objective functions as a result of different design variables affecting the response of the structure. Surrogate based multi-objective optimization algorithms such as Polynomial Response Surface (PRS) [93], radial based, and Kriging (KR) methods [92] are generally applied to generate the objective functions and to present results in a set of Pareto optimal solutions (a cloud of optimal points when multiple conflicting objective functions do not acquire a simultaneous

optimum [93]). As a result, designers can choose the final design according to particular limitations or requirements. One of these algorithms that incorporates an evolutionary approach to the problem is the genetic algorithm. Multi-objective optimization genetic algorithms (MOGAs) [110, 111] are suitable and fast for solving multi-objective problems because of their excellent advantages such as simple constraint-handling techniques [91].

A number of different approaches were employed to evaluate the usefulness of a hybrid tube in comparison with a bare metal tube. For instance, one study considered the ratio between mean crushing load of hybrid tubes and metal tubes [88]. The results of Table 3-6 show that, after including the cost parameter (related to thickness of composite section) in the objective functions, PMTC values for the 24 and 32 layers are in the same range which are higher than the values for 16 layers. Moreover, the mean crushing value of the hybrid tube with 32 layers is greater than 24 layers. Therefore, the problem was defined in two ways: dual objective optimization of (1) PMTC and the load efficiency factor and (2) mean crushing load and the load efficiency factor of hybrid tubes with 32 layers of FRP section with a pre-specified stacking sequence $[90/\theta_1/\theta_2/0]_{ns}$ $(-90 < \theta_i < 90, n = 4)$ where θ_1, θ_2, are the design variables in the optimization process in such a way that the maximum load does not exceed 220 kN.

In most crashworthiness optimization problems, the application of neural networks is attractive because of complexity of analytical models and the computational cost of numerical models to frame the correlations between crashworthiness functions and different design variables. In the present optimization problem, in order to construct each objective and constraint as nonlinear functions in terms of the design variables, three distinct back-propagation neural networks [112] as surrogate models were created. Back-propagation neural networks are able to recognize the nonlinearities by the steepest gradient descent method [91]. The architecture of each network is 3-4-1 in which the transfer functions for the three layers are “tangent sigmoid”, “tangent sigmoid” and “linear” respectively (in-detail information about the relations can be found in [91]).

Training and testing of the neural networks were performed by the "Trainbr" function in MATLAB [113] using 39 numerical simulations which were chosen using the design of experiment (DOE) technique: Latin hypercube sampling (LHS) designs [93, 114]. Twenty-six simulations were used for training and the remaining simulations were used to evaluate the accuracy of surrogate models. The number of neurons was adjusted until the desired accuracy was achieved. The numerical and simulated objective functions for the training and testing points are listed in Table 3-7. The results show that the maximum relative error in the mean crushing load, maximum load and PMTC are 9.4%, 7.5% and 10.6% respectively.

Table 3-7. Crashworthiness functions simulated by neural networks in comparison with numerical results

Design variables		Numerical results				Simulated NN results			
θ_1	θ_2	$P_{mean}(kN)$	$P_{max}\ (kN)$	$\frac{P_{mean}}{P_{max}} * 100$	$PMTC$	$P_{mean}(kN)$	$P_{max}\ (kN)$	$\frac{P_{mean}}{P_{max}} * 100$	$PMTC$
0	-15	94.6	178	0.53	10.1	94.0	186	0.53	10.4
0	-45	90.6	183	0.49	8.8	91.2	186	0.50	9.5
0	-75	89.2	204	0.44	8.4	89.9	203	0.42	8.7
0	-90	88.0	211	0.42	8.0	87.6	214	0.42	7.9
0	0	101	191	0.53	12.0	97.9	186	0.53	11.9
15	-15	94.1	178	0.53	9.9	98.0	185	0.52	9.9
15	-30	89.1	195	0.46	8.3	92.9	185	0.50	9.2
15	-60	92.1	193	0.48	9.3	89.4	192	0.48	8.6
15	-75	87.3	204	0.43	7.8	87.6	204	0.44	8.0
15	-90	85.4	210	0.41	7.2	85.0	214	0.42	7.6

30	-30	90.0	195	0.46	8.6	95.4	183	0.48	8.8
30	-45	88.1	174	0.51	8.0	88.2	184	0.49	8.1
30	-75	83.5	203	0.41	6.6	82.6	203	0.46	7.3
45	-15	89.1	182	0.49	8.3	88.8	183	0.45	8.8
60	-45	88.3	196	0.45	8.1	88.0	196	0.44	7.8
60	-60	86.9	206	0.42	7.7	87.2	204	0.43	7.4
60	-15	82.4	204	0.40	6.2	81.9	204	0.40	6.7
75	-30	82.3	200	0.41	6.2	82.7	201	0.40	5.9
75	-90	81.4	213	0.38	5.9	81.4	213	0.38	6.5
75	-60	81.0	212	0.38	5.8	82.2	225	0.39	5.6
90	-90	82.9	240	0.35	6.4	81.9	239	0.34	6.6
0	15	102	179	0.57	12.4	102	186	0.55	12.4
45	0	93.4	183	0.51	9.7	89.2	183	0.46	9.2
90	0	91.7	211	0.44	9.1	83.1	215	0.43	8.4
15	45	92.2	183	0.50	9.3	92.3	184	0.50	9.5
30	30	98.4	194	0.51	11.3	96.4	182	0.50	11.4
30	45	87.6	170	0.52	7.9	88.6	182	0.49	8.6
30	75	82.7	186	0.44	6.4	85.8	185	0.45	6.3
45	15	89.4	185	0.48	8.4	90.6	183	0.48	8.9
45	45	90.0	169	0.53	8.6	89.9	182	0.49	8.3
45	60	85.2	194	0.44	7.1	84.6	179	0.46	7.3
45	75	84.6	173	0.49	6.9	84.5	174	0.44	6.9

60	15	87.0	191	0.45	7.7	89.1	192	0.47	7.6
60	60	81.7	171	0.48	6.0	81.8	170	0.47	6.1
75	30	85.7	197	0.44	7.3	82.1	196	0.44	7.1
75	60	79.3	175	0.45	5.3	79.7	175	0.44	4.4
90	15	84.5	209	0.40	6.9	83.9	208	0.42	7.6
90	30	83.1	209	0.40	6.5	83.7	199	0.40	6.2
90	75	77.8	215	0.36	4.8	77.7	212	0.35	4.7

The response surfaces of the networks are shown in Fig. 3-14. They exhibit nonlinear behavior in terms of the stacking sequence of the composite section of the metal-composite square hybrid tube (a result which was predictable based on the numerical results in Table 3-7). The exact maximum values for the crashworthiness functions are shown in Table 3-8 along with the corresponding values for θ_1 and θ_2.

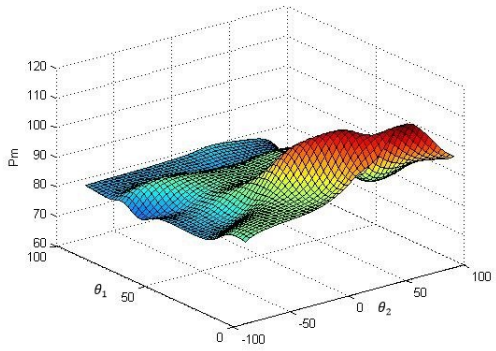

(a)

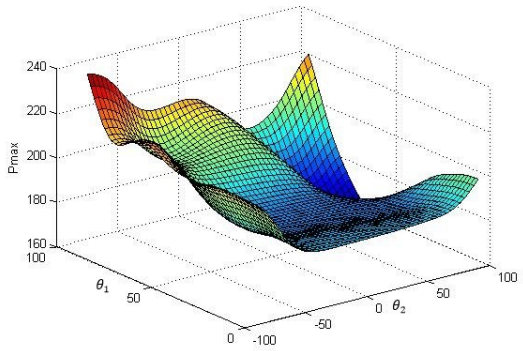

(b)

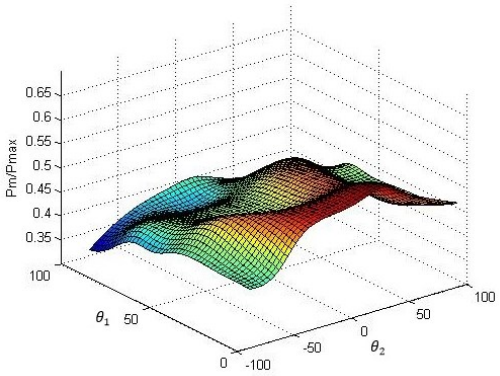

(c)

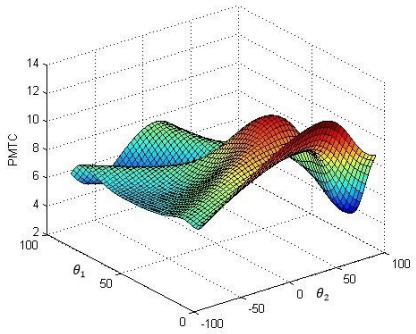

(d)

Fig. 3-14. Response surfaces of a) mean crushing load, b) Maximum load and c) load efficiency factor d) PMTC

Table 3-8. Optimized design variables for each crashworthiness function

Crashworthiness function	θ_1	θ_2	Maximum value
P_m	0	48	113
P_{max}	90	-90	240
$\frac{P_m}{P_{max}}$	0	25	0.554
PMTC	0	33	12.6

The non-dominated sorting genetic algorithm (NSGA-II) [110] was selected as the optimization algorithm to attain the Pareto optimal set. NSGA-II ranks solutions with fast non-dominated arrangement and assigns weight based values on their ranks [91]. In order to obtain results with good repeatability, the algorithm was executed several times. The resulting Pareto optimal solutions are demonstrated in Fig. 3-15 and they explain the trade-off between mean crushing load and load efficiency factor. Each point in this figure represents a possible optimal solution with a unique set of design variables.

The three optimum points were selected as examples of θ_1 and θ_2. The stacking sequence $[90/0/45/0]_{4s}$ has the highest mean crushing load and the stacking sequence $[90/2/25/0]_{4s}$ has the maximum ratio between the mean crushing load and the maximum load in the optimal solutions. The stacking sequence $[90/5/30/0]_{4s}$ has the maximum value of the product of the two optimized functions. The appropriate choice may be governed by manufacturing restrictions. For instance, the filament winding technique may not to be able to achieve small off-axis angles. In addition the spatial (geometric) constraints may limit the thickness of the FRP section. Furthermore, the FRP thickness drives the cost of the raw materials.

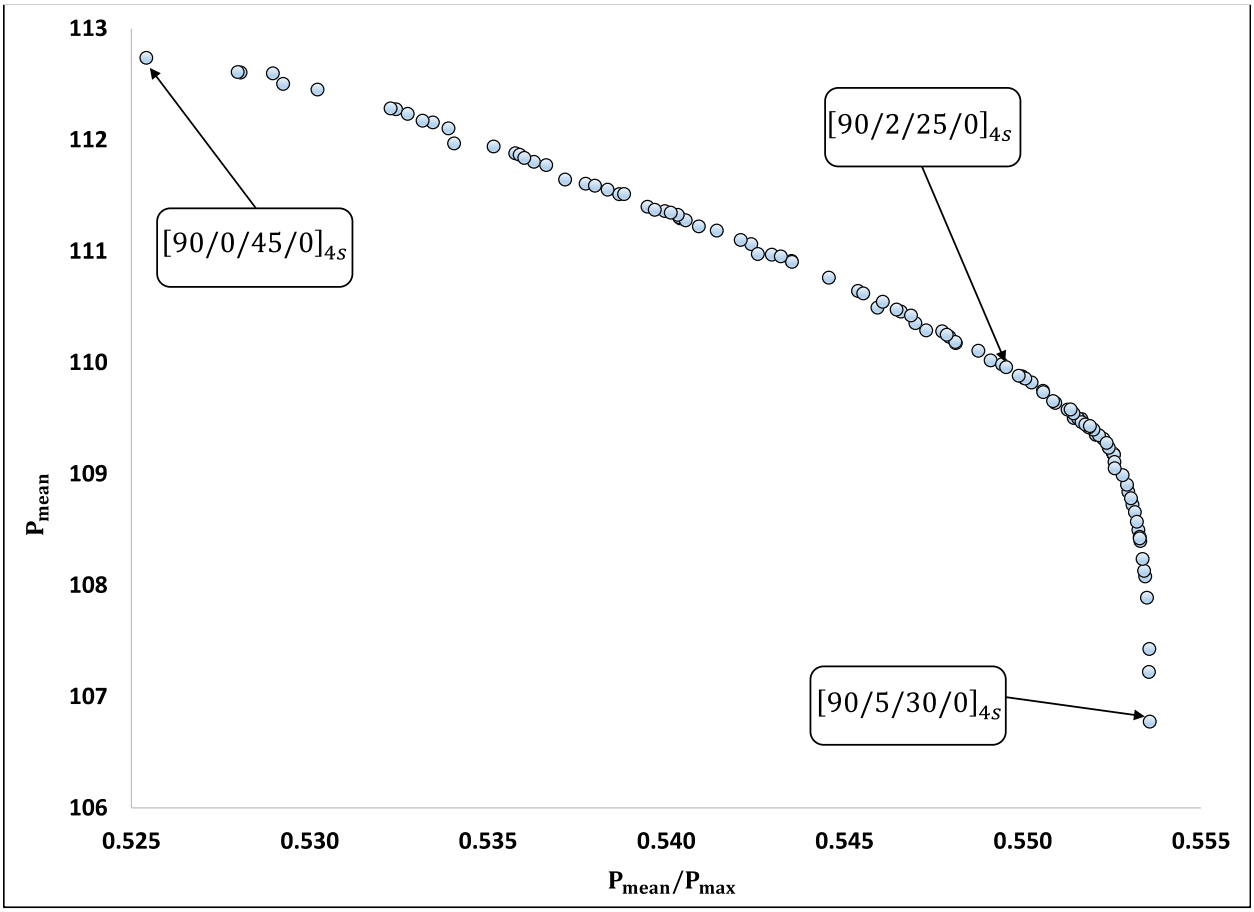

Fig. 3-15. Pareto optimal solutions of the defined multi-objective optimization problem

3.6. Conclusion

The effects of thickness and stacking sequence of the composite section of the 304 stainless steel-S2 glass/epoxy square hybrid tube were studied on crashworthiness functions including energy absorption, mean crushing load, maximum load, and the ratio between the difference of mean crushing load of hybrid and metal tube and thickness of the FRP section numerically using LS-DYNA software to reduce the costly time-consuming experimental methods. The resultant functions were compared with previously obtained experimental results to produce a reliable model.

The simulated responses were shown to be highly non-linear with the variables, making the design process challenging. To represent the non-linear relations, 3 neural networks were created using simulated functions of 39 different combinations of stacking sequences for the composite section. Two multi-objective optimization problems were introduced: 1) mean crushing load and load efficiency factor and 2) PMTC and load efficiency factor. In each case, maximum crushing load was used as the constraint. Design variables were chosen as θ_1 and θ_2 in the $[90/\theta_1/\theta_2/0]_{ns}$ $(-90 < \theta_i < 90, n = 4)$ stacking sequence. The non-dominated sorting genetic algorithm (NSGA-II) was used to optimize the design variables and the results were represented as Pareto Frontier solutions. While the crashworthiness functions except for maximum load show nonlinear behavior with respect to the design variables, they exhibit plateaus for the $[90/\theta_1/\theta_2/0]_{4s}$ stacking sequence in the range where $0 < \theta_1 < 5$ and $25 < \theta_2 < 45$. This resulted in very narrow series of optimized points for multi-objective optimization problem.

In this study, for the sake of computational cost, only one shell element was used through the thickness of the composite section. As a result, it was not possible to model delamination and frictional dissipated energy between delaminated layers. Despite this limitation, the relatively simple numerical model was able to reproduce the failure modes and load-displacement results for different configurations. In addition, it can provide a better estimate of the mean crush load for metal composite hybrid tubes than analytical modeling of the mean crushing load of metal-composite hybrid tubes using equivalent bending stiffness and strength of the hybrid section [115]. Future studies provide the opportunity to use tie-break

contact interfaces (simulating cohesive zone models) or thick shell elements in LS-DYNA to predict the remaining experimental failure modes such as delamination.

Chapter 4

4. Conclusion and future work

4.1. Conclusion

The available methods to predict the energy absorption of metal-composite tubes having different constituents (fiber and matrix materials), fiber orientations, and stacking sequence for the FRP section and different geometrical parameters are either deficient or numerically/experimentally expensive, limiting their applicability. Experimental methods coupled with numerical simulations or analytical modeling may able to shed some lights on the effect of each design variables on different crashworthiness functions such as maximum crushing load, mean crushing load, and specific energy absorption (SEA). However, it was previously shown that the relationships between the design variables and crashworthiness functions are complex and sometimes counterintuitive which make the design process complicated.

In this study, the effects of different stacking sequences and thicknesses on the collapse mode, the crushing load efficiency, and the specific absorbed energy of hybrid tubes were experimentally investigated in comparison with bare metal square tubes. It was shown that overwrapping a composite around the stainless steel metal tube can (1) change its collapse mode from a splitting mode (with very low energy absorption) to a symmetric or mixed mode (with much higher energy absorption) and (2) lower the load oscillation around the mean crushing load. The greater effect of FRP strengthening on slender metal tubes was also emphasized. Based on experiments, it was shown that number of layers of the FRP section has a significant effect the energy absorption of the hybrid tubes. Furthermore, a new triggering mechanism was developed that changed the collapse mode to a symmetric mode and as a result improved the crush load efficiency in hybrid square tubes.

In general, the experimental results indicate that the thickness of the metal and FRP sections and the stacking sequence of the composite section in the hybrid tubes is significant and complicated enough to justify the development of a model of the response. Such a model can help explain counterintuitive behavior (including the reduced energy absorption exhibited by tubes with 8 layers of composite). Therefore, the experimental results for different configurations of fiber orientation and stacking sequences [103] were used to build a numerical model [116]. The steel tube was meshed using $1\,\text{mm} \times 1\,\text{mm}$ 8-noded hexahedral solid elements (based on a mesh convergence study) using ELFORM=1 (in solid element formulation) with hourglass control to prevent zero-energy shapes. The FRP section in the hybrid tubes was meshed with $1\,\text{mm} \times 1\,\text{mm}$ reduced integration Belytschko-Tsay shell elements that can capture the response of each layer by an integration point. Lamination shell theory was also activated in the elements to simulate the shear stress through the thickness. The models were validated with experimental results under quasi-static crushing for different stacking sequences and thicknesses. The effect of stacking sequence and thickness of the composite section on crashworthiness functions including energy absorption, mean crushing load, maximum load, and the ratio between the difference of mean crushing load of hybrid and metal tube and thickness of the FRP section and failure modes of the hybrid tubes were explained using the numerical model.

The simulated responses were shown to be highly non-linear with respect to the input variables, making the design process challenging. To represent the non-linear relations between crashworthiness functions and design variables, 4 neural networks were created using simulated functions of 41 different combinations of stacking sequence for the FRP sections. It was show that the maximum relative error between the numerical and simulated objective functions (mean crushing load, maximum load and PMTC) were 9.4%, 7.5% and 10.6%, respectively. To find a best combination of design variables, two multi-objective optimization problems were introduced using: 1) mean crushing load and load efficiency factor and 2) PMTC and load efficiency factor in which

$$PMTC = \frac{P_m\ of\ hybrid\ tube\ -\ P_m\ of\ metal\ tube}{Thickness\ of\ the\ composite\ section}$$

In each case, maximum crushing load was used as the constraint (introduced by the maximum allowable load by the testing frame). Design variables were chosen as θ_1 and θ_2 in the $[90/\theta_1/\theta_2/0]_{ns}$ $(-90 < \theta_i < 90, n = 4)$ stacking sequence. The stacking sequence was chosen to include 0° and 90° layers. 90° layer was used to avoid the splitting mode for the metal section at the same time to absorb energy by fiber fracture failure mode. A 0° layer was used in the direction of loading to make the tube stiffer in the process of progressive lobe formation. The non-dominated sorting genetic algorithm (NSGA-II) was used to optimize the design variables and the results were represented as Pareto Frontier solutions. While the crashworthiness functions except for maximum load show nonlinear behavior with respect to the design variables, they exhibit plateaus for the $[90/\theta_1/\theta_2/0]_{4s}$ stacking sequence in the range where $0 < \theta_1 < 5$ and $25 < \theta_2 < 45$. This resulted in very narrow series of optimized points for multi-objective optimization problem.

For the sake of computational cost, only a single shell element was used through the thickness of the composite section. As a result, it was not possible to model delamination and frictional dissipated energy between delaminated layers. Despite this limitation, the relatively simple numerical model was able to reproduce the failure modes and load-displacement results for different configurations. In addition, it can provide a better estimate of the mean crush load for metal composite hybrid tubes than analytical modeling of the mean crushing load of metal-composite hybrid tubes using equivalent bending stiffness and strength of the hybrid section [115].

Finally, a parametric study has been conducted using the current developed model to identify the role of each involving material property such as tensile/compressive stiffness and strength, ductility, etc. on energy absorption of metal-composite square tubes.

4.2. Future work

Previous studies have indicated that delamination itself does not significantly affect the energy absorption but it causes the delaminated layers to slide on each other and produce frictional energy dissipation [87]. The effect of fiber orientation and stacking sequence on delamination, and as result the effect of delamination and the frictional dissipation energy

between delaminated layers on crashworthiness parameters needs to be addressed numerically and experimentally. Because of computational cost of using one solid or shell element for each layer, experimental configurations should be designed to confirm if there is a chance of modeling the failure mode. For instance, a $[[\theta_1]_4/[\theta_2]_4/[\theta_3]_4/[\theta_4]_4]$ stacking sequence can be used and each 4 layers could be modeled by just one shell element. Another potential approach is utilizing new layered solid element formulation in LS-DYNA: TSHELL elements. The element is basically layered solid element which has 8 nodes as the same as solid elements and uses 3D stress state [117]. One layer of TSHELL elements were able to predict the delamination effect load-displacement data.

To facilitate the prediction of crashworthiness functions, an analytical model can be developed for metal-composite square hybrid tubes which considers the effect of fiber orientation and stacking sequence of FRP section. Theoretical modeling of mean crushing load of metal, composite and metal-composite hybrid tubes with different geometries have been studied in different papers [12, 13, 16, 115, 118-123]. Wierzbicki and Abramowicz [119] presented crushing behavior of square metal tubes by a self-consistent method and a kinematic method of plasticity with a constant value of flow stress σ_0 which considered the tube material as rigid-perfectly plastic. Energy was dissipated by extensional and inextensional deformations at stationary and moving plastic hinge lines. Finally, mean crushing load was calculated based on flow stress and geometrical dimensions. In another study [122], the authors studied the diamond failure mode of metal-composite cylindrical tubes to derive the mean crushing load for one layer of composite having fiber orientation in hoop direction. The composite part was considered as perfectly plastic material in the calculation. Mirzaei et al. [115] extended the approach and used Tsai-Hill failure criteria to model the mean crushing load for a metal-composite cylindrical tube having an arbitrary stacking sequence and fiber orientation for each layer. The model developed by Mirzaei et al. considered all layers to fail at the same time to determine the neutral axis needed to calculate the equivalent bending stiffness of the metal-composite wall. However, using the combination of elastica based theory and progressive failure of FRP may be a more reasonable approach. Abramowicz utilized an Elastica based theory to predict plastic

deformation (lob formation) of metal square tubes [118]. Strain in each layer of FRP section can be compared with calculated strain (derived from predicted lob formation by Abramowicz [118]) in each region of the metal section to define a progressive failure for the FRP section having an arbitrary stacking sequence and fiber orientation for each layer.

The bond between the metal and composite sections is often the weakest point in crushing process and may lead to very low energy absorption. The effect of surface preparation, bonding using adhesives, and the effect of humidity and temperature on the bonding needs to be studied experimentally and numerically [74, 75].

In this work, the stainless steel square tubes employed were bent, welded, and formed from metal sheets. The process could introduce pre-stress in the metal tube. Additionally, in the curing process of composite section on stainless steel, different coefficients of thermal expansion of metal and composite section may introduce residual stresses that impact the subsequent failure behavior. Modeling of manufacturing process is a challenging task because it requires a great deal of information such as material properties as a function of temperature in heating and cooling processes. However, development of accurate models of this process would enable engineers to design better energy absorption elements.

In this study [116], the capability of Digital Image Correlation (DIC) to measure the effect of machine compliance, sample alignment, and in-plane strains on the stainless steel square tubes was shown but not investigated in-detail. In-plane strains and failure modes in the form of displacements measured by DIC could be used to provide a complementary data for the modeling process of energy absorption elements tested under quasi-static and impact loadings.

Finally, in this work, to train the back propagation artificial neural networks, Levenberg-Marquardt method was used. In general, it is very hard to decide which training algorithm is the fastest for a problem because of the complexity of problem, the error goal, the number of variables, and the number of objective functions. However, there are other methods such as Resilient Backpropagation, Scaled Conjugate Gradient, Polak-Ribiére Conjugate Gradient, etc. [113] that may speed up the training process. Hence, a comparison should be made

between different methods to define the best one in terms of computational cost and accuracy for a specific problem.

5.Appendix

The effect of geometrical parameters such as thickness, ratio between square side and thickness, and the length of the square metal, composite and hybrid tubes have been

reported before [13, 18, 48, 51, 64, 103, 118, 124]. In order to define the effect of different material properties of the FRP section on crashworthiness functions or load-displacement results of glass/epoxy 304 stainless steel hybrid square tubes, a parametric study was done. The study assists to understand if crashworthiness functions and failure modes are sensitive to significant variation of each material property. A physical range was defined for each material property based on the reported properties of glass fiber reinforced plastics in literature [18, 88, 125]. The material properties in Table 5-1 for M21-37%/7581 and M21-45%/120 composites were obtained from Hexcel corporation website.

Table 5-1. Reported properties for different types of glass fiber/epoxy composites

	E_{ft} GPa	E_{mt} GPa	G_{12} GPa	X_t MPa	X_c MPa	Y_t MPa	Y_c MPa	ε_{ft} %	ε_{fc} %	S MPa
S2-glass/8552 [116]	46.5	12.1	4.47	1480	820	40.2	145	3.28	1.84	149
M21-37%/7581	25.5	-	-	444	692	-	-	-	-	-
M21-45%/120	24.8	-	-	320	674	-	-	-	-	-
E-glass/epoxy [88]	30.9	8.3	2.8	798	480	40	140	-	-	70
Glass/polyester [18]	33.5	8	5	400	200	30	50	-	-	30
E-glass/epoxy [125]	45	12	5.5	1020	620	40	140	2.3	1.4	70
S-glass/epoxy [125]	55	16	7.6	1620	690	40	140	2.9	1.3	80

To do the parametric study, S2-glass/8552 304 stainless steel hybrid square tube with $[90/-45/45/0]_{2s}$ was chosen as the base configuration. Table 5-2 shows the selected values

for each material property for parametric study. As a result, the load-displacement data of the base configuration was compared with the variations in each property.

Table 5-2. selected values for each material property of glass/epoxy composites

Property	Description	Range
E_{ft}	Young's modulus in fiber direction under tensile loading (GPa)	25, 35, and 55
E_{mt}	Young's modulus in transverse direction under tensile loading (GPa)	8 and 10.677
G_{12}	In-plane shear modulus (GPa)	3 and 6
X_t	Tensile strength in fiber direction (MPa)	400, 900, and 1900
X_c	Compressive strength in fiber direction (MPa)	200, 500 and 1100
Y_t	Tensile strength in transverse direction (MPa)	30 and 50
Y_c	Compressive strength in transverse direction (MPa)	50, 80, and 110
ε_{ft}	Strain at failure in fiber direction under tensile loading (%)	2, 3, and 5
ε_{fc}	Strain at failure in fiber direction under compressive loading (%)	1, 1.5, and 2.5
S	In-plane shear strength (MPa)	30, 50, and 110

Changing E_{mt}, G_{12}, FAILT, X_t, Y_t, and S did not show any significant change in load-displacement data compared with the base configuration (no change in load variation and mean crushing load which confirm the same failure modes). In fact, making the material of matrix brittle/ductile or weaker/stronger in tensile direction did not alter the crashworthiness functions. In addition, considering the effect of changing the shear strength

of the FRP section on tensile fiber mode, tensile matrix mode, and compressive matrix mode in Chang-Chang failure criterion employed in MAT 54 material model [11] and using $[90/-45/45/0]_{2s}$ stacking sequence, the results show that shear strength is not an effective parameter in crushing process which was not anticipated. This suggest that shearing is not a dominant failure mode or the MAT 54 material mode were not able to capture the failure mode which is expected considering no specific shear-related criteria in the model.

Contrary to small effect of tensile strength in fiber direction and tensile strain-to-failure in fiber direction, the same quantities in compressive direction not only change the load-displacement data including the maximum and mean crushing loads (Fig. 5-1 and 5-2) but they are able to change the failure modes to global buckling after two successive symmetric failure modes (Fig 5-3). By increasing DFAILC (compressive strain-to-failure) from the base value (1.84%) to 2.5%, the maximum load and mean crushing load were also increased.

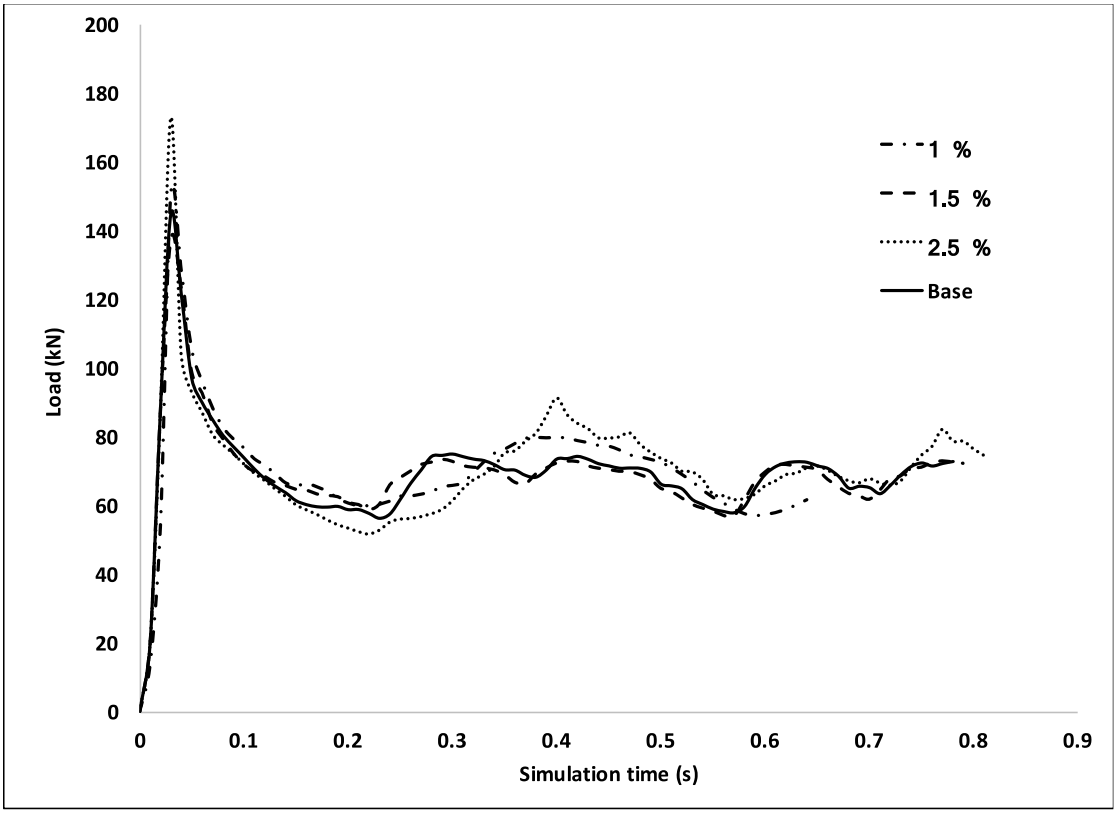

Fig 5-1. Effect DFAILC on the load-displacement data

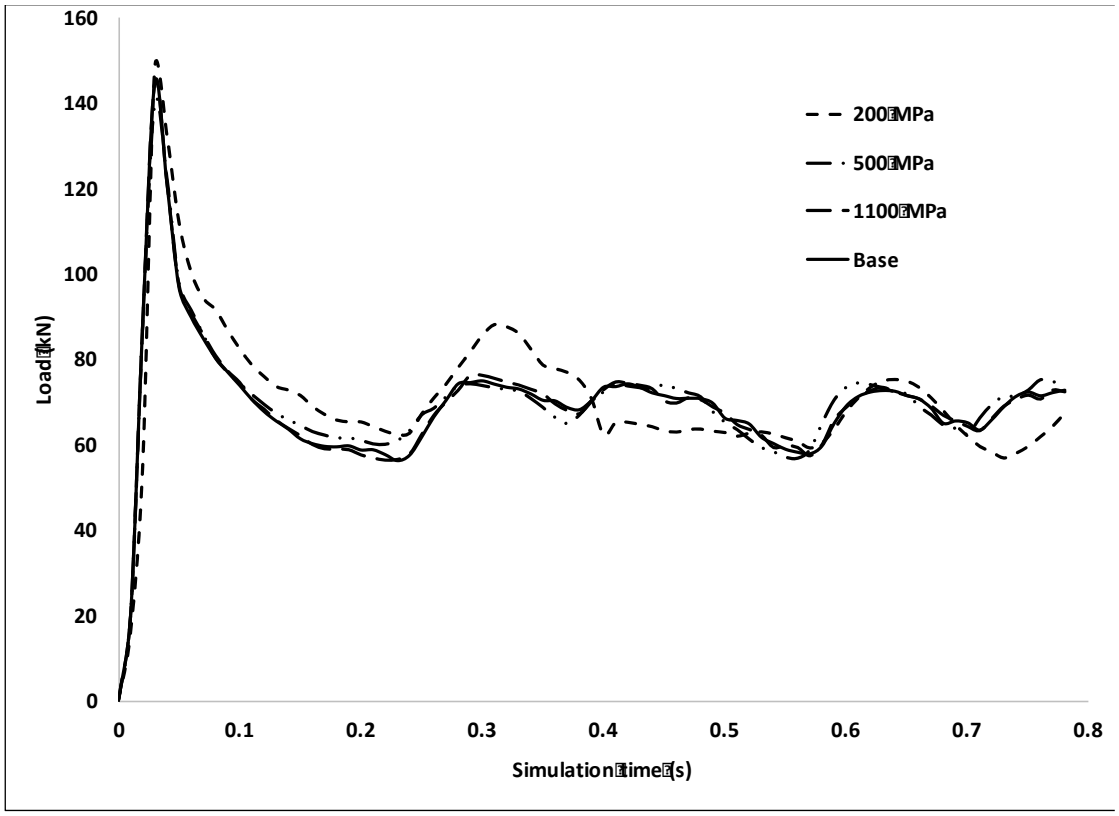

Fig 5-2. Effect of compressive strength in fiber direction on load-displacement data

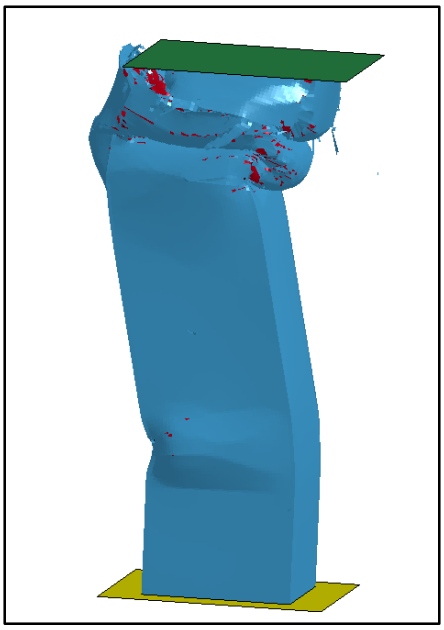

Fig 5-3. Change the failure mode to global buckling as a reason of changing DFAILC to 1%

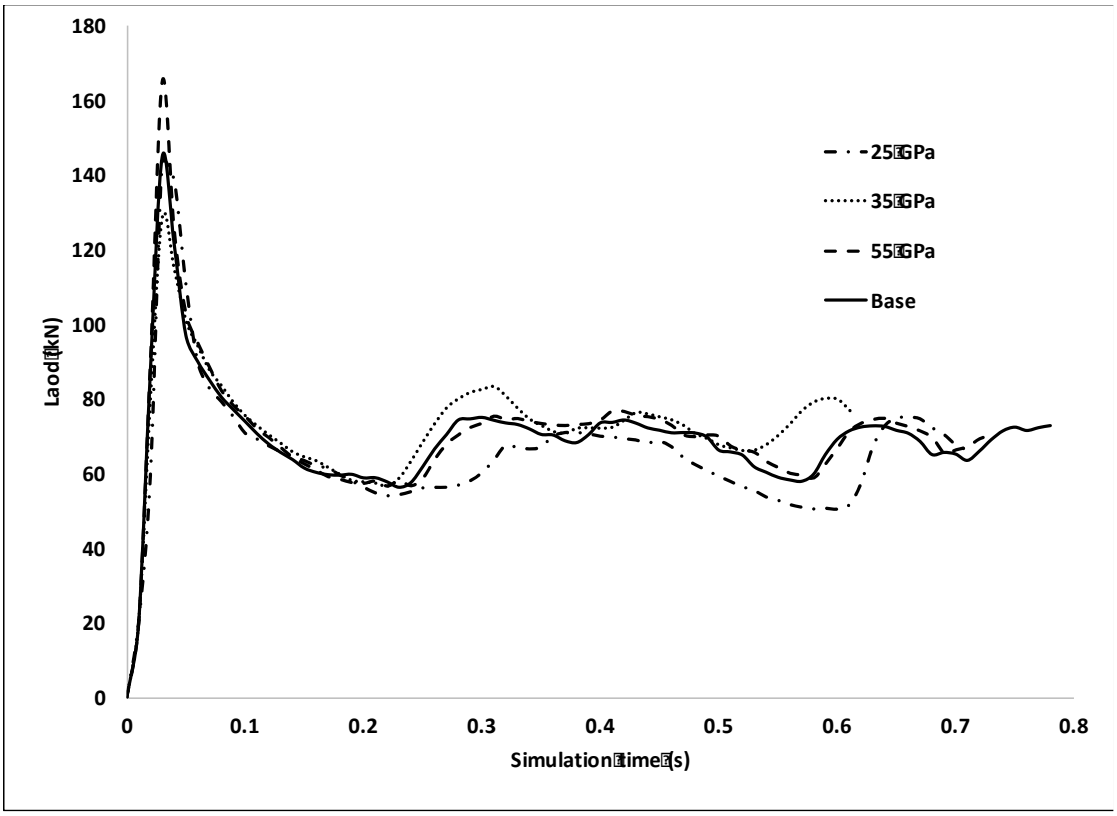

Fig 5-4. Young's modulus in fiber direction under tensile loading on load-displacement data

Based on the results, properties of FRP section in fiber direction under compressive loading have effect on crashworthiness function of the hybrid tubes. However, there is no clear relationship between the functions and the properties. In addition, the limited range of reported values for the properties in literature makes it hard to make a concrete conclusion.

6. References

[1] Lu G, Yu T. Energy absorption of structures and materials: Elsevier, 2003.

[2] Mahdi E, Sebaey T. An experimental investigation into crushing behavior of radially stiffened GFRP composite tubes. Thin-Walled Structures. 2014;76:8-13.

[3] Mamalis AG, Manolakos D, Demosthenous G, Ioannidis M. Crashworthiness of composite thin-walled structures: CRC Press, 1998.

[4] Feraboli P, Masini A. Development of carbon/epoxy structural components for a high performance vehicle. Composites Part B: Engineering. 2004;35:323-30.

[5] Thornton P, Jeryan R. Crash energy management in composite automotive structures. International Journal of Impact Engineering. 1988;7:167-80.

[6] Niknejad A, Assaee H, Elahi SA, Golriz A. Flattening process of empty and polyurethane foam-filled E-glass/vinylester composite tubes–An experimental study. Composite Structures. 2013;100:479-92.

[7] Kathiresan M, Manisekar K, Manikandan V. Crashworthiness analysis of glass fibre/epoxy laminated thin walled composite conical frusta under axial compression. Composite Structures. 2014;108:584-99.

[8] Mamalis A, Robinson M, Manolakos D, Demosthenous G, Ioannidis M, Carruthers J. Crashworthy capability of composite material structures. Composite Structures. 1997;37:109-34.

[9] Bisagni C, Di Pietro G, Fraschini L, Terletti D. Progressive crushing of fiber-reinforced composite structural components of a Formula One racing car. Composite Structures. 2005;68:491-503.

[10] Kim JS, Yoon HJ, Shin KB. A study on crushing behaviors of composite circular tubes with different reinforcing fibers. International Journal of Impact Engineering. 2011;38:198-207.

[11] Feraboli P, Masini A. Development of carbon/epoxy structural components for a high performance vehicle. Composites Part B-Engineering. 2004;35:323-30.

[12] Song HW, Wan ZM, Xie ZM, Du XW. Axial impact behavior and energy absorption efficiency of composite wrapped metal tubes. International Journal of Impact Engineering. 2000;24:385-401.

[13] Shin KC, Lee JJ, Kim KH, Song MC, Huh JS. Axial crush and bending collapse of an aluminum/GFRP hybrid square tube and its energy absorption capability. Composite Structures. 2002;57:279-87.
[14] Kalhor R, Akbarshahi H, Case SW. Multi-Objective Optimization of Axial Crush Performance of Square Metal–Composite Hybrid Tubes. ASME 2013 International Mechanical Engineering Congress and Exposition: American Society of Mechanical Engineers; 2013. p. V009T10A35-VT10A35.
[15] Mamalis AG, Manolakos DE, Ioannidis MB, Papapostolou DP. On the response of thin-walled CFRP composite tubular components subjected to static and dynamic axial compressive loading: experimental. Composite Structures. 2005;69:407-20.
[16] Bambach MR, Elchalakani M. Plastic mechanism analysis of steel SHS strengthened with CFRP under large axial deformation. Thin-Walled Structures. 2007;45:159-70.
[17] Bambach MR, Elchalakani M, Zhao XL. Composite steel-CFRP SHS tubes under axial impact. Composite Structures. 2009;87:282-92.
[18] Palanivelu S, Van Paepegem W, Degrieck J, Vantomme J, Kakogiannis D, Van Ackeren J, et al. Crushing and energy absorption performance of different geometrical shapes of small-scale glass/polyester composite tubes under quasi-static loading conditions. Composite Structures. 2011;93:992-1007.
[19] Zhao XL, Zhang L. State-of-the-art review on FRP strengthened steel structures. Engineering Structures. 2007;29:1808-23.
[20] Hollaway LC, Cadei J. Progress in the technique of upgrading metallic structures with advanced polymer composites. Progress in Structural Engineering and Materials. 2002;4:131-48.
[21] Meredith J, Bilson E, Powe R, Collings E, Kirwan K. A Performance Versus Cost Analysis of Prepreg Carbon Fibre Epoxy Energy Absorption Structures. Composite Structures. 2015.
[22] McGregor C, Vaziri R, Xiao XR. Finite element modelling of the progressive crushing of braided composite tubes under axial impact. International Journal of Impact Engineering. 2010;37:662-72.
[23] Ochelski S, Gotowicki P. Experimental assessment of energy absorption capability of carbon-epoxy and glass-epoxy composites. Composite Structures. 2009;87:215-24.

[24] Deslauriers P. Numerical modeling of composite structures for advanced automotive applications 2006.
[25] Mamalis A, Manolakos D, Demosthenous G, Ioannidis M. Analysis of failure mechanisms observed in axial collapse of thin-walled circular fibreglass composite tubes. Thin-Walled Structures. 1996;24:335-52.
[26] Mamalis A, Manolakos D, Ioannidis M, Papapostolou D. Crashworthy characteristics of axially statically compressed thin-walled square CFRP composite tubes: experimental. Composite Structures. 2004;63:347-60.
[27] Mamalis A, Manolakos D, Ioannidis M, Papapostolou D. On the experimental investigation of crash energy absorption in laminate splaying collapse mode of FRP tubular components. Composite Structures. 2005;70:413-29.
[28] Fairfull A, Hull D. Energy absorption of polymer matrix composite structures- Frictional effects. Structural Failure. 1989:255-79.
[29] Hull D. A Unified Approach to Progressive Crushing of Fiber-Reinforced Composite Tubes. Composites Science and Technology. 1991;40:377-421.
[30] Mamalis A, Manolakos D, Demosthenous G, Ioannidis M. The static and dynamic axial crumbling of thin-walled fibreglass composite square tubes. Composites Part B: Engineering. 1997;28:439-51.
[31] Mamalis A, Manolakos D, Demosthenous G, Ioannidis M. Analytical modelling of the static and dynamic axial collapse of thin-walled fibreglass composite conical shells. International Journal of Impact Engineering. 1997;19:477-92.
[32] Ghasemnejad H, Blackman BRK, Hadavinia H, Sudall B. Experimental studies on fracture characterisation and energy absorption of GFRP composite box structures. Composite Structures. 2009;88:253-61.
[33] Savona SC, Hogg P. Effect of fracture toughness properties on the crushing of flat composite plates. Composites Science and Technology. 2006;66:2317-28.
[34] Farley GL. Effect of Fiber and Matrix Maximum Strain on the Energy-Absorption of Composite-Materials. Journal of Composite Materials. 1986;20:322-34.
[35] Farley GL. Energy absorption of composite materials. Journal of Composite Materials. 1983;17:267-79.

[36] Hamada H, Coppola JC, Hull D, Maekawa Z, Sato H. Comparison of Energy-Absorption of Carbon Epoxy and Carbon Peek Composite Tubes. Composites. 1992;23:245-52.
[37] Warrior N, Turner T, Robitaille F, Rudd C. Effect of resin properties and processing parameters on crash energy absorbing composite structures made by RTM. Composites Part A: applied science and manufacturing. 2003;34:543-50.
[38] Ataollahi S, Taher ST, Eshkoor RA, Ariffin AK, Azhari CH. Energy absorption and failure response of silk/epoxy composite square tubes: Experimental. Composites Part B-Engineering. 2012;43:542-8.
[39] Mamalis A, Manolakos D, Viegelahn G. The axial crushing of thin PVC tubes and frusta of square cross-section. International Journal of Impact Engineering. 1989;8:241-64.
[40] Hull D. A unified approach to progressive crushing of fibre-reinforced composite tubes. Composites Science and Technology. 1991;40:377-421.
[41] Ramakrishna S. Microstructural design of composite materials for crashworthy structural applications. MATERIALS & DESIGN. 1997;18:167-73.
[42] Berry J, Hull D. Effect of speed on progressive crushing of epoxy glass cloth tubes. INSTITUTE OF PHYSICS CONFERENCE SERIES: PLENUM PUBL CORP 233 SPRING ST, NEW YORK, NY 10013; 1984. p. 463-70.
[43] Bejan L, Poterasu VF. Woven composite material design by orthotropic compliance averaging method using mathematica. Computer Methods in Applied Mechanics and Engineering. 1999;179:53-65.
[44] Fairfull AH, Hull D. Effects of Specimen Dimensions on the Specific Energy Absorption of Fibre Composite Tubes. In: Matthews FL, Buskell NCR, Hodgkinson JM, Morton J, editors. Sixth International Conference on Composite Materials. London, United Kingdom: Elsevier; 1987. p. 3.36-3.45.
[45] Babbage JM, Mallick PK. Static axial crush performance of unfilled and foam-filled aluminum-composite hybrid tubes. Composite Structures. 2005;70:177-84.
[46] Farley GL. Effect of Specimen Geometry on the Energy Absorption Capability of Composite Materials. Journal of Composite Materials. 1986;20:390-400.

[47] Mamalis A, Manolakos D, Viegelahn G. Crashworthy behaviour of thin-walled tubes of fibreglass composite materials subjected to axial loading. Journal of Composite Materials. 1990;24:72-91.
[48] Farley GL. Effect of Specimen Geometry on the Energy-Absorption Capability of Composite-Materials. Journal of Composite Materials. 1986;20:390-400.
[49] Hamada H, Ramakrishna S. Scaling effects in the energy absorption of carbon-fiber peek composite tubes. Composites Science and Technology. 1995;55:211-21.
[50] Mamalis A, Manolakos D, Demosthenous G, Ioannidis M. Energy absorption capability of fibreglass composite square frusta subjected to static and dynamic axial collapse. Thin-Walled Structures. 1996;25:269-95.
[51] Abdewi EF, Sulaiman S, Hamouda A, Mahdi E. Effect of geometry on the crushing behaviour of laminated corrugated composite tubes. Journal of materials processing technology. 2006;172:394-9.
[52] Thornton PH. The Crush Behavior of Pultruded Tubes at High-Strain Rates. Journal of Composite Materials. 1990;24:594-615.
[53] Mamalis A, Manolakos D, Ioannidis M, Papapostolou D. On the response of thin-walled CFRP composite tubular components subjected to static and dynamic axial compressive loading: experimental. Composite Structures. 2005;69:407-20.
[54] Farley GL. The Effects of Crushing Speed on the Energy-Absorption Capability of Composite Tubes. Journal of Composite Materials. 1991;25:1314-29.
[55] Laananen DH, Winkelman KL. Analysis of energy-absorbing seat configurations for aircraft. International Journal of Crashworthiness. 1996;1:355-68.
[56] Lau STW, Said MR, Yaakob MY. On the effect of geometrical designs and failure modes in composite axial crushing: A literature review. Composite Structures. 2012;94:803-12.
[57] Palanivelu S, Van Paepegem W, Degrieck J, Van Ackeren J, Kakogiannis D, Van Hemelrijck D, et al. Experimental study on the axial crushing behaviour of pultruded composite tubes. Polymer Testing. 2010;29:224-34.
[58] Feraboli P. Development of a Corrugated Test Specimen for Composite Materials Energy Absorption. Journal of Composite Materials. 2008;42:229-56.

[59] Eshkoor RA, Oshkovr SA, Sulong AB, Zulkifli R, Ariffin AK, Azhari CH. Effect of trigger configuration on the crashworthiness characteristics of natural silk epoxy composite tubes. Composites Part B-Engineering. 2013;55:5-10.
[60] Siromani D, Henderson G, Mikita D, Mirarchi K, Park R, Smolko J, et al. An experimental study on the effect of failure trigger mechanisms on the energy absorption capability of CFRP tubes under axial compression. Composites Part A: applied science and manufacturing. 2014;64:25-35.
[61] Cheng Q, Altenhof W, Li L. Experimental investigations on the crush behaviour of AA6061-T6 aluminum square tubes with different types of through-hole discontinuities. Thin-Walled Structures. 2006;44:441-54.
[62] El-Hage H, Mallick PK, Zamani N. A numerical study on the quasi-static axial crush characteristics of square aluminum tubes with chamfering and other triggering mechanisms. International Journal of Crashworthiness. 2005;10:183-95.
[63] Qureshi OM, Bertocchi E. Crash behavior of thin-Walled box beams with complex sinusoidal relief patterns. Thin-Walled Structures. 2012;53:217-23.
[64] Lee S, Hahn CS, Rhee M, Oh JE. Effect of triggering on the energy absorption capacity of axially compressed aluminum tubes. Materials & Design. 1999;20:31-40.
[65] Hou T, Pearce G, Prusty B, Kelly D, Thomson R. Pressurised composite tubes as variable load energy absorbers. Composite Structures. 2015;120:346-57.
[66] Warrior NA, Turner TA, Robitaille F, Rudd CD. Effect of resin properties and processing parameters on crash energy absorbing composite structures made by RTM. Composites Part a-Applied Science and Manufacturing. 2003;34:543-50.
[67] Daniel L, Hogg P, Curtis P. The crush behaviour of carbon fibre angle-ply reinforcement and the effect of interlaminar shear strength on energy absorption capability. Composites Part B: Engineering. 2000;31:435-40.
[68] Hadavinia H, Ghasemnejad H. Effects of Mode-I and Mode-II interlaminar fracture toughness on the energy absorption of CFRP twill/weave composite box sections. Composite Structures. 2009;89:303-14.
[69] Farley GL. Energy-Absorption of Composite-Materials. Journal of Composite Materials. 1983;17:267-79.

[70] Warrior N, Turner T, Robitaille F, Rudd C. The effect of interlaminar toughening strategies on the energy absorption of composite tubes. Composites Part A: applied science and manufacturing. 2004;35:431-7.
[71] Solaimurugan S, Velmurugan R. Progressive crushing of stitched glass/polyester composite cylindrical shells. Composites Science and Technology. 2007;67:422-37.
[72] Thornton P, Edwards P. Energy absorption in composite tubes. Journal of Composite Materials. 1982;16:521-45.
[73] Bambach MR. Axial capacity and crushing behavior of metal-fiber square tubes - Steel, stainless steel and aluminum with CFRP. Composites Part B-Engineering. 2010;41:550-9.
[74] Hollaway L, Cadei J. Progress in the technique of upgrading metallic structures with advanced polymer composites. Progress in Structural Engineering and Materials. 2002;4:131-48.
[75] Bouchet J, Jacquelin E, Hamelin P. Dynamic axial crushing of combined composite aluminium tube: the role of both reinforcement and surface treatments. Composite Structures. 2002;56:87-96.
[76] Kim HC, Shin DK, Lee JJ, Kwon JB. Crashworthiness of aluminum/CFRP square hollow section beam under axial impact loading for crash box application. Composite Structures. 2014;112:1-10.
[77] Aidi B, Case SW. Experimental and Numerical Analysis of Notched Composites Under Tension Loading. Applied Composite Materials. 2015;22:837-55.
[78] McGregor CJ, Vaziri R, Poursartip A, Xiao X. Simulation of progressive damage development in braided composite tubes under axial compression. Composites Part a-Applied Science and Manufacturing. 2007;38:2247-59.
[79] Mamalis AG, Manolakos DE, Ioannidis MB, Papapostolou DP. The static and dynamic axial collapse of CFRP square tubes: Finite element modelling. Composite Structures. 2006;74:213-25.
[80] Xiao XR. Modeling Energy Absorption with a Damage Mechanics Based Composite Material Model. Journal of Composite Materials. 2009;43:427-44.
[81] Xiao X, Botkin ME, Johnson NL. Axial crush simulation of braided carbon tubes using MAT58 in LS-DYNA. Thin-Walled Structures. 2009;47:740-9.

[82] Feraboli P, Wade B, Deleo F, Rassaian M, Higgins M, Byar A. LS-DYNA MAT54 modeling of the axial crushing of a composite tape sinusoidal specimen. Composites Part A: applied science and manufacturing. 2011;42:1809-25.
[83] Palanivelu S, Van Paepegem W, Degrieck J, Kakogiannis D, Van Ackeren J, Van Hemelrijck D, et al. Parametric study of crushing parameters and failure patterns of pultruded composite tubes using cohesive elements and seam, Part I: Central delamination and triggering modelling. Polymer Testing. 2010;29:729-41.
[84] Palanivelu S, Van Paepegem W, Degrieck J, Van Ackeren J, Kakogiannis D, Wastiels J, et al. Parametric study of crushing parameters and failure patterns of pultruded composite tubes using cohesive elements and seam: Part II - Multiple delaminations and initial geometric imperfections. Polymer Testing. 2010;29:803-14.
[85] Siromani D, Awerbuch J, Tan T-M. Finite element modeling of the crushing behavior of thin-walled CFRP tubes under axial compression. Composites Part B: Engineering. 2014;64:50-8.
[86] Jacob GC, Fellers JF, Simunovic S, Starbuck JM. Energy absorption in polymer composites for automotive crashworthiness. Journal of Composite Materials. 2002;36:813-50.
[87] Elmarakbi A. Finite Element Analysis of Delamination Growth in Composite Materials using LS-DYNA: Formulation and Implementation of New Cohesive Elements: INTECH Open Access Publisher, 2011.
[88] El-Hage H, Mallick PK, Zamani N. A numerical study on the quasi-static axial crush characteristics of square aluminum-composite hybrid tubes. Composite Structures. 2006;73:505-14.
[89] Lanzi L, Castelletti L, Anghileri M. Multi-objective optimisation of composite absorber shape under crashworthiness requirements. Composite Structures. 2004;65:433-41.
[90] Lanzi L, Bisagni C, Ricci S. Neural network systems to reproduce crash behavior of structural components. Computers & Structures. 2004;82:93-108.
[91] Jiang Z, Gu M. Optimization of a fender structure for the crashworthiness design. Materials & Design. 2010;31:1085-95.

[92] Acar E, Guler M, Gerceker B, Cerit M, Bayram B. Multi-objective crashworthiness optimization of tapered thin-walled tubes with axisymmetric indentations. Thin-Walled Structures. 2011;49:94-105.
[93] Hou S, Han X, Sun G, Long S, Li W, Yang X, et al. Multiobjective optimization for tapered circular tubes. Thin-Walled Structures. 2011;49:855-63.
[94] Marzbanrad J, Ebrahimi MR. Multi-objective optimization of aluminum hollow tubes for vehicle crash energy absorption using a genetic algorithm and neural networks. Thin-Walled Structures. 2011;49:1605-15.
[95] Queipo NV, Haftka RT, Shyy W, Goel T, Vaidyanathan R, Tucker PK. Surrogate-based analysis and optimization. Progress in Aerospace Sciences. 2005;41:1-28.
[96] Goel T, Haftka RT, Shyy W, Queipo NV. Ensemble of surrogates. Structural and Multidisciplinary Optimization. 2007;33:199-216.
[97] Balali V, Zahraie B, Roozbahani A. Integration of ELECTRE III and PROMETHEE II decision-making methods with an interval approach: Application in selection of appropriate structural systems. Journal of Computing in Civil Engineering. 2012;28:297-314.
[98] Papila N, Shyy W, Griffin L, Dorney DJ. Shape optimization of supersonic turbines using global approximation methods. Journal of Propulsion and Power. 2002;18:509-18.
[99] Goel T, Vaidyanathan R, Haftka RT, Shyy W, Queipo NV, Tucker K. Response surface approximation of Pareto optimal front in multi-objective optimization. Computer Methods in Applied Mechanics and Engineering. 2007;196:879-93.
[100] Zarei H, Kroger M, Albertsen H. An experimental and numerical crashworthiness investigation of thermoplastic composite crash boxes. Composite Structures. 2008;85:245-57.
[101] Hanefi EH, Wierzbicki T. Axial resistance and energy absorption of externally reinforced metal tubes. Composites Part B. 1996;27:387-94.
[102] El-Hage H, Mallick PK, Zamani N. A numerical study on the quasi-static axial crush characteristics of square aluminum–composite hybrid tubes. Composite Structures. 2006;73:505-14.
[103] Kalhor R, Case SW. The effect of FRP thickness on energy absorption of metal-FRP square tubes subjected to axial compressive loading. Composite Structures. 2015;130:44-50.

[104] Kalhor R, Case SW. The effect of FRP thickness on energy absorption of metal-FRP square tubes subjected to axial compressive loading. Composite Structures.
[105] LS-DYNA Thoery Manual. Livermore, CA: Livermore Software Technology Corp.; 2013.
[106] Douthett J. Heat Treating of Stainless Steels, Heat Treating. ASM Handbook: ASM International; 1991. p. 769–92.
[107] Pagano NJ, Tandon GP. Thermoelastic Model for Multidirectional Coated-Fiber Composites - Traction Formulation. Composites Science and Technology. 1990;38:247-69.
[108] Feraboli P, Wade B, Deleo F, Rassaian M, Higgins M, Byar A. LS-DYNA MAT54 modeling of the axial crushing of a composite tape sinusoidal specimen. Composites Part a-Applied Science and Manufacturing. 2011;42:1809-25.
[109] LS-DYNA Keyword User's Manual, Version R 7.0. Livermore, CA: Livermore Software Technology Corp.; 2013.
[110] Deb K, Pratap A, Agarwal S, Meyarivan T. A fast and elitist multiobjective genetic algorithm: NSGA-II. Evolutionary Computation, IEEE Transactions on. 2002;6:182-97.
[111] Marler RT, Arora JS. Survey of multi-objective optimization methods for engineering. Structural and Multidisciplinary Optimization. 2004;26:369-95.
[112] Rumelhart DE, Hinton GE, Williams RJ. Learning internal representations by error propagation. DTIC Document; 1985.
[113] MATLAB 8.0 and Statistics Toolbox 8.1. The MathWorks, Inc.
[114] Park J-S. Optimal Latin-hypercube designs for computer experiments. Journal of statistical planning and inference. 1994;39:95-111.
[115] Mirzaei M, Shakeri M, Sadighi M, Akbarshahi H. Experimental and analytical assessment of axial crushing of circular hybrid tubes under quasi-static load. Composite Structures. 2012;94:1959-66.
[116] Kalhor R, Akbarshahi H, Case SW. Numerical modeling of the effects of FRP thickness and stacking sequence on energy absorption of metal–FRP square tubes. Composite Structures. 2016;147:231-46.
[117] Chatiri M, Güll T, Matzenmiller A. An assessment of the new LS-DYNA layered solid element: basics, patch simulation and its potential for thick composite structure analysis. 7th European LS-DYNA Conference, Salzburg2009.

[118] Abramowicz W. The effective crushing distance in axially compressed thin-walled metal columns. International Journal of Impact Engineering. 1983;1:309-17.
[119] Wierzbicki T, Abramowicz W. On the Crushing Mechanics of Thin-Walled Structures. Journal of Applied Mechanics-Transactions of the Asme. 1983;50:727-34.
[120] Abramowicz W, Jones N. Dynamic axial crushing of square tubes. International Journal of Impact Engineering. 1984;2:179-208.
[121] Mamalis AG, Manolakos DE, Demosthenous GA, Johnson W. Axial Plastic Collapse of Thin Bi-Material Tubes as Energy Dissipating Systems. International Journal of Impact Engineering. 1991;11:185-96.
[122] Hanefi E, Wierzbicki T. Axial resistance and energy absorption of externally reinforced metal tubes. Composites Part B-Engineering. 1996;27:387-94.
[123] Akbarshahi H, Sadighi M, Shakeri M, Mirzaei M. Mathematical Model for Axial Crushing of Hybrid Square Tubes. Composite Science and Technology, Pts 1 and 2. 2011;471-472:664-9.
[124] Jimenez MA, Miravete A, Larrode E, Revuelta D. Effect of trigger geometry on energy absorption in composite profiles. Composite Structures. 2000;48:107-11.
[125] Baker A, Mallick P. Composite engineering handbook. Marcel Decker Inc, New York. 1997.